

The CECOM Center for Night Vision and Electro-Optics

AD-A218 213

OPTOELECTRONIC WORKSHOPS

XI

SUPERLATTICE DISORDERING



December 7, 1988

Accession For	
NTIS GRA&I	<input checked="" type="checkbox"/>
DTIC TAB	<input type="checkbox"/>
Unannounced	<input type="checkbox"/>
Justification	
By	
Distribution/	
Availability Codes	
Dist	Avail and/or Special
A-1	

sponsored jointly by

ARO-URI Center for Opto-Electronic Systems Research
The Institute of Optics, University of Rochester

REPORT DOCUMENTATION PAGE

1a. REPORT SECURITY CLASSIFICATION Unclassified		1b. RESTRICTIVE MARKINGS	
2a. SECURITY CLASSIFICATION AUTHORITY		3. DISTRIBUTION/AVAILABILITY OF REPORT Approved for public release; distribution unlimited.	
2b. DECLASSIFICATION/DOWNGRADING SCHEDULE		5. MONITORING ORGANIZATION REPORT NUMBER(S) <i>ARO 24626.108-PH-01R</i>	
4. PERFORMING ORGANIZATION REPORT NUMBER(S)	7a. NAME OF MONITORING ORGANIZATION U. S. Army Research Office		
6a. NAME OF PERFORMING ORGANIZATION University of Rochester	6b. OFFICE SYMBOL (if applicable)	7b. ADDRESS (City, State, and ZIP Code) P. O. Box 12211 Research Triangle Park, NC 27709-2211	
6c. ADDRESS (City, State, and ZIP Code) The Insitute of Optics Rochester, NY 14627	9. PROCUREMENT INSTRUMENT IDENTIFICATION NUMBER <i>DAAL03-86-K-0173</i>		
8a. NAME OF FUNDING/SPONSORING ORGANIZATION U. S. Army Research Office	8b. OFFICE SYMBOL (if applicable)	10. SOURCE OF FUNDING NUMBERS	
8c. ADDRESS (City, State, and ZIP Code) P. O. Box 12211 Research Triangle Park, NC 27709-2211	PROGRAM ELEMENT NO.		PROJECT NO.
		TASK NO.	WORK UNIT ACCESSION NO.
11. TITLE (Include Security Classification) Optoelectronic Workshop XI: Superlattice Disordering			
12. PERSONAL AUTHOR(S) Susan Houde-Walter			
13a. TYPE OF REPORT Technical	13b. TIME COVERED FROM TO	14. DATE OF REPORT (Year, Month, Day) December 7, 1988	15. PAGE COUNT
16. SUPPLEMENTARY NOTATION The view, opinions and/or findings contained in this report are those of the author(s) and should not be construed as an official Department of the Army position, policy, or decision, unless so designated by other documentation.			
17. COSATI CODES		18. SUBJECT TERMS (Continue on reverse if necessary and identify by block number)	
FIELD	GROUP	SUB-GROUP	
		Workshop; superlattice disordering. <i>DES</i>	
19. ABSTRACT (Continue on reverse if necessary and identify by block number)			
<p>↓</p> <p>This workshop on "Superlattice Disordering" represents the eleventh of a series of intensive academic/ government interactions in the field of advanced electro-optics, as part of the Army sponsored University Research Initiative. By documenting the associated technology status and dialogue it is hoped that this baseline will serve all interested parties towards providing a solution to high priority Army requirements. Responsible for program and program execution are Dr. Nicholas George, University of Rochester (ARO-URI) and Dr. Rudy Buser, NVEOC.</p>			
20. DISTRIBUTION/AVAILABILITY OF ABSTRACT <input type="checkbox"/> UNCLASSIFIED/UNLIMITED <input type="checkbox"/> SAME AS RPT. <input type="checkbox"/> DTIC USERS		21. ABSTRACT SECURITY CLASSIFICATION Unclassified	
22a. NAME OF RESPONSIBLE INDIVIDUAL Nicholas George	22b. TELEPHONE (Include Area Code) 716-275-2417	22c. OFFICE SYMBOL	

The CECOM Center for Night Vision and Electro-Optics

OPTOELECTRONIC WORKSHOPS

XI

SUPERLATTICE DISORDERING



December 7, 1988

Preparation For	
DTIC	<input checked="" type="checkbox"/>
US	<input type="checkbox"/>
UK	<input type="checkbox"/>
Other	<input type="checkbox"/>
Prepared by	
Approved by	
Approved by Coles	
Dist	Special

sponsored jointly by

A-1

ARO-URI Center for Opto-Electronic Systems Research
The Institute of Optics, University of Rochester

**OPTOELECTRONIC WORKSHOP
ON
SUPERLATTICE DISORDERING**

**Organizer: ARO-URI-University of Rochester
and CECOM Center for Night Vision and Electro-Optics**

- 1. INTRODUCTION**
- 2. SUMMARY -- INCLUDING FOLLOW-UP**
- 3. VIEWGRAPH PRESENTATIONS**
 - A. Center for Opto-Electronic Systems Research
Organizer -- Susan Houde-Walter**

**Overview and Status of Work at Univeristy of Rochester
Susan Houde-Walter**
 - B. CECOM Center for Night Vision and Electro-Optics
Organizer -- John Pollard**

**The Status of MBE at C²NVEO
Jack Dinan**

**Electronic Structure Calculations: Impurities, Superlattices
Ronald Graft**

**Photorefectance Studies of Group II-VI Systems
Paul Amirtharaj**

**Properties of CdTe/InSb Interlayers
Michael Martinka**

**Non-Linear Optical Properties
Gary Wood**

**Laser Diode Arrays
David Caffey**
- 4. LIST OF ATTENDEES**

1. INTRODUCTION

This workshop on "Superlattice Disorder" represents the eleventh of a series of intensive academic/ government interactions in the field of advanced electro-optics, as part of the Army sponsored University Research Initiative. By documenting the associated technology status and dialogue it is hoped that this baseline will serve all interested parties towards providing a solution to high priority Army requirements. Responsible for program and program execution are Dr. Nicholas George, University of Rochester (ARO-URI) and Dr. Rudy Buser, CCNVEO.

2. SUMMARY AND FOLLOW-UP ACTIONS

Dr. Buser opened the session with remarks on the NVEOC mission in optical materials research. Dr. Buser stressed the directions in which epitaxial growth and processing efforts must go to achieve sophisticated new device types needed by the military, and the Army in particular.

The first talk was a tutorial in response to a request from NVEOC personnel on the implications of the quantum size effect in III-V semiconductors for lasers, modulators, and detectors. The tutorial, given by Prof. Houde-Walter, emphasized the differences between performance and characteristics of quantum well and double heterostructure lasers, bulk and quantum well modulators utilizing the quantum-confined Stark effect, and some newly proposed GaInSb/InAs strained layer superlattice structures which may mimic the absorption spectra of HgCdTe.

Prof. Houde-Walter next gave a presentation on the current research at the Institute of Optics in superlattice disordering and its application to monolithic integration in III-V semiconductor optoelectronics. Methods for improving state-of-the-art lateral resolution in AlGaAs/GaAs were described and results from preliminary calculations were presented.

Current efforts in molecular beam epitaxy at NVEOC were next given by Dr. John Dinnan. Fabrication of CdTe/InSb buffer layers for HgCdTe structures and CdTe/CdZnTe superlattice structures was discussed, as was MBE growth of InSb on CdTe and CdTe on InSb. The studies of InSb/CdTe interfaces revealed a chemical reaction between InSb and CdTe which resulted in non-abrupt heterostructure definition. Improvement in interface quality was achieved by careful control of component flux ratios during growth.

Dr. Ronald Graft, also from NVEOC, followed with a discussion of computationally efficient numerical modeling techniques for simulating the presence of impurities in bulk semiconductors and for modeling superlattices. A recursion method, used to describe the effect of impurities and point defects, and a renormalization method, which was used to model superlattices, were presented.

Dr. Paul Armirharaj gave a review of the photoreflectance technique and discussed his application of the method to II-VI semiconductors. A demonstration of the sensitivity of the technique to processing (implant and anneal) and characterization of CdZnTe alloys and CdTe/ZnTe superlattices were presented.

The properties of CdTe/InSb interfaces and molecular beam epitaxial growth of In₂Te₃ layers on InSb (100) substrates were described by Dr. Michael Martinka of NVEOC. In an effort to achieve InSb/In₂Te₃/InSb and InSb/In₂Te₃/CdTe multilayers, InSb and CdTe were grown on epitaxial In₂Te₃ layers. Characterization revealed pronounced mixing of the alloys, consistent with thermodynamics of the InSb/In₂Te₃ interface.

Dr. Gary Wood of NVEOC gave a presentation of results from a joint NVEOC/Rockwell International/University of Illinois collaboration on optical nonlinearities in semiconductor multi-quantum wells. The physical origins of nonlinearities in bulk and quantum well semiconductors were discussed in

detail. HgCdTe multi-quantum wells with a sawtooth profile were designed, grown, and their electrical properties were characterized. Afterwards Prof. Houde-Walter compared NVEOC's data using a well-known figure of merit for nonlinear materials $(X^{(3)}/\alpha\tau)$.

The last presentation by NVEOC was given by Dr. David Caffey on laser diode arrays. Blocks of commercial diode arrays were used to pump zig-zag YAG oscillators. Adequate heat sinking in a dense array of lasers was a concern. Despite some thermal detuning of the optical emission of the pump, good pumping efficiencies were achieved.

The seminar concluded with a lively discussion of the process of developing new materials into state of the art devices. Dr. John Pollard expressed interest in improvement of the noise characteristics of avalanche photodiodes and Prof. Houde-Walter suggested that quantum well avalanche structures might have improved signal-to-noise ratios.

Follow-up has included informal swapping of technical papers and continued discussions between Prof. Houde-Walter and NVEOC personnel on heat sinking laser diodes and the unique ability of impurity-induced disordering to generate window transparency and reduce facet damage in high-power laser diode arrays.

ARO-URI UNIVERSITY OF ROCHESTER AND C²NVEO OPTOELECTRONIC WORKSHOP

SUBJECT: Application of Superlattices and Quantum Well Structures

Small Conference Room, Bldg 305

Wednesday, 7 Dec 88 at 1000

AGENDA

1000	Introduction	Dr. Rudy Buser
1005	Overview and Status of Work at University of Rochester	Susan Houde-Walter
1100	The Status of MBE at C²NVEO	Jack Dinan
1120	Electronic Structure Calculations Impurities, Superlattices	Ron Graft
1140	Photoreflectance Studies of Group II-VI Systems	Paul Amirtharaj
1200	Properties of CdTe/InSb Interlayers	Mike Martinka
1220	Non-linear Optical Properties	Gary Wood
1240	Laser Diode Arrays	Dave Caffey
1300	Discussion	

POC: John Pollard, X45780

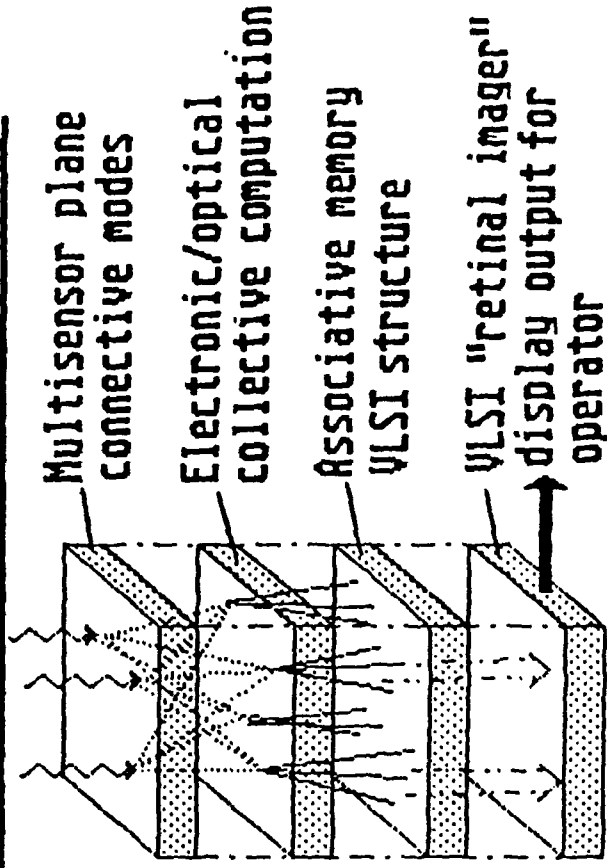
INTRODUCTION.

RUDY BUSER.

DECEMBER 7, 1988.
CECOM CENTER FOR NIGHT VISION
AND ELECTRO-OPTICS

Dr. Buser indicated the importance of controlled layer growth for the next generation of device structures and the impact this has already had on the laser technology. The disordering of superlattices to obtain controlled electronic properties was particularly interesting and provides the material scientists with new tools to fabricate special devices. He also discussed in the opening remarks the future possibility of providing a new sensor-processor which was integrated on one focal plane. The conceptual structure is given in the following viewgraph which combines a detector plane with an electronic/optical "neural net" type processor coupled with an associative memory and output display for autonomous recognition systems. This will necessitate the development of the growth of superlattice type structures in semiconductor materials and their appropriate modification under controlled conditions. The future investment at C2NVEO will provide for the controlled growth of materials using the methods of molecular beam and chemical beam epitaxy.

INTEGRATED DETECTOR PROCESSOR

<p><u>STATUS OF E-D SIGNAL PROCESSING</u></p> <p>Simplistic processing pursued</p> <ul style="list-style-type: none"> • Time delay and integration • Multiplexing • Responsivity correction • Automatic gain control 	<p><u>ISSUES</u></p> <ul style="list-style-type: none"> • Architecture selection • Interconnection technology • Integrated component technology
<p><u>REQUIREMENT FOR ADVANCED PROCESSING</u></p> <ul style="list-style-type: none"> • Processing speed • Improved signal/noise • Power reduction • Low weight • Small size 	<p><u>FUTURE INTEGRATED SENSOR/PROCESSOR</u></p> 

CECOM CENTER FOR NIGHT VISION
AND ELECTRO-OPTICS.

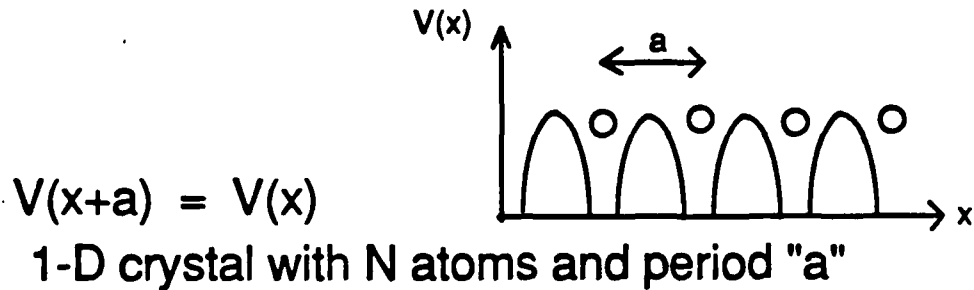
**CENTER FOR OPTO-ELECTRONIC SYSTEMS RESEARCH
OVERVIEW AND STATUS OF WORK**

THE QUANTUM SIZE EFFECT
AND ITS IMPLICATIONS
FOR LASERS, MODULATORS AND DETECTORS
IN OPTO-ELECTRONICS
and
SUPERLATTICE DISORDERING

SUSAN HOUDE-WALTER
URI Center for Opto-Electronics
The Institute of Optics
University of Rochester
(716) 275-7629

In Collaboration with
GARY WICKS
The Institute of Optics
University of Rochester

SEMICONDUCTOR CRYSTALS



Solutions to Shrödinger equation with periodic potential are Bloch functions:

$$\Psi_k(x) = e^{ikx} u_k(x)$$

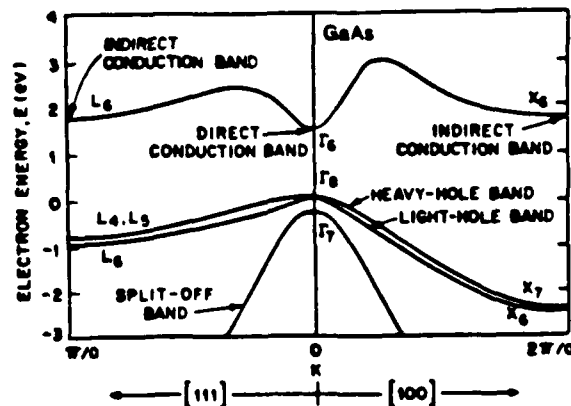
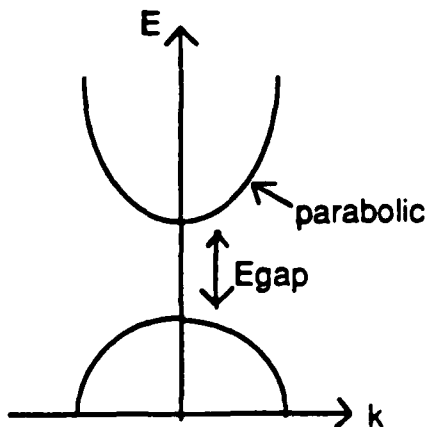
$$\text{where } u_k(x) = u_k(x+a)$$

k is crystal momentum:

$$k = \frac{2m\pi}{Na}$$

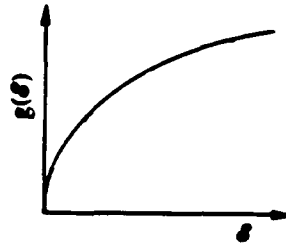
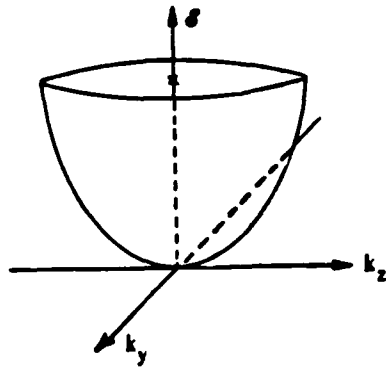
Result: certain energies are not allowed; "band gap"

Nearly free electron:
$$E = \frac{\hbar^2 k^2}{2m^*}$$



QUANTUM SIZE EFFECTS

Nearly free electron model (bulk):



density of states

$$E = \frac{\hbar^2}{2m} (k_x^2 + k_y^2 + k_z^2)$$

Particle in an infinitely deep 1-D well of width L_z

Schrödinger eqn.:

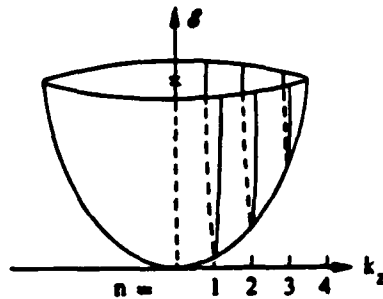
$$\frac{-\hbar^2}{2m} \frac{d^2\Psi}{dz^2} = E \Psi$$

$$E_n = \frac{\hbar^2}{2m} \left(\frac{n\pi}{L_z} \right)^2 \quad n = 1, 2, 3, \dots$$

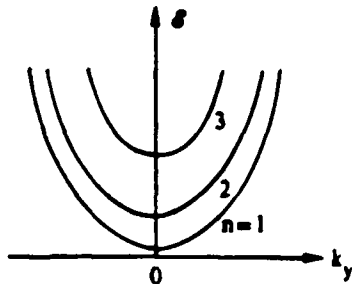
$$\Psi_n = A \sin \left(\frac{n\pi z}{L_z} \right)$$

>> discrete number of bound states.

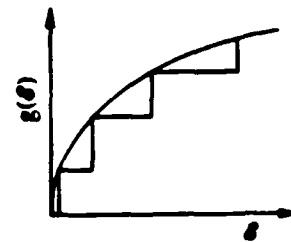
3-D Semiconductor Crystal, 1-D Confinement



$$E = \frac{\hbar^2}{2m} \left\{ k_x^2 + k_y^2 + \left(\frac{n\pi}{L_z} \right)^2 \right\}$$

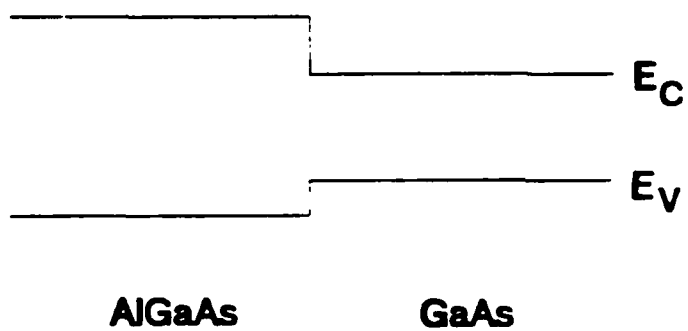
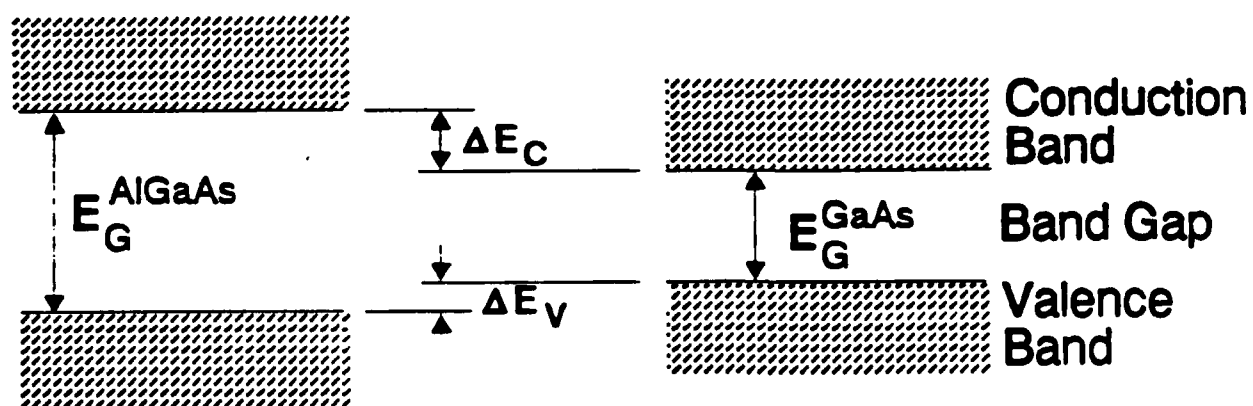


like 2-D nearly free electron model for each n

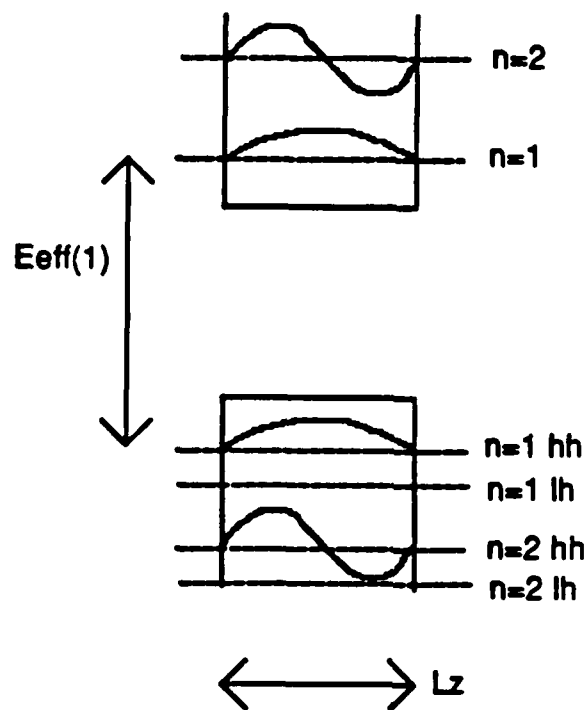


result: constant density of states for each n .

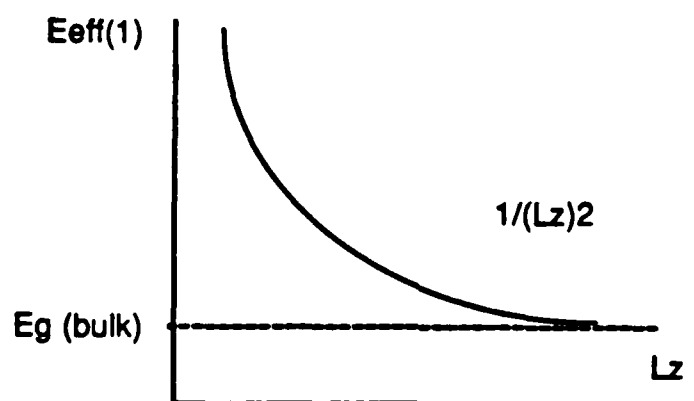
Heterojunction Energy Bands



Quantum Well - infinite potential barrier



$$L_z < \lambda_{\text{elec}} (=200 \text{ \AA in GaAs})$$



Particle in a 1-D well of finite height, V_0 , and width L_z :

In the well:

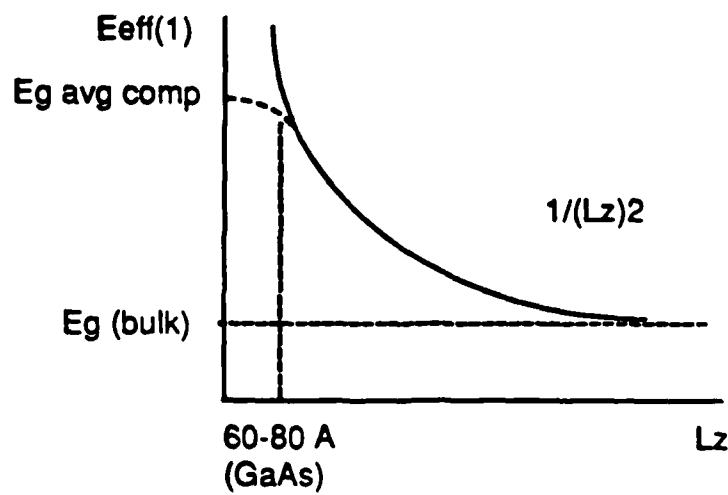
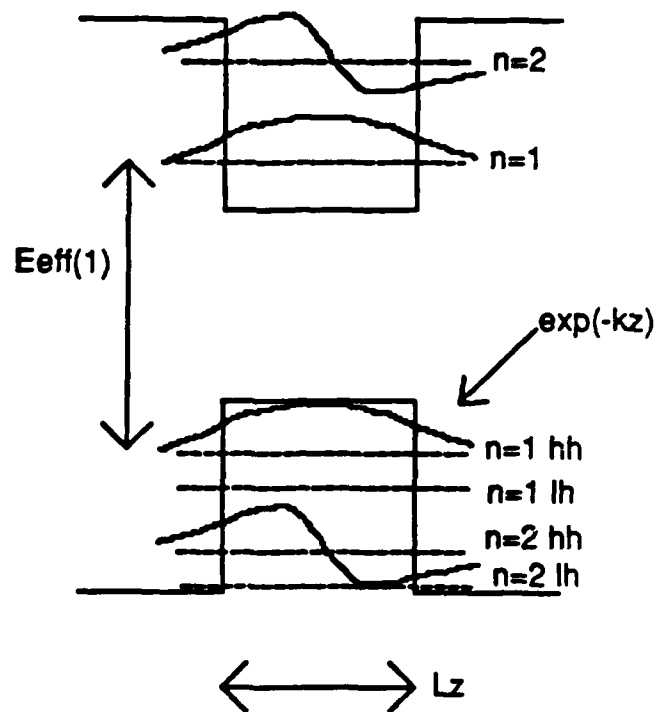
$$\frac{d^2\Psi}{dz^2} + k_2^2\Psi = 0 \quad k_2 = \frac{\sqrt{2mE}}{\hbar}$$

In the barrier region:

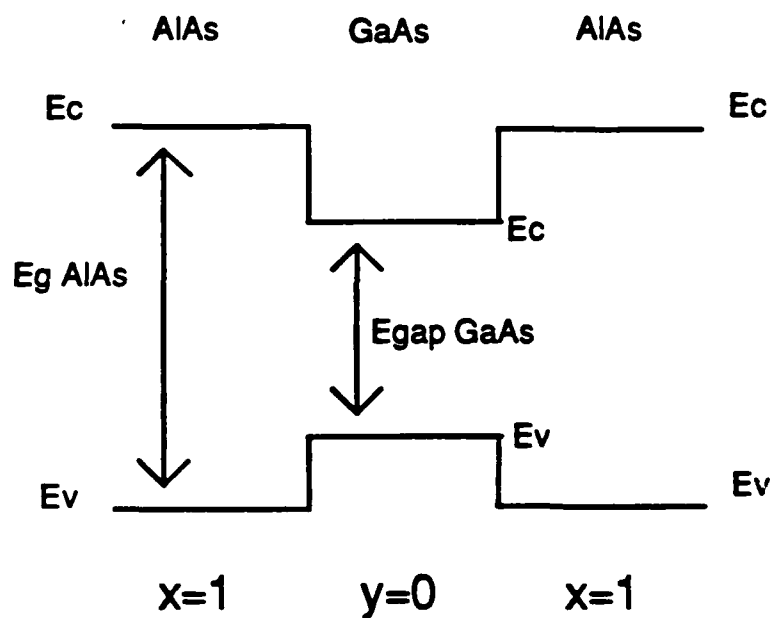
$$\frac{d^2\Psi}{dz^2} + k_1^2\Psi = 0 \quad k_1 = \frac{\sqrt{2m(V_0 - E)}}{\hbar}$$

$$\Psi = \begin{cases} A e^{k_1 z} & z < -\frac{L_z}{2} \\ B \sin(k_2 z) & -\frac{L_z}{2} < z < \frac{L_z}{2} \\ C e^{-k_1 z} & z > \frac{L_z}{2} \end{cases}$$

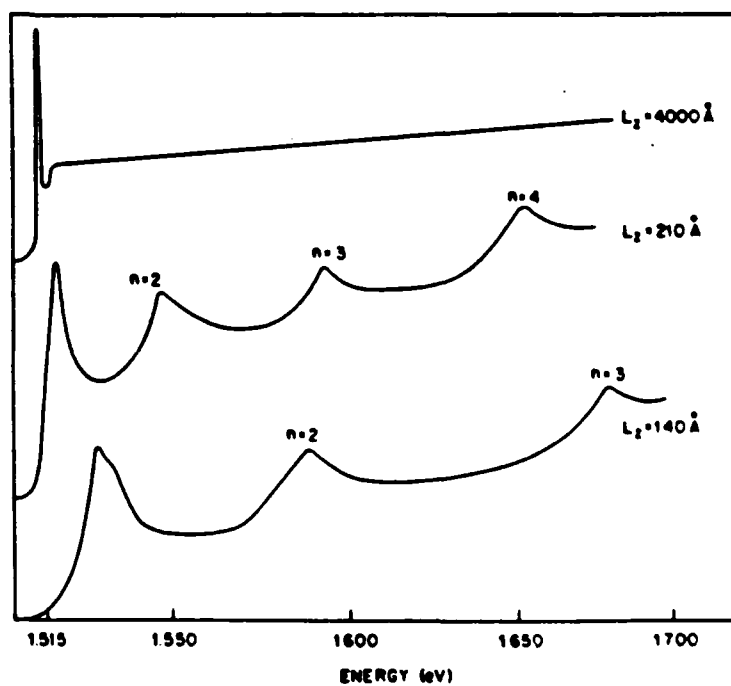
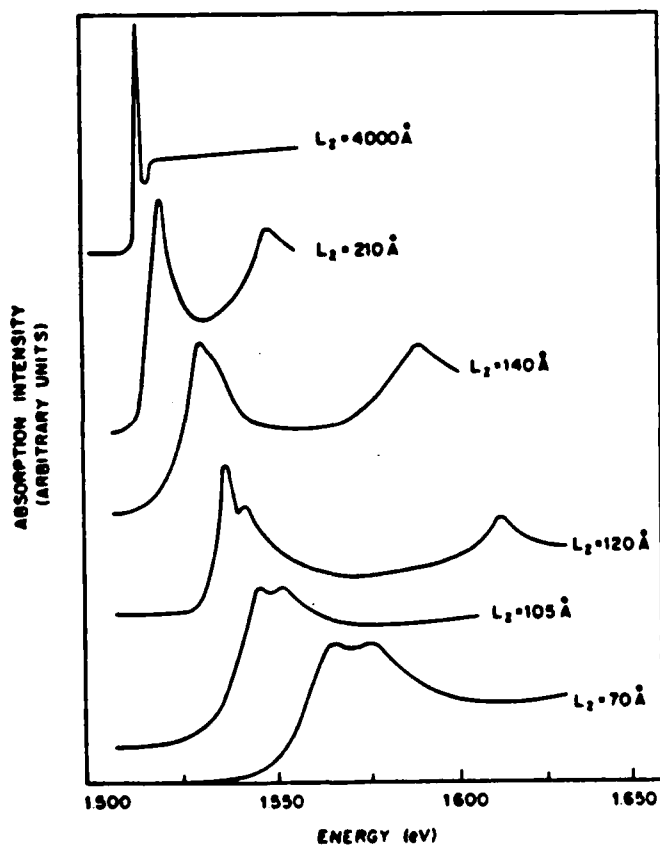
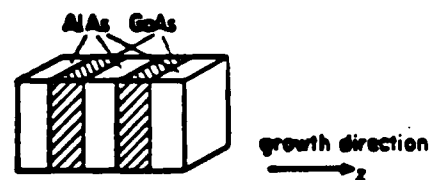
Quantum Well - finite potential barrier



Form lattice-matched heterostructure, e.g.:
 $(\text{Al}_x\text{Ga}_{1-x}\text{As}/\text{Al}_y\text{Ga}_{1-y}\text{As})$



GeAs-AlAs Quantum-Well Structure.



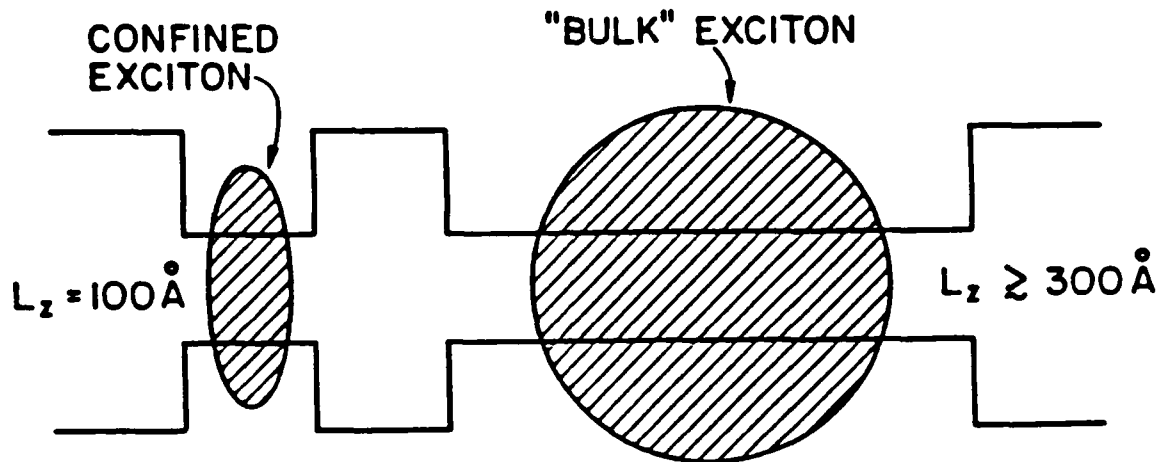
FROM: R. DINGLE, FESTKÖRPERPROBLEME XV (1975).

OTHER FEATURES OF ABSORPTION SPECTRA

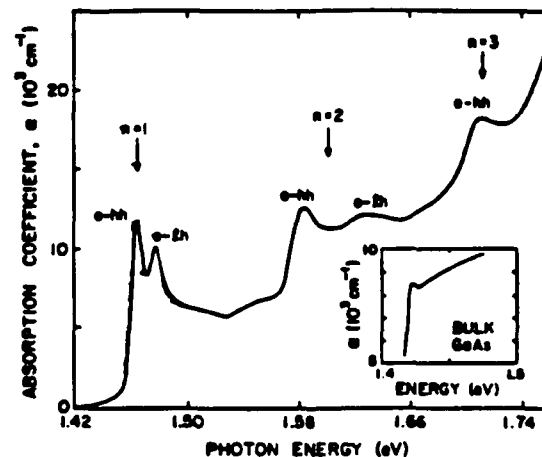
1. Room temperature excitons

exciton: hydrogen-like e-h pair bound together by Coulomb force

confined in QW, e-h pair has smaller orbit radius \Rightarrow stronger binding energy



excitons absorb/emit light at $h\nu = E_g - E_{ex}$ where E_{ex} is the energy required to thermally ionize exciton



From: J. Ralston, Ph.D. thesis, Cornell Univ. 1988

Consequence: absorption spectra is further sharpened

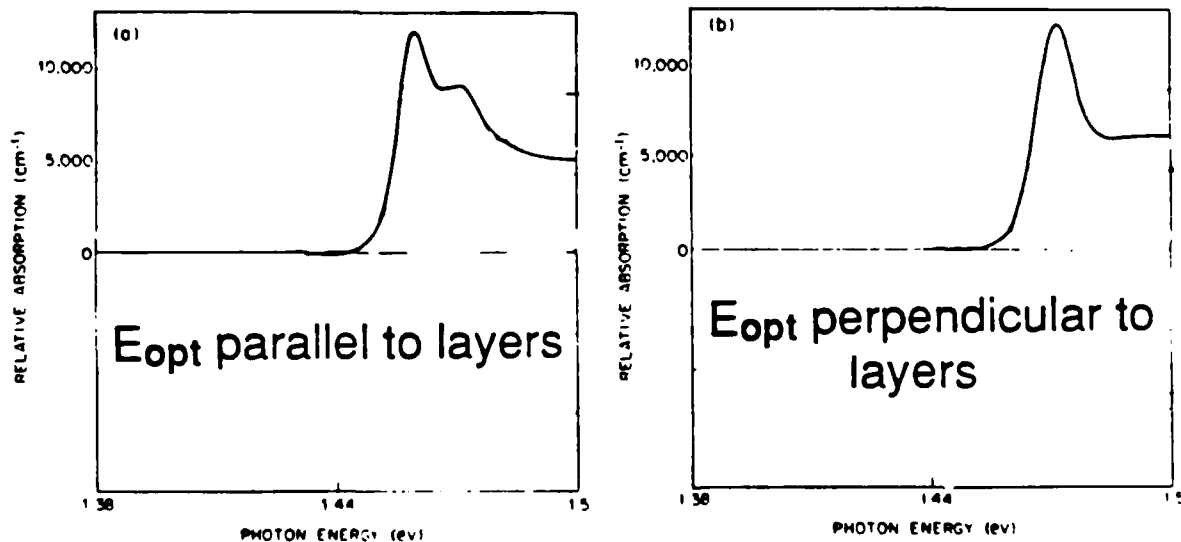
2. Polarization Selectivity

Angular momentum selection rules yield different oscillator strengths for light and heavy hole transitions:

Heavy hole: $\sigma = 3$ $\pi = 0$

Light hole: $\sigma = 1$ $\pi = 4$

Light polarized | parallel to layers: both lh & hh excitons
perpendicular \longrightarrow only lh excitons



Modified from: Weiner, et al APL 50, p843 (3/30/87)

Consequences:

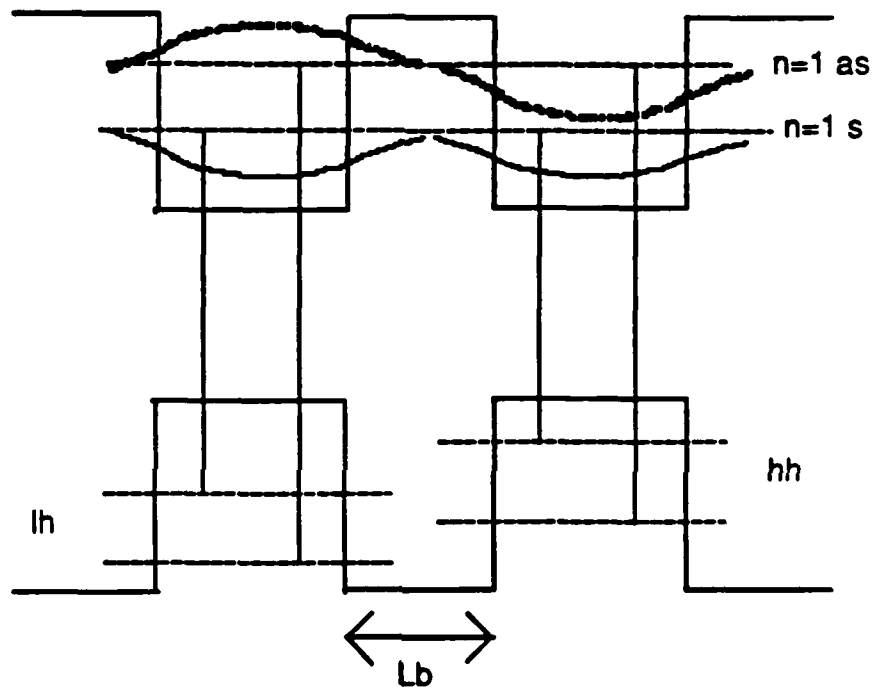
- birefringence

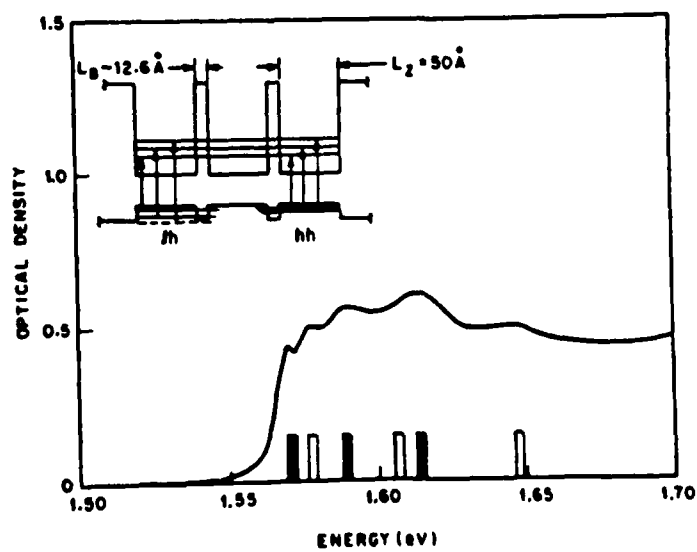
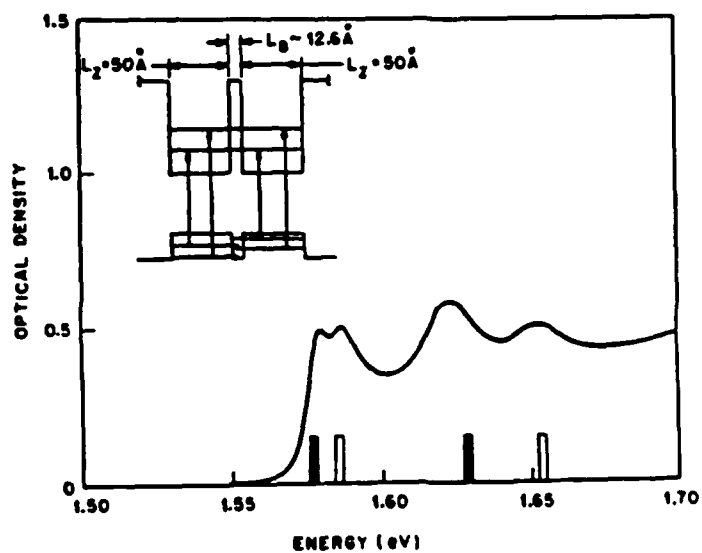
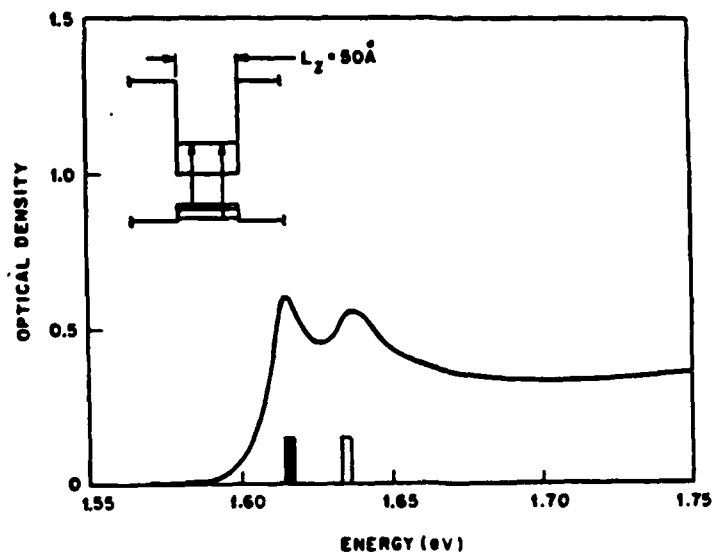
- extra polarization selectivity in waveguides

Two Coupled Quantum Wells

(n coupled quantum wells = superlattice)

(n uncoupled quantum wells = multi-quantum well)





FROM: R. DINGLE ibid.

How do dimensional constraints affect refractive index?

Dielectric constant:

$$\epsilon = \epsilon_1 + i\epsilon_2 = (n + ik)^2$$

where n = refractive index
 k = extinction coefficient:

$$k = \frac{1}{2} \frac{\hbar c}{\hbar \omega} \alpha$$

Kramers-Kronig relations:

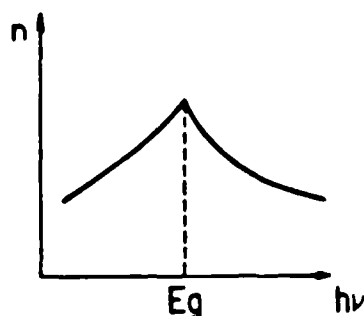
$$\epsilon_1(\omega) = 1 + \frac{2}{\pi} P \int_0^{\infty} \frac{\omega' \epsilon_2(\omega')}{\omega'^2 - \omega^2} d\omega'$$

$$\epsilon_2(\omega) = -\frac{2\omega}{\pi} P \int_0^{\infty} \frac{\epsilon_1(\omega')}{\omega'^2 - \omega^2} d\omega'$$

Calculated refractive indices:

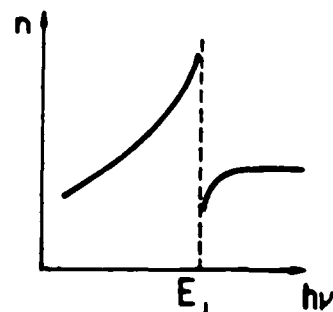
bulk semiconductor

$$\epsilon_2 \propto A(\hbar\nu - E_g)^{1/2}$$



quantum well

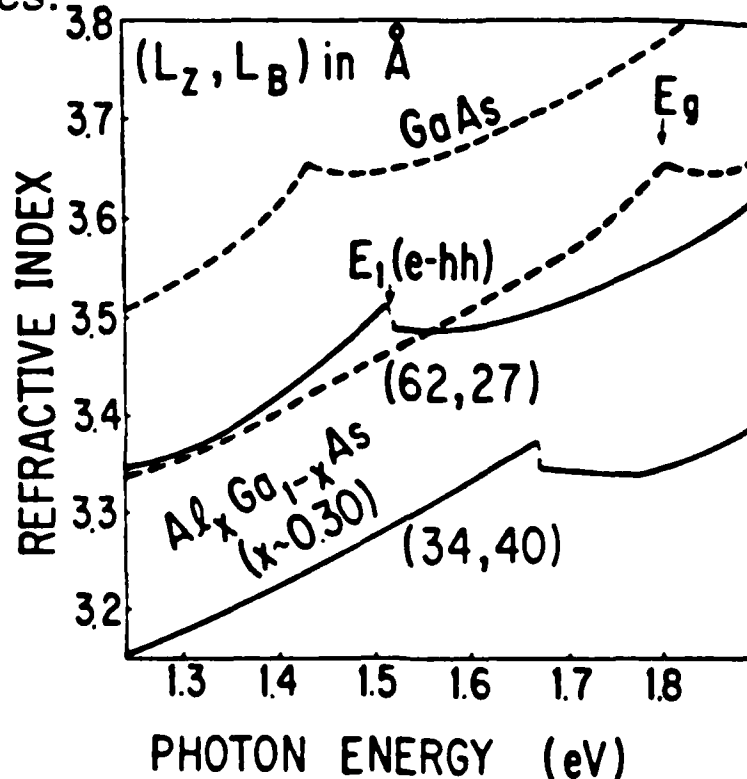
$$\epsilon_2 \propto \{A\theta(\hbar\nu - E_1) + B\delta(\hbar\nu - E_1)\}$$



Experimental:

ref: Y. Suzuki and H. Okamoto, J. Elec. Mats. 12, 397 (1983)

Compare refractive index (dispersion) of bulk $\text{Al}_{0.30}\text{Ga}_{0.70}\text{As}$ to GaAs/AlAs SL's with various barrier thicknesses:



Note: for a fixed average alloy composition, one can make large changes in refractive index by tailoring heterostructure dimensions.

>>useful degrees of freedom in device design

lasers

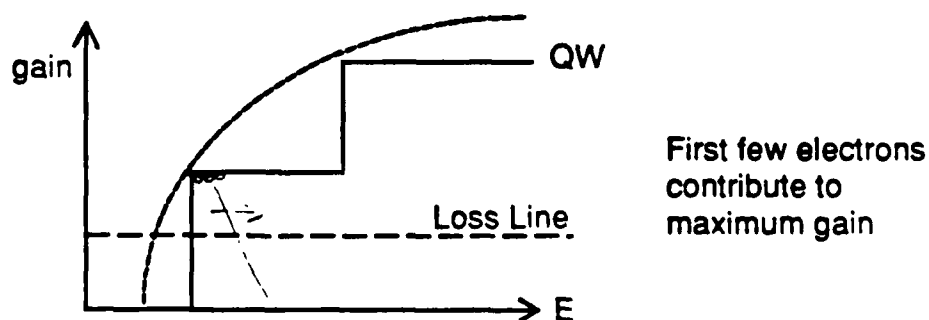
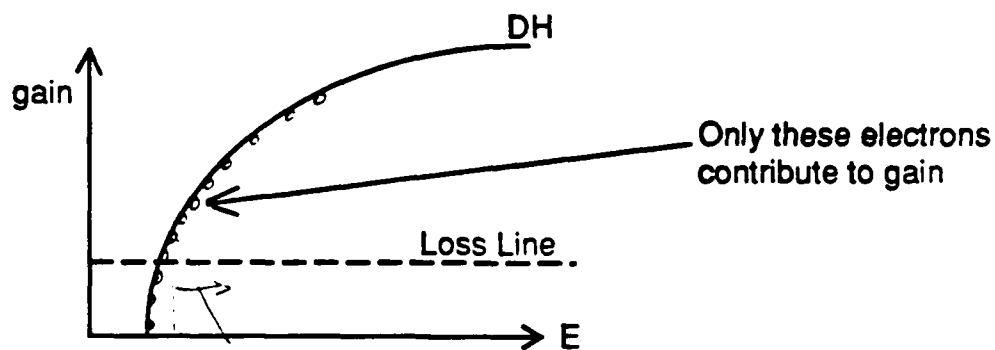
waveguides, lenses, modulators

detectors

QSE IMPLICATIONS FOR LASERS

(based on invited talk by A. Yariv, LEOS '88 (THE-3))

$$\text{gain} \propto \int dE \rho(E) [f_c(N,E) - f_v(N,E)] \frac{h/T_2}{(E - h\nu)^2 + (\frac{h}{T_2})^2}$$

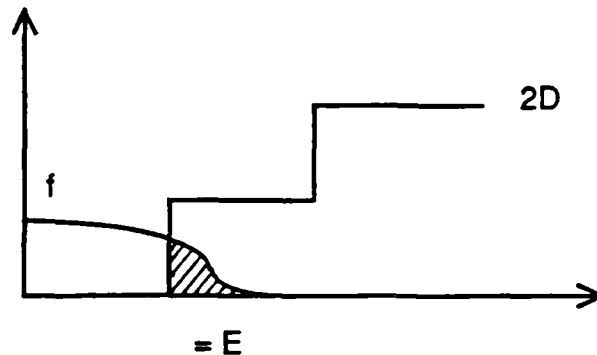


* Approx. gain is calculated by assuming a constant density of states in the conduction band and a constant density of states in the valence band

1. Threshold Current

ref.: Arakawa, et al, IEEE JQE, QE-21, p666 (10/85)

Semiconductor is transparent when conduction band Fermi level penetrates the density of states

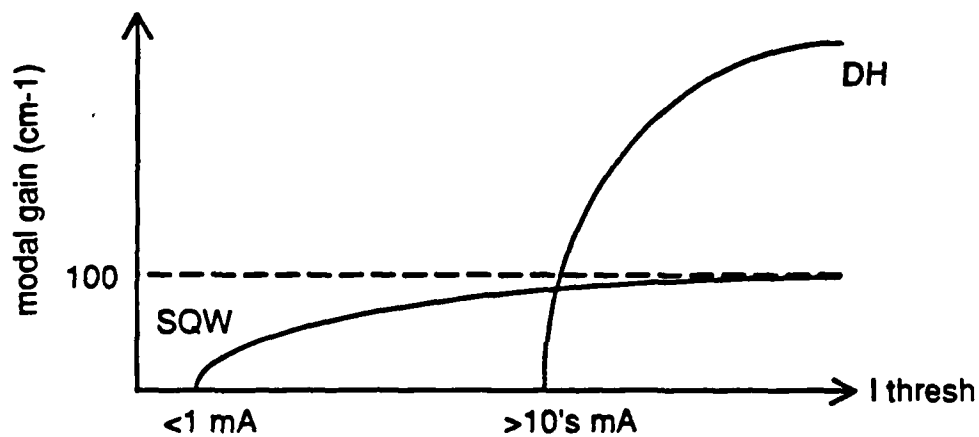


$$\begin{aligned}
 N_{2D}^{Tr} &= \frac{m^*}{\pi h^2} \int_{\epsilon_1}^{\infty} \frac{dE_c}{e^{(E_c - \epsilon_1)/kT} + 1} \\
 &= \ln 2 \frac{m^* kT}{\pi h^2} \\
 &\approx 1.5 \times 10^{12} \frac{\text{elec}}{\text{cm}^2} \Rightarrow 1.5 \times 10^{18} \frac{\text{elec}}{\text{cm}^3}
 \end{aligned}$$

Transparency is independent of confinement geometry

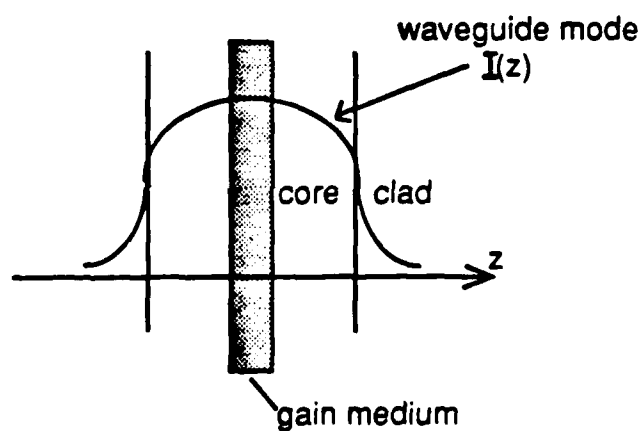
$$I_{Tr} \approx \frac{e N_{2D}^{Tr}}{\tau_p} V_{\text{active}}$$

Quantum well lasers typically have 20-40x smaller active volume >> proportionately smaller threshold



Modal gain = confinement factor \times gain

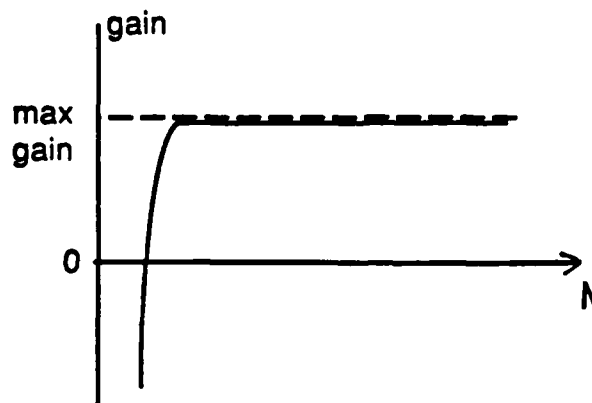
$$\Gamma = \frac{\int_{L_z} |E_{\text{opt}}|^2 dz}{\int_{-\infty}^{\infty} |E_{\text{opt}}|^2 dz}$$



Typically

$$\Gamma \cong \frac{L_z}{2000 \text{ \AA}}$$

2. Maximum Gain



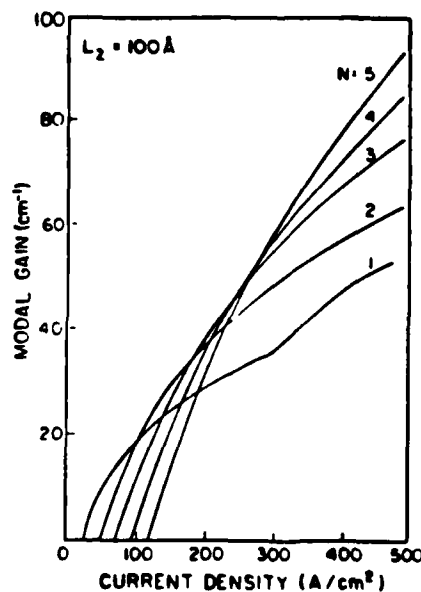
*Since maximum gain is approx. 100 cm^{-1} , require low losses to achieve lasing in SQW laser.

*Increase modal gain by increasing Γ : use MQW's.

>>Therefore, use MQW's (typically $N=3$)

$$g_{\text{max modal}}(N \text{ QW's}) \cong N g_{\text{max modal}}(\text{SQW})$$

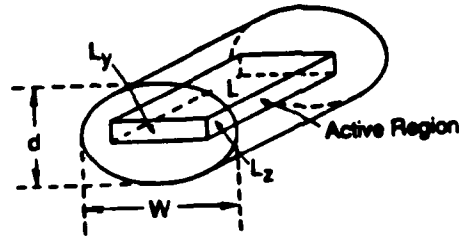
where N = number of QW's



From: Arakawa, et al IEEE JQE QE-21, p666 (10/85)

3. More on Current Threshold

ref.: Yariv, APL 53, p1033 (9/19/88)



$$I_{\text{Thresh}}^{3D} \propto N_{3D}^{\text{Tr}} (WL_z L) + \underbrace{\frac{Wd}{g'_{3D}} \ln \frac{1}{R} + \frac{WLd}{g'_{3D}} \alpha_{\text{scatt}}}_{\substack{\text{mirror \& scattering} \\ 20\%}}$$

80%

$$I_{\text{Thresh}}^{2D} \propto N_{2D}^{\text{Tr}} (WL) + \underbrace{\frac{Wd}{g'_{2D}} \ln \frac{1}{R} + \frac{WLd}{g'_{2D}} \alpha_{\text{scatt}}}_{80\%}$$

20%

*The dominant contribution to threshold approaches zero as end mirror reflectivities approach unity.

e.g. for $R \rightarrow 1$ and $\alpha = 0$ the minimum threshold current density is

$$I_{\text{Thresh min/cm}^2} = 60 \text{ A/cm}^2$$

>>> $I_{\text{Thresh}} = 0.1 \text{ mA}$ for typical device dimensions
($W = 1.5 \mu\text{m}$, $L = 120 \mu\text{m}$)

4. Laser Linewidth

ref.: Derry, et al, APL 53, p271 (7/25/88)

QW lasers have narrower linewidths

$$\Delta\nu = (1 + \alpha^2) \Delta\nu_{\text{Schalow-Townes}}$$

$$\text{where } \alpha = \frac{d\chi_R/dN}{d\chi_I/dN}$$

and $\chi = \chi_R + i\chi_I$, complex susceptibility

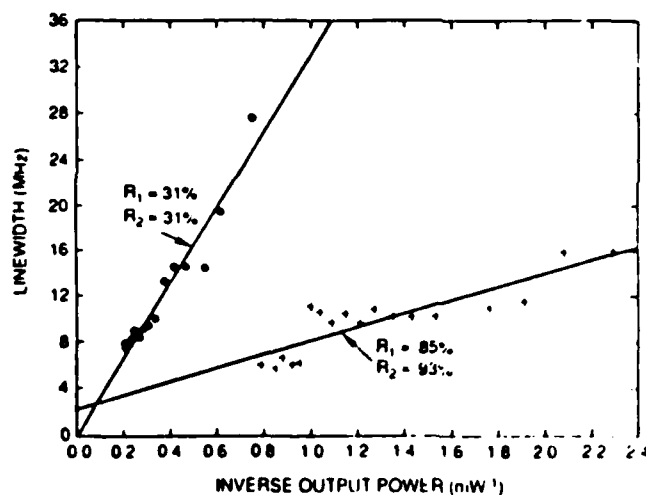


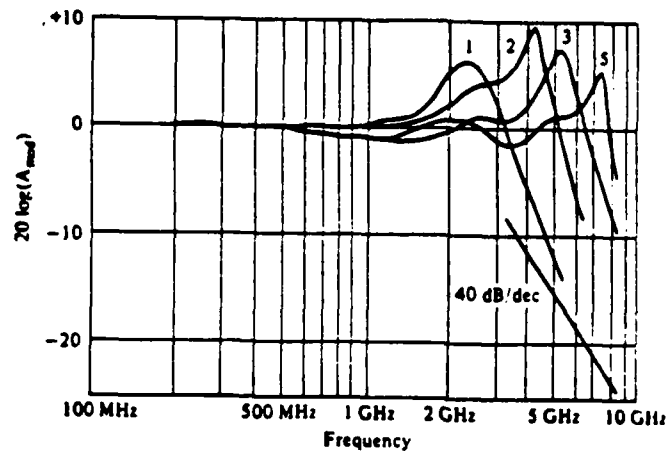
FIG. 1 Spectral linewidth as a function of the reciprocal of the output power at facet with reflectivity R_1 for an uncoated buried heterostructure GRIN SCH SQW laser and for the same laser with coated facet reflectivities $R_1 = 85\%$ and $R_2 = 93\%$

Slope:	DH:	74.7 MHz mW
	QW (R=31%):	28.3
	QW (R=90%):	5.9

$$\Delta\nu \cong 6 \text{ MHz @ } 1.3 \text{ mW}$$

5. Modulation Bandwidth

ref.: Arakawa (as above)



$$f_r \propto \sqrt{\frac{g' P_o}{\tau_p}}$$

where $g' = dg/dn$

P_o = power inside cavity

and τ_p = photon lifetime in cavity

QW lasers have about twice modulation bandwidth of DH lasers.

In sum:

QW lasers can be designed to have:

- lower current thresholds than DH lasers; these low thresholds can be further reduced by reflective coatings,

- smaller (2-3x) modal gain than DH lasers (for single QW lasers); same modal gain for MQW lasers (typically 2-3 QW's),

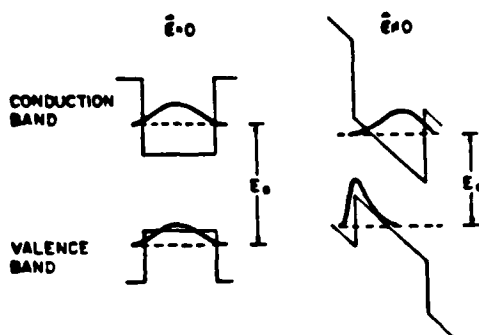
- narrower linewidths (about 5x narrower than equivalent DH lasers),

- twice the modulation bandwidth of DH lasers.

QSE IMPLICATIONS FOR MODULATORS

1. Quantum Confined Stark Effect

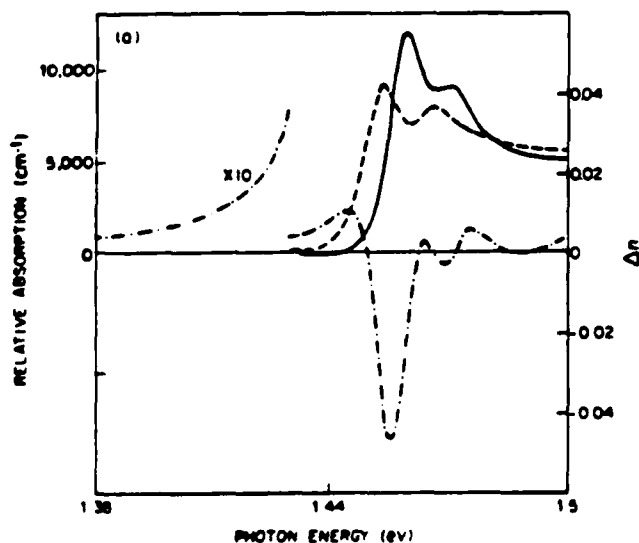
ref.: D.A.B. Miller, et al, Phys. Rev. B, 32, 1043 (85)



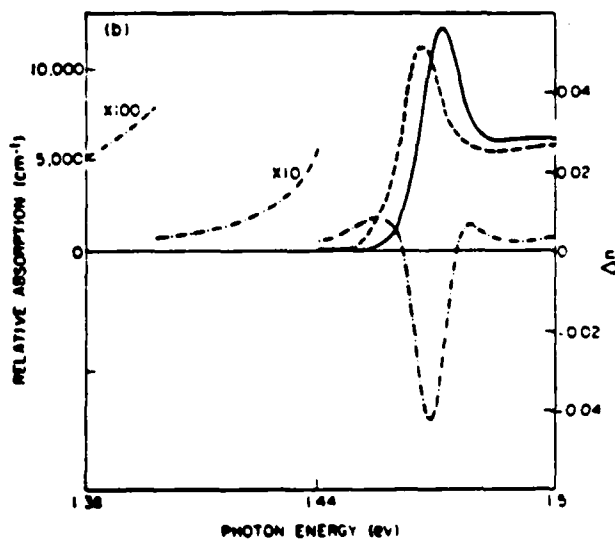
E_{appl} perpendicular to plane of layers
 $E=10^4$ V/cm (typically across 10^{-4} cm)

E_g decreases as E_{appl} becomes stronger

E_{opt} parallel to layers



E_{opt} perpendicular to layers



From: Weiner, et al, APL 50, p843 (3/30/87)

A. Electro-absorption: waveguide intensity modulator
ref.: Wood, JLWT 6, p743 (6/88)

$\Delta\alpha_{MQW} = 50\times \Delta\alpha_{GaAs}$ bulk (is comparable to $LiNbO_3$)

residual absorption for typical device = 2 dB

typical device speeds = 3-5 GHz

B. Electro-refraction: Phase modulators

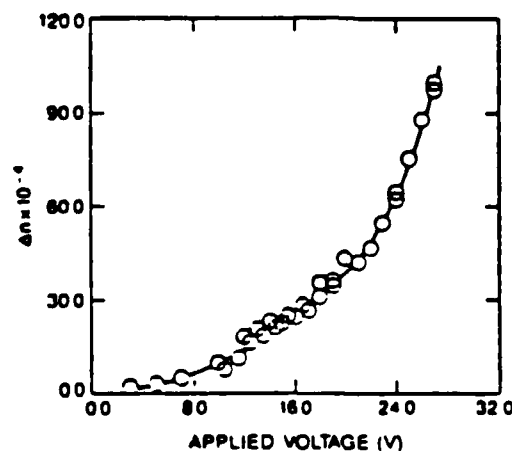
ref.: Weiner, et al, APL 50, p842 (3/30/87)
Zucker, IGWO '88, paper MA-2

Not useable near band edge due to unacceptable absorption losses

Far from band edge, $10^{-4} < \Delta n < 10^{-3}$ with minimum chirp

Dominant electro-optic effect is quadratic with E_{app}

$$\Delta n \cong -\frac{1}{2} n^3 s E_{app}^2$$



Bias to achieve small modulation voltages with min. chirp.

2. Other Modulators

A. Exciton Field Ionization

E_{app} parallel to layer interface: rip exciton apart with large fields (10^5 V/cm)

2-5x larger Δn than QCSE (penalty is higher field strength)

B. coupled quantum wells

C. direct to doubly indirect switching of superlattices

QSE Implications for Long Wavelength Detectors

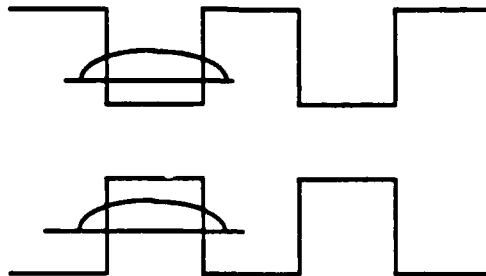
ref.: C. Mailhot and D. Smith J. Vac. Sci. Technol. B 5 p1268
(Jul/Aug 87)

Propose Type-II strained layer GaInSb/InAs SL
to replace HgCdTe:

- *III-V's are relatively easy to process
- *Relaxed tolerances (e.g. bandgap less sensitive to QW thickness than on HgCdTe alloy composition)
- *Reduced dark current

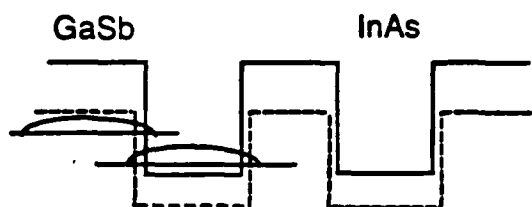
Type I Superlattice:

Bottom of conduction band and top of valence band
coincide in space.

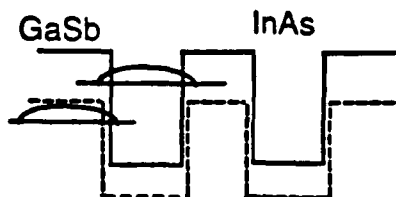


Type II Superlattice:

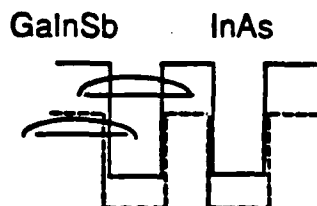
Bottom of conduction band and top of valence band
don't coincide in space.



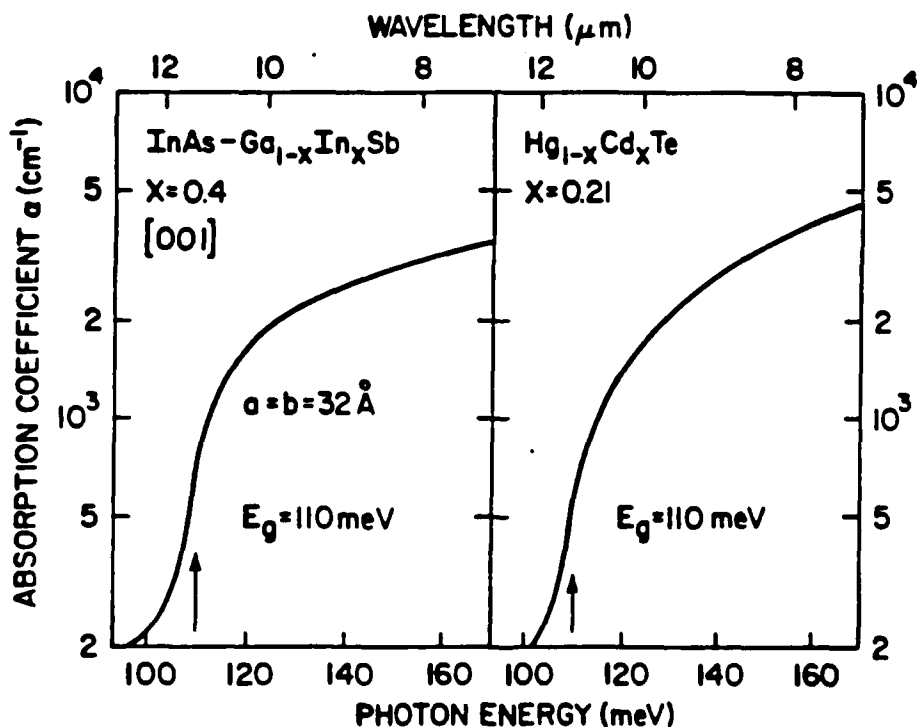
Negative bandgap in bulk;
negligible overlap of
wavefunctions



Tuneable bandgap by
QSE; negligible overlap
of wavefunctions



Introduce strain by barrier
alloy; suppresses
bandgap so can further
squeeze QW; result is
significant overlap of e-h
wavefunctions



from D. Smith and C. Mailhot J. Appl. Phys. **62** p2545
(9/15/87)

QSE materials is a new class of materials with extra useful degrees of freedom

Many parameters:

QW thickness, barrier thickness

Number of QW's

Well, barrier compositions, doping

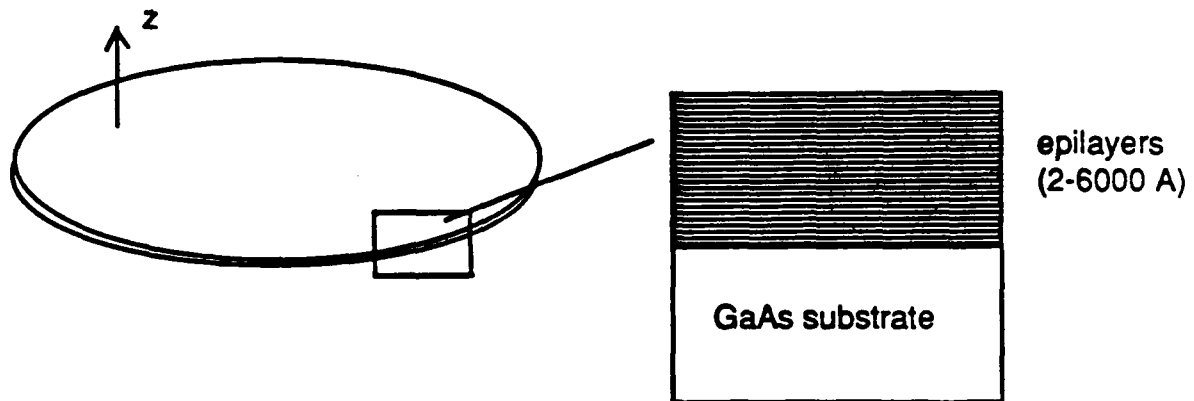
Extent of optical confinement

Etc.

>> well suited to design and engineering of opto-electronic circuitry

>> good candidate for monolithic integration

Heterostructures are grown epitaxially
molecular beam epitaxy
metallorganic chemical vapor deposition



INTEGRATION: grow one structure, use same base material for all components

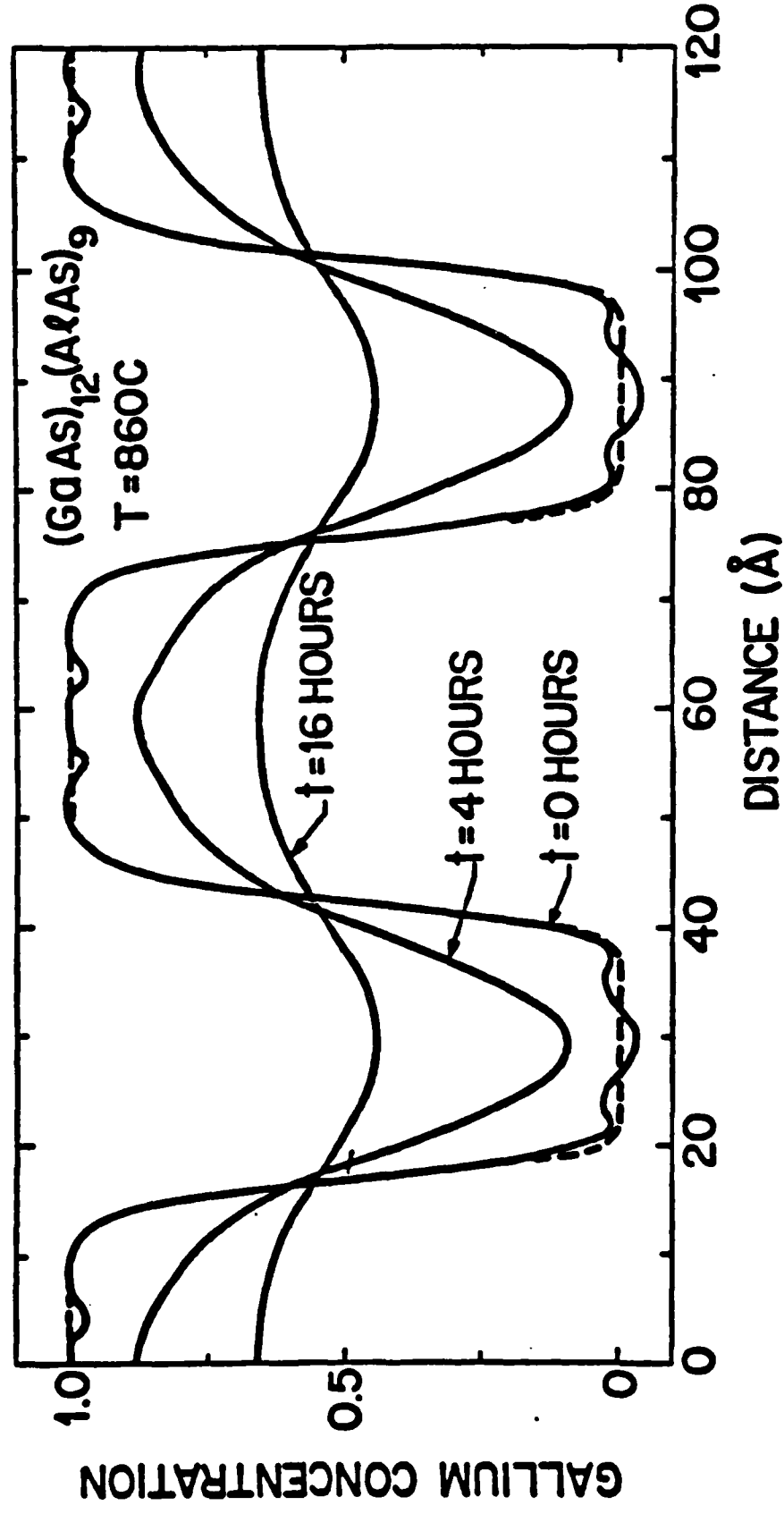
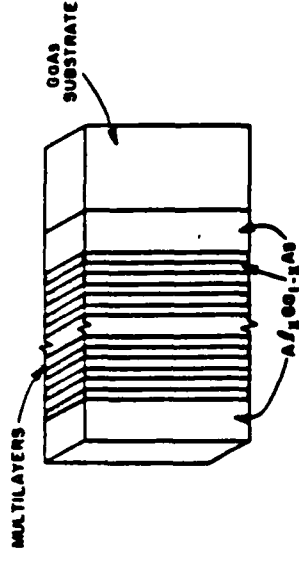
define components (e.g. ridge waveguides, heterostructure lasers) by removing surrounding material (ion beam etching, cleaving, etc.)

Disadvantage:
scattering, band bending, not planar, etc.

Objective: change bandgap and refractive index locally to define components

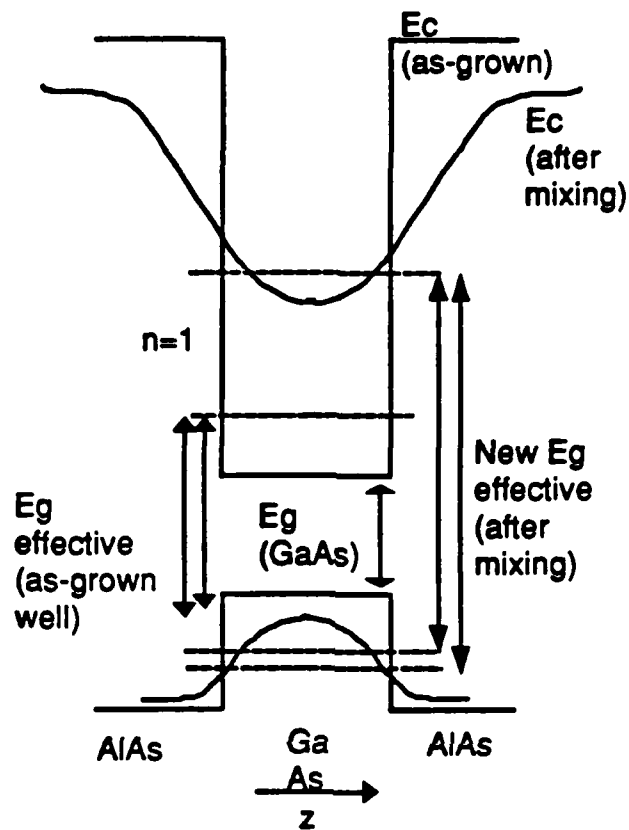
New Method: smooth abruptness of heterostructures locally

SL's are stable at moderate temperatures



FROM: P. DERNIER, et al, Bull. Amer. Phys. Soc. 22, 293 (1977).

Partial Mixing of heterostructure interfaces:



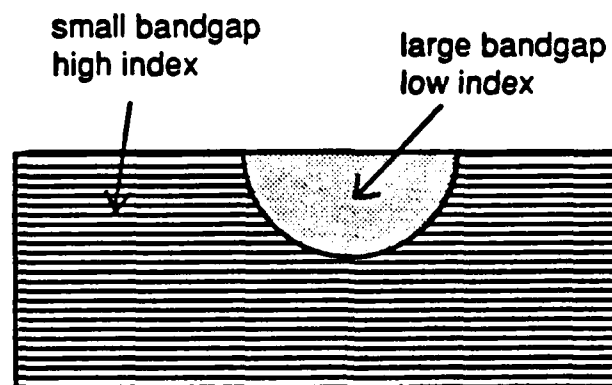
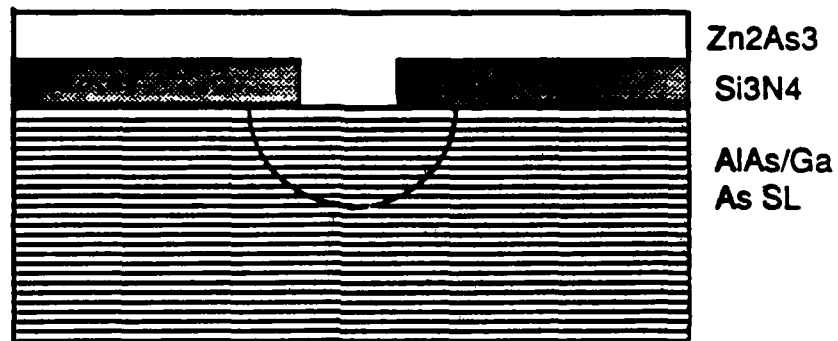
Use to tune emission wavelength of lasers

ref: M. Camras, et al., Appl. Phys. Lett., 54, p5637 (1983)

Mixing is enhanced by impurity transport

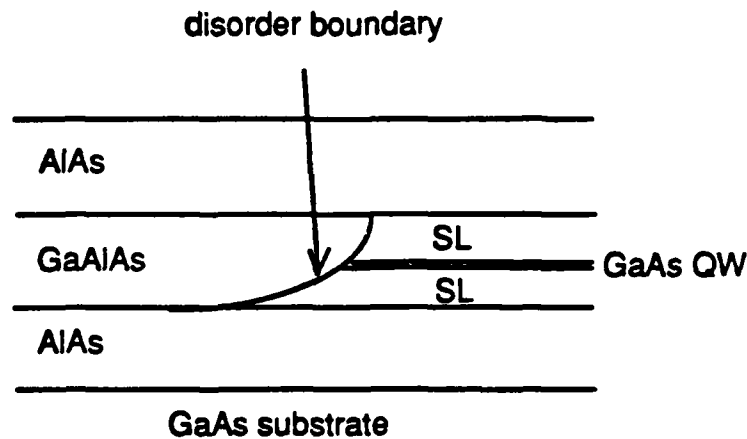
ref: W.D. Laidig, et al, Appl. Phys. Lett. 38, 776 (1981)

**MASKED Zn DIFFUSION INTO
SL**



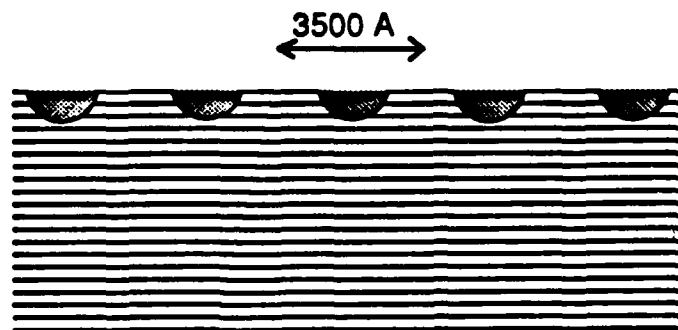
Waveguides:

ref.: F. Julien, et al., Appl. Phys. Lett., 50, 866 (1987)



Grating Couplers:

ref.: J. Ralston, et al., GaAs & Related Compounds (1985), 367.

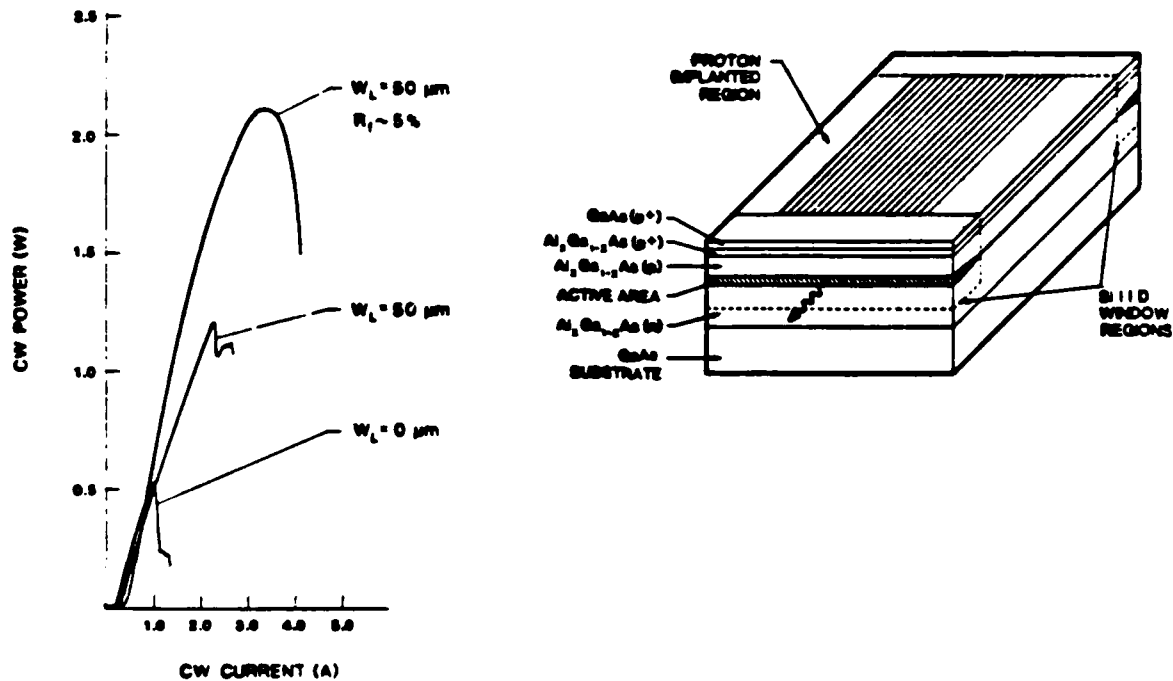


Masked Se implantation, grating period $\Lambda = 3500\text{\AA}$, $\lambda = 1.15\text{ }\mu\text{m}$

Lasers:

Reduce facet damage by increasing E_g at output windows.

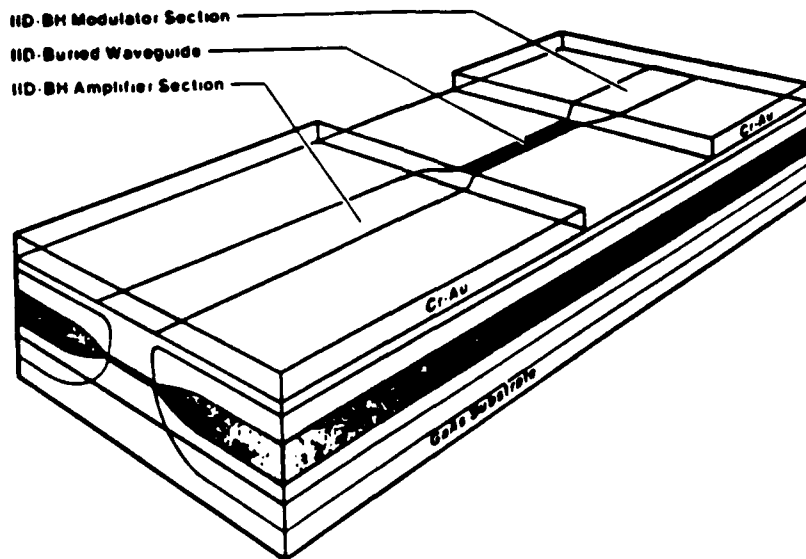
ref.: R. Thornton, et al, Appl. Phys. Lett., **49**, 1572 (1986).



Monolithic Integration:

Laser, waveguide and modulator

ref: R. Thornton, et al., J. Lightwave Tech., **6**, 786 (June 1988).



General Phenomenon:

Alloy	Species	Site
	P, Ga, Al, V _{III}	
$\text{Al}_x\text{Ga}_{1-x}\text{As}/\text{Al}_y\text{Ga}_{1-y}\text{As}$	Zn	III
	Si, Ge	
	S, Se	
$\text{GaP}/\text{GaAs}_{1-x}\text{P}_x$	Zn	V
$\text{InP}/\text{Ga}_{1-y}\text{In}_y\text{As}_{1-x}\text{P}_x$	Zn	III, V

Electrically inactive species:

Ga, Al implant and anneal- collisional mixing
 P implant and anneal - collisional mixing, strain(?)
 V_{III} - Ga gettering into cap layer

Electrically active impurities:

Impurity diffusion from ext. or grown-in sources
 Ion implantation - two stages:
 collisional
 impurity mixing

Can pattern by beam writing or photolithography
 waveguides and gratings
 low threshold lasers
 high power lasers

THIS WORK: Brian Olmsted
(in collaboration with Gary Wicks)

GOAL: Monolithic Optoelectronic Integration

>>improved lateral resolution for component definition

Zn diffusion



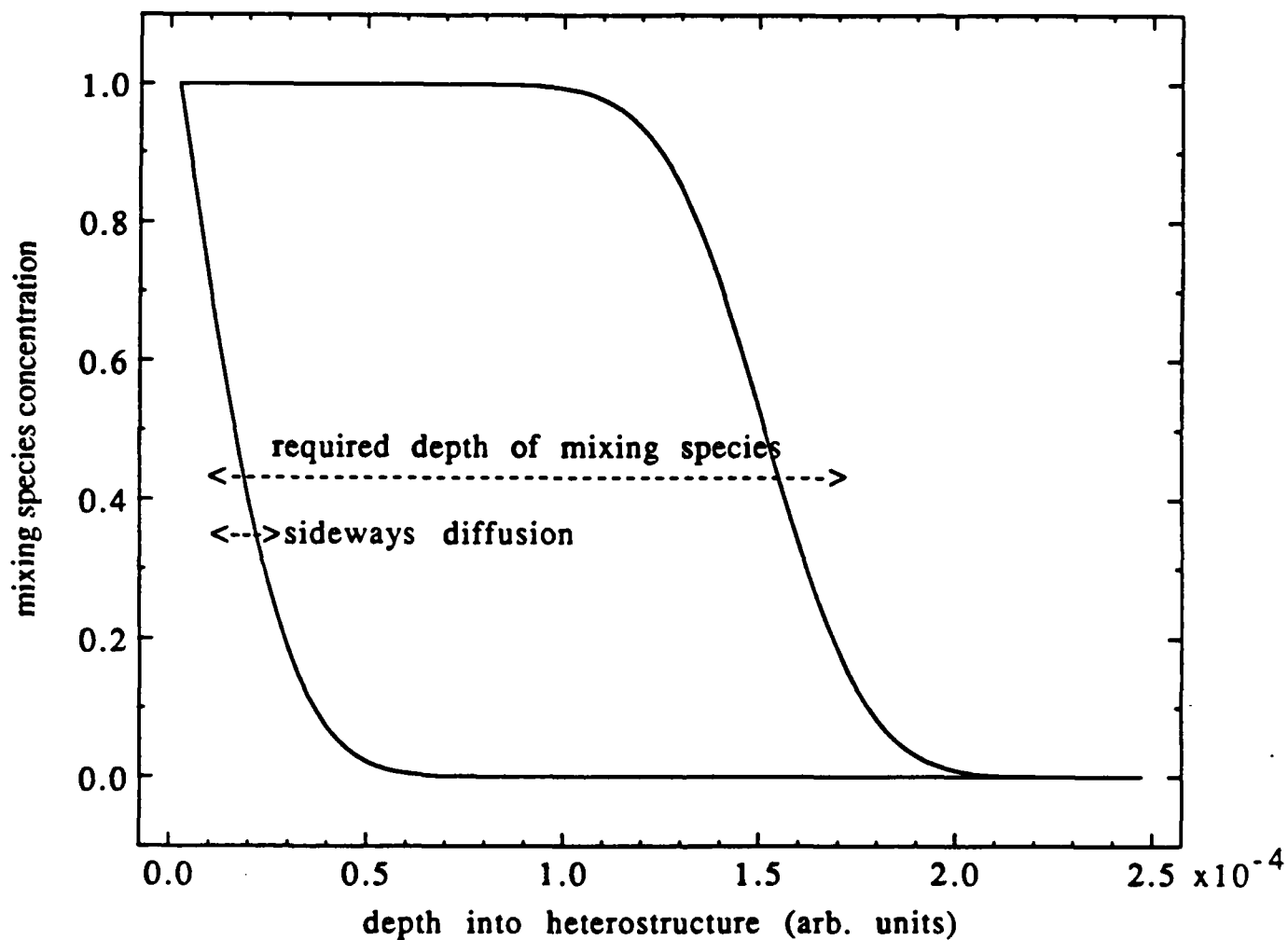
1 μ m

Si diffusion

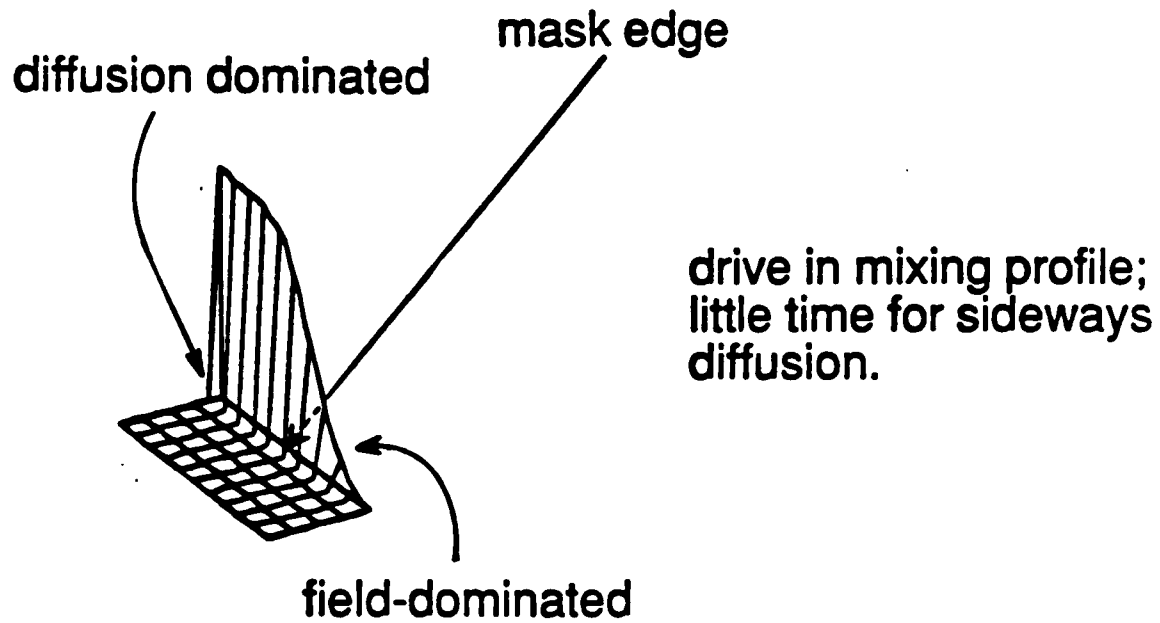


1 μ m

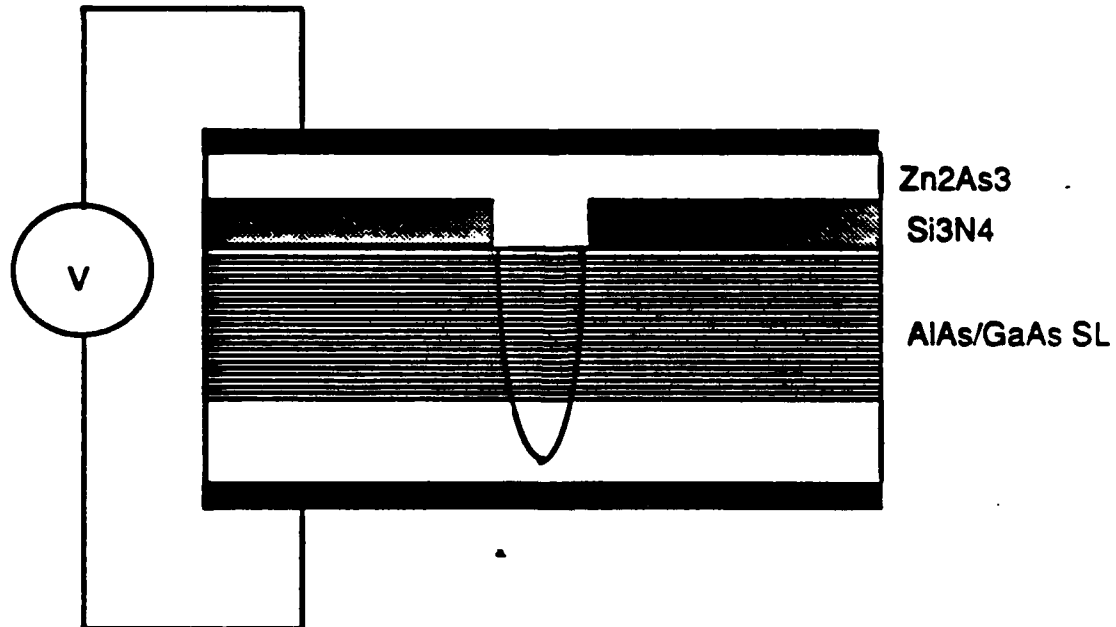
Control diffusion of mixing species by applied electric field



drive in mixing species perpendicular to heterostructure layers; little time for sideways diffusion.



Use evaporated source or gettering layer:



Use to study IID mechanism, fabricate components.

***Improve lateral resolution**

currently sideways mixing is greater than
penetration ==> improve by order of magnitude

***Design low loss structures**

currently $\alpha=3-4 \text{ cm}^{-1}$ ==> $\alpha<1 \text{ cm}^{-1}$

***Build integrated optoelectronic systems including
basic optical component types:**

sources

lasers

modulators

electroabsorption

electrorefraction

passive components

waveguides

couplers

detectors

**CECOM CENTER FOR NIGHT VISION AND ELECTRO-OPTICS
STATUS OF MBE AT C²NVEOC**

THE STATUS OF MBE AT C2NVEO

JACK DINAN

DECEMBER 7, 1988.
CECOM CENTER FOR NIGHT VISION
AND ELECTRO-OPTICS.

MBE at CCNVEO

CdTe / InSb

II - VI SUPERLATTICES

HgCdTe

***IN SITU* ARRAY PROCESSING**

CdTe / InSb

substrate / buffer for HgCdTe epitaxy

2D gas

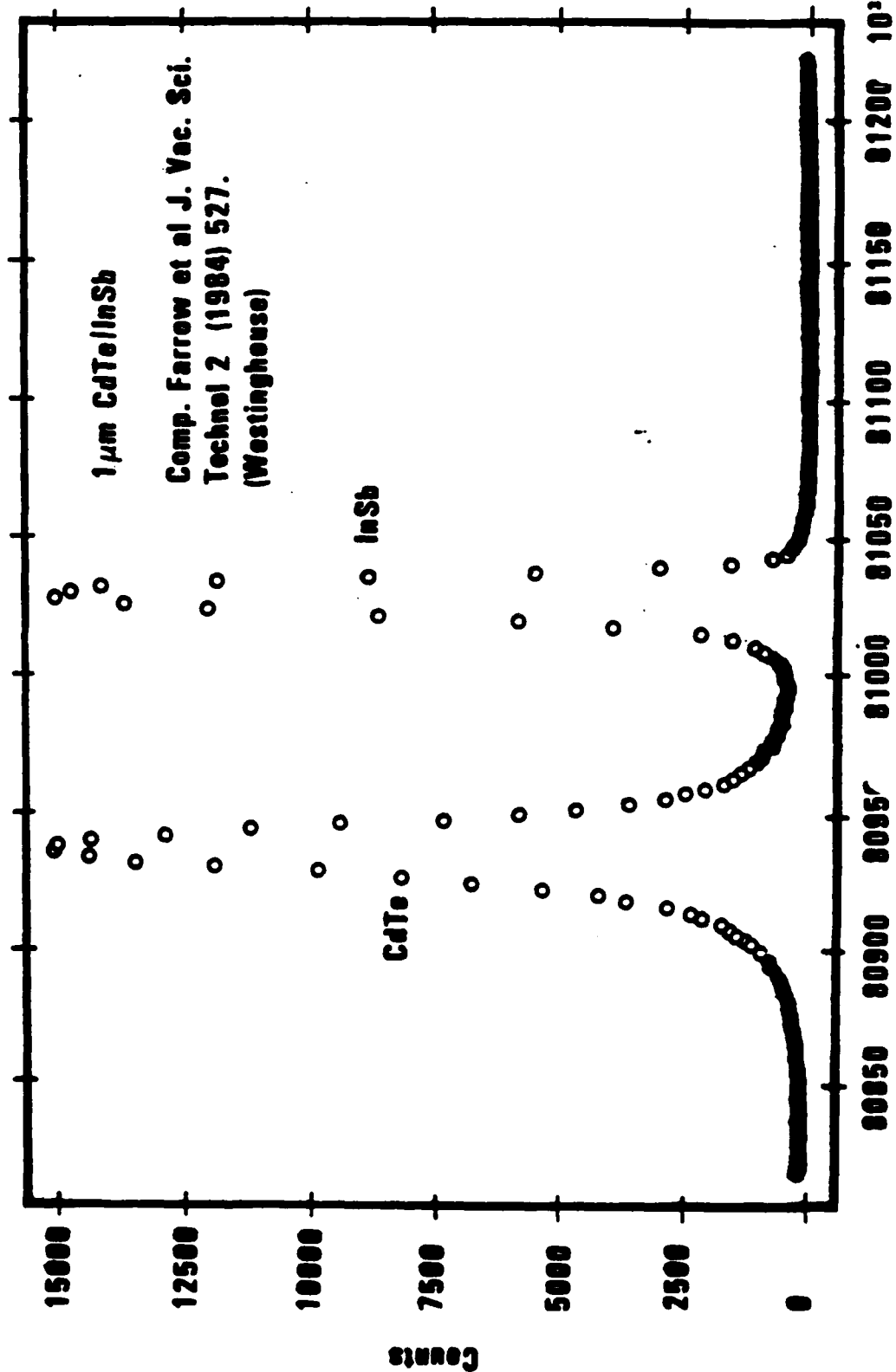
resonant tunneling structure

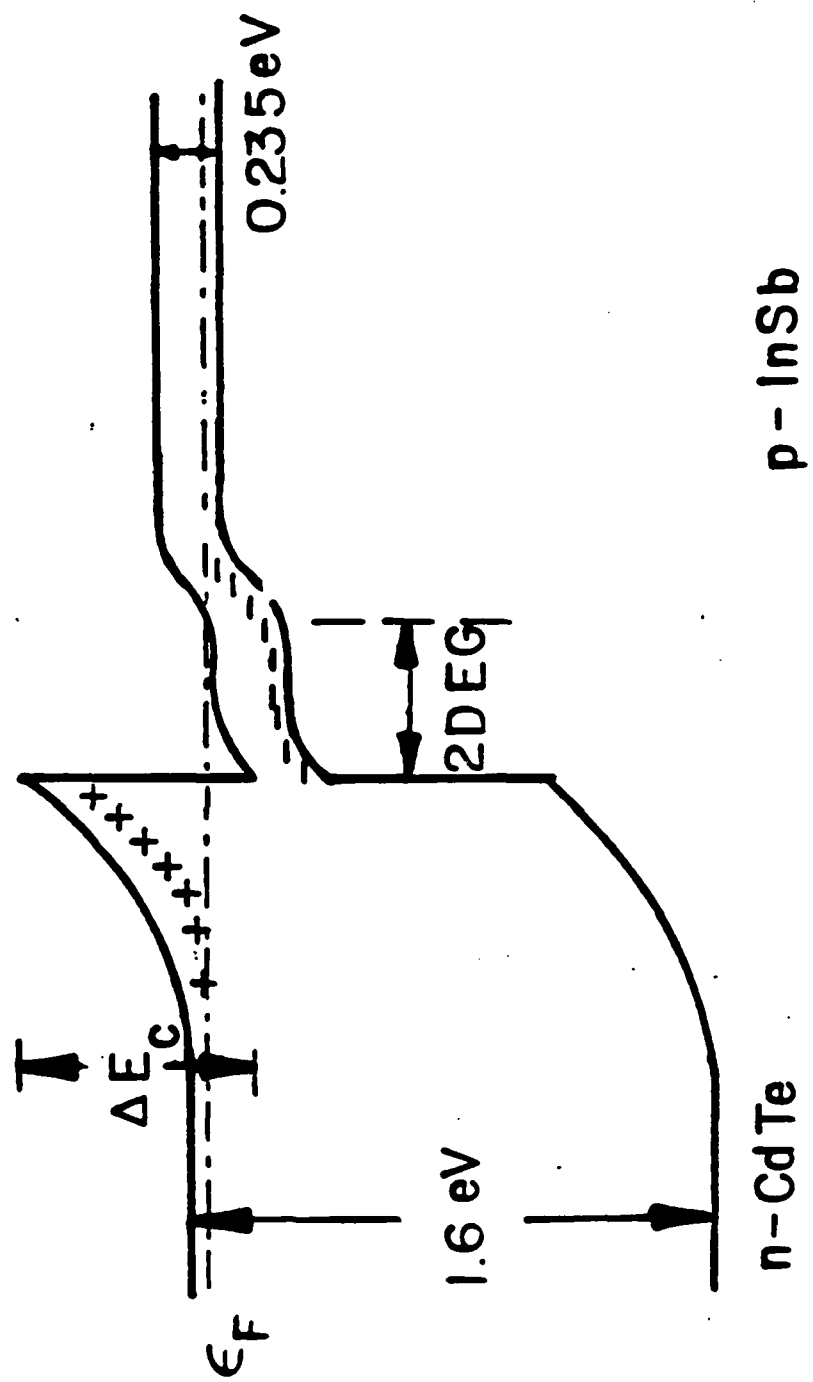
quantum well detector

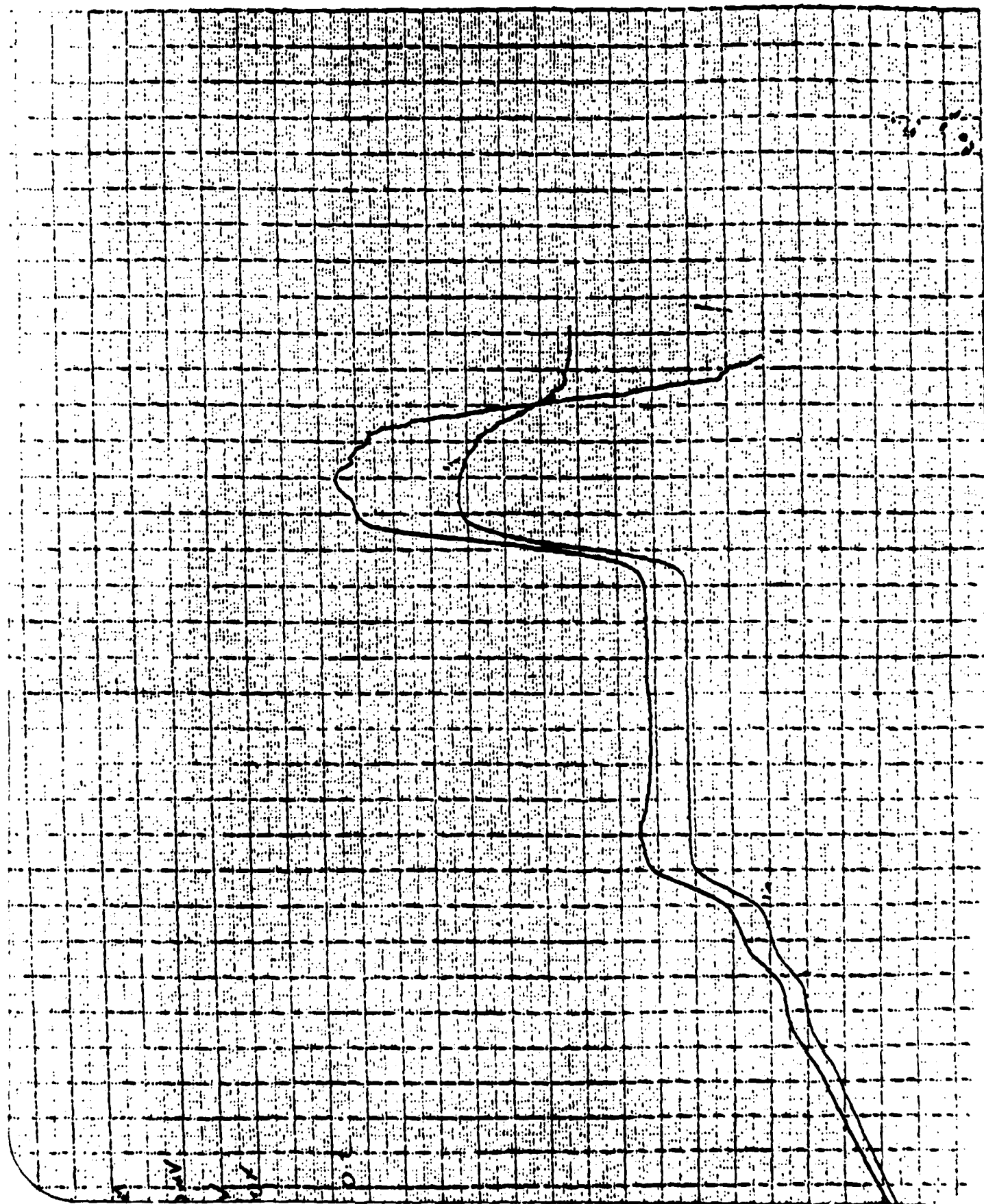
quantum well laser

POD1 7810, 'CdTe-INSB GOLDING THETA-2THETA scan

Omega/Twotheta scan (006) reflection





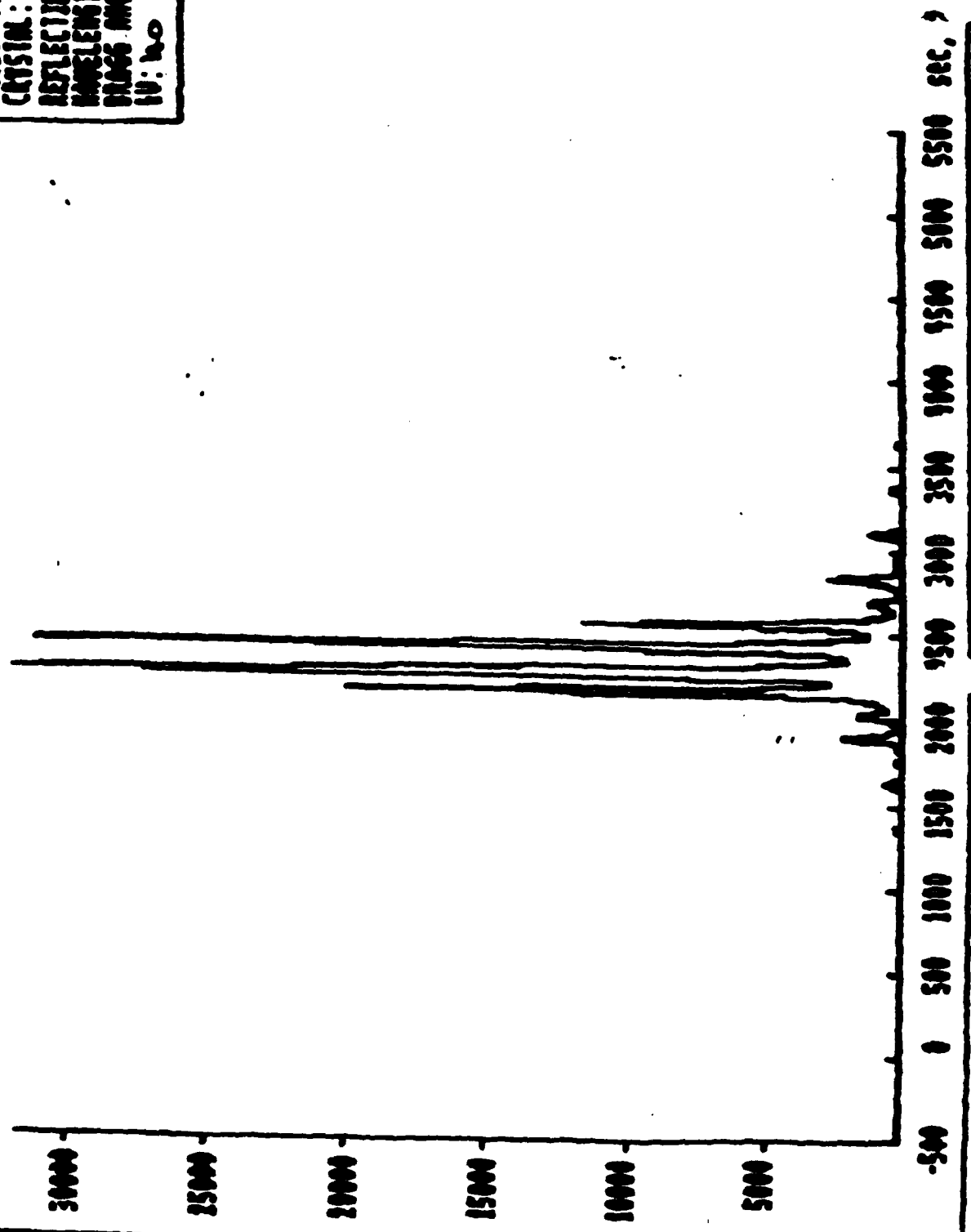




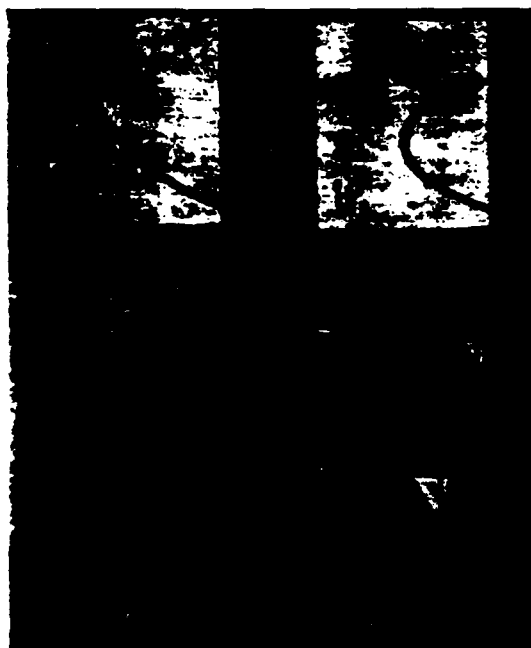
0627003.M03
21.50 4/7/1988
CRYSTAL: InSb
REFLECTION: 001
WAVELENGTH: 1.51
SCATTER ANGLE: 27.35
HV: 40 MA: 20

450°A CdTe - 450°A InSb

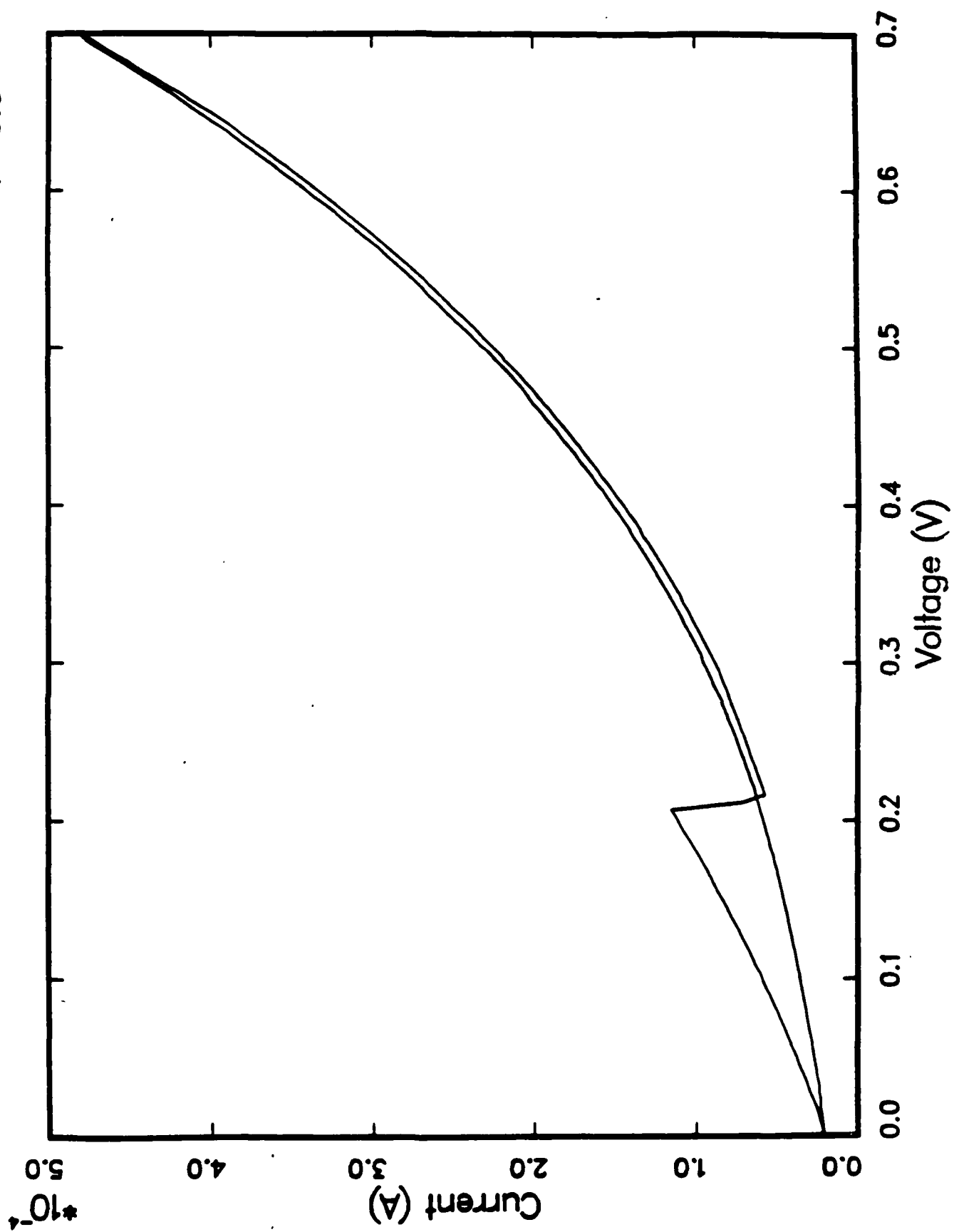
Intensity







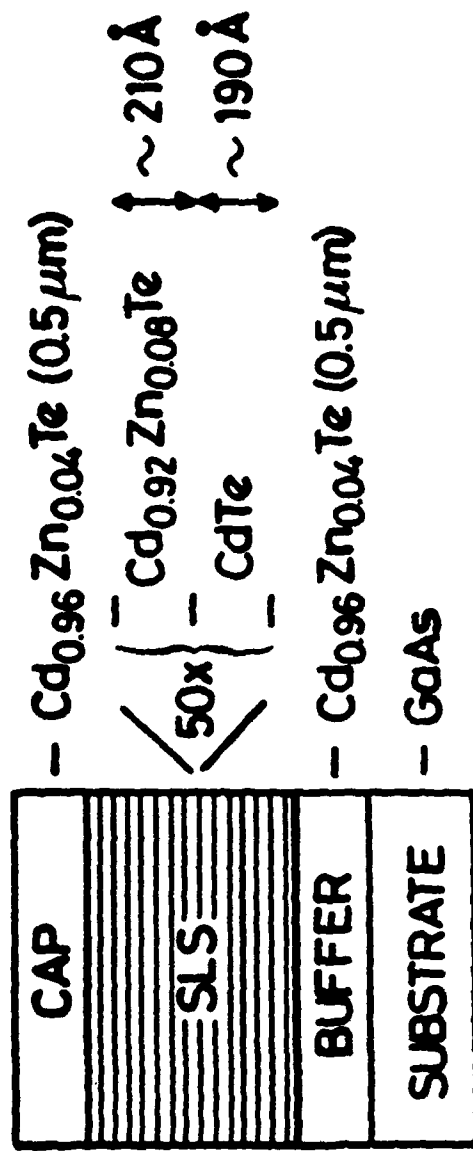
$T = 9.3$

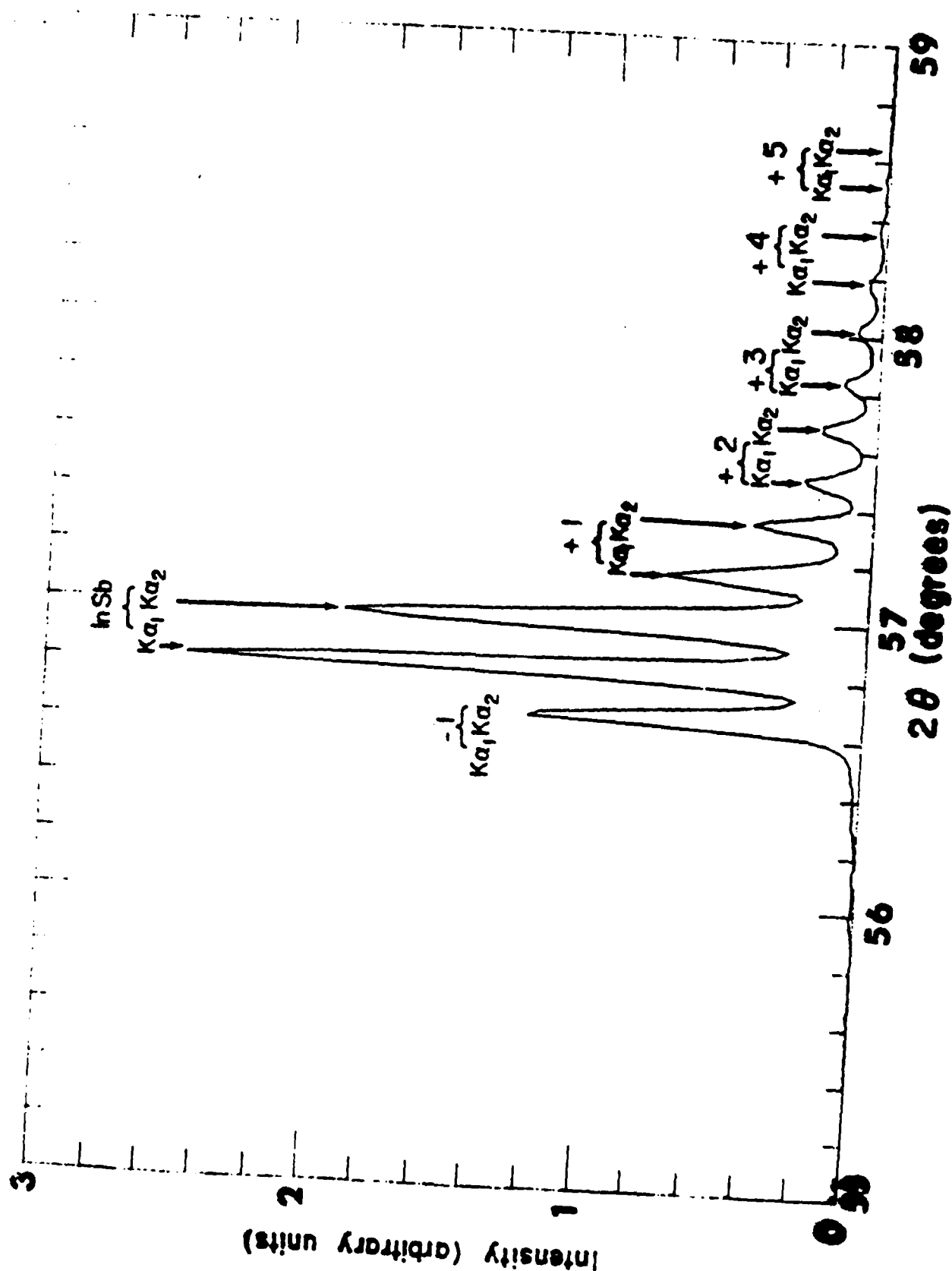


II - VI SUPERLATTICES

CdTe / CdZnTe superlattices

dislocation-filter for HgCdTe epitaxy





IN - SITU PROCESSING OF ARRAYS

growth

mesa etching

metalization

passivation

**CECOM CENTER FOR NIGHT VISION AND ELECTRO-OPTICS
ELECTRONIC STRUCTURE CALCULATIONS: IMPURITIES, SUPERLATTICES**

**ELECTRONIC STRUCTURE
CALCULATIONS:
IMPURITIES, SUPERLATTICES.**

RONALD GRAFT.

**DECEMBER 7, 1988.
CECOM CENTER FOR NIGHT VISION
AND ELECTRO-OPTICS.**

ELECTRONIC STRUCTURE CALCULATIONS

OUTLINE

Recursion Method

General Remarks.

Application to point impurities and defects.

Renormalization Method

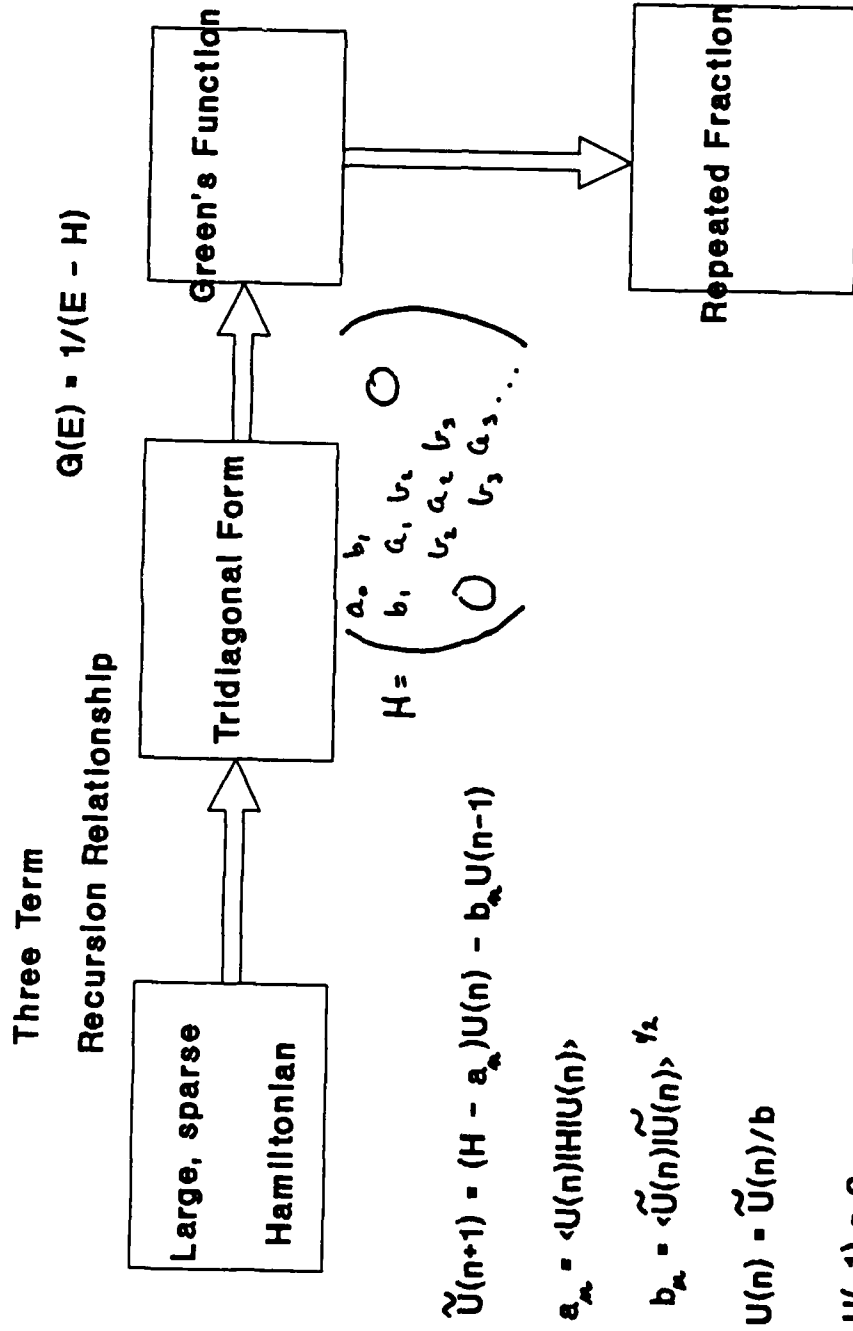
General Remarks.

Application to Superlattices.

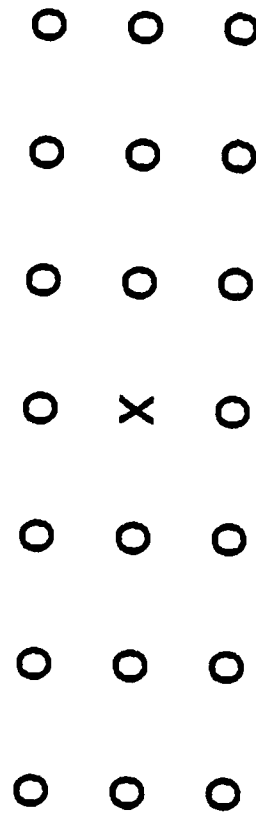
**COLLABORATORS: Prof L. Resca and D. Lohrmann
The Catholic University of America
Washington, DC**

**Prof G. Pastore-Parravicini
University of Pisa
Pisa, Italy**

RECURSION METHOD



EXAMPLE: POINT IMPURITY IN A SQUARE LATTICE



Assume an orthonormal basis of one orbital per atom and nearest neighbor interaction.

$$H = H_0 + V$$

$$H = E_0 \sum_{n,m} |\phi_{nm}\rangle \langle \phi_{nm}| + T_0 \sum_{n,m} |\phi_{nm}\rangle \langle \phi_{nm}| + V_0 |\phi_{00}\rangle \langle \phi_{00}| + Ze^2 \sum_{n,m \neq 0} |\phi_{nm}\rangle \langle \phi_{nm}| / R_{nm}$$

(n,m) labels the lattice sites; $R_{nm} = (n^2 + m^2)^{1/2}$

EXAMPLE (CONTINUED)

Take $U(0) = |\phi_{\infty}\rangle$. Eg, $|\phi_{\infty}\rangle = |s\rangle$; $E_s = \langle s | H | s \rangle = E_0$

Then, $a_0 = E_0$ and

$$\tilde{U}(1) = (H - E_0)|\phi_{\infty}\rangle$$

$$= E_0|\phi_{\infty}\rangle + T_0[|\phi_{-10}\rangle + |\phi_{10}\rangle + |\phi_{0-1}\rangle + |\phi_{01}\rangle]$$

$$+ V_0|\phi_{\infty}\rangle - E_0|\phi_{\infty}\rangle$$

$$b_1 = \langle \tilde{U}(1) | \tilde{U}(1) \rangle^{1/2} = \text{sqrt}(4T_0^2 + V_0^2)$$

$$U(1) = \tilde{U}(1) / b_1$$

$$a_1 = \langle U(1) | H | U(1) \rangle$$

ETC

RECURSION METHOD (Summary)

We have applied this method to singly and doubly ionized donors in Silicon using a 5 orbital basis set.

Main contributions:

Incorporation of coulomb tail.

Efficient computational algorithm (compared to Cambridge Library) that uses much of the crystalline symmetry. Can readily calculate 50-60 exact a,b pairs corresponding to several hundred thousand atom clusters.

Devised a method to separate impurity levels from spurious levels in the gap due to finite cluster effects.

Have verified many valley scattering effects and relative contribution of the coulomb tail to deep impurity levels. (Singly ionized doubly \sim 300-400 mev.) \sim 150mev;

Biggest Problems:

Form of the impurity potential.

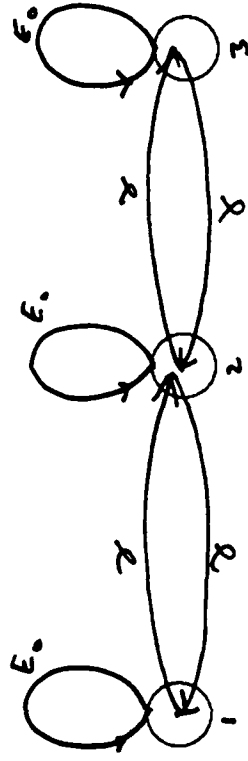
Termination of the continued fraction.

Tightbinding parameterization (good effective masses etc).

RENORMALIZATION METHOD

A SYSTEMATIC REDUCTION OF THE DEGREES OF FREEDOM OF THE HAMILTONIAN.

EXAMPLE:



$$H = \begin{pmatrix} E_0 & \gamma & 0 \\ \gamma & E_0 & \gamma \\ 0 & \gamma & E_0 \end{pmatrix}$$

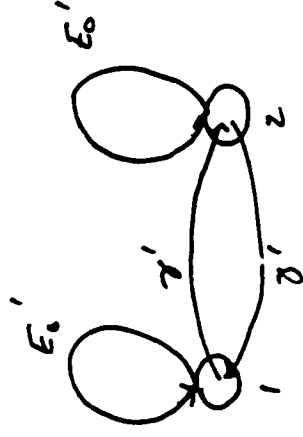
$$|H - EI| = 0$$

Has solution $E = E_0, E_0 + \sqrt{2}\gamma, E_0 - \sqrt{2}\gamma$

As an alternate, consider the following transformation:

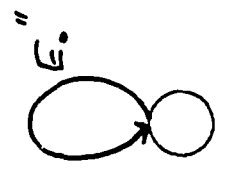
$$E'_0 = E_0 + \gamma \cdot 1.0 / (E - E_0) \cdot \gamma ; \quad \gamma' = \gamma \cdot 1.0 / (E - E_0) \cdot \gamma$$

$$H_{\text{eff}} = H_{AA} + \sum (E)$$



RENORMALIZATION METHOD (Continued)

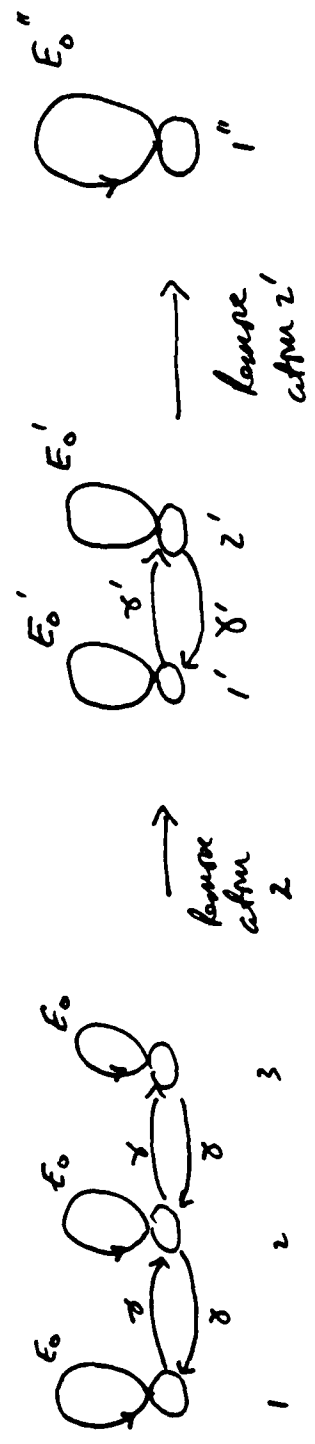
Now repeat the transformation one more time, thereby reducing the degrees of freedom to 1:



$$E_0'' = E_0' + \gamma^2 (E - E_0') = E$$

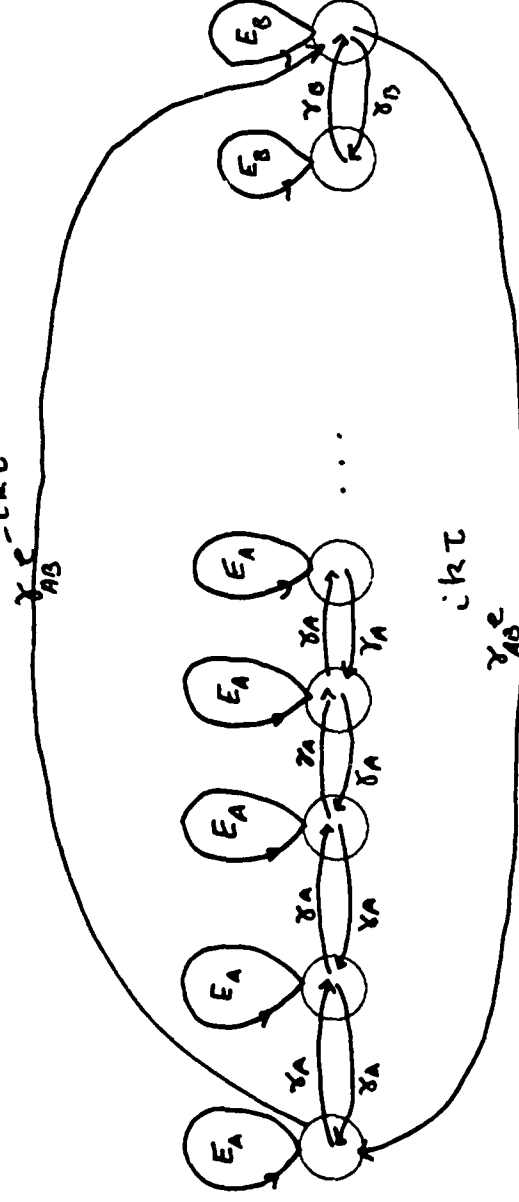
A little manipulation gives

$$E = E_0 : E_0 + \sqrt{2\gamma} : E_0 - \sqrt{2\gamma}$$



RENORMALIZATION METHOD (Continued)

This can be readily generalized to a one dimensional superlattice:



The preceding transformation can be applied simultaneously

to, eg, all even numbered sites in slab A, then slab B.

By continuing this process, the renormalized Hamiltonian,

H_R , can be reduced to a single degree of freedom as before.

The number of transformations is $O(2 \log_2 N)$.

For $N = N_A = N_B = 1000$,

≈ 20 steps are required

RENORMALIZATION METHOD (Continued)

The method can be further generalized to a real superlattice by the following observations:

- (1) If translational symmetry in the plane perpendicular to the superlattice direction is included, the 3 dimensional superlattice becomes a linear chain,
- (2) The self energy and hopping parameters become matrices, In the case of CdTe/HgTe, 10×10 . Since the material is a compound, alternate atomic planes are not identical so that two sets of matrices are required.

RENORMALIZATION METHOD

(Summary)

The renormalization method is particularly suited to large repeat periods where conventional methods become intractable because of large matrix size.

It is much simpler to implement and run than the complex k method.

It is more general than envelope function methods requiring a similar band structure of the constituent materials and somewhat questionable boundary conditions at the interface.

We have run Silicon (MOS) and obtained excellent results.

Have an implementation for CdTe/HgTe (strain-free) that also gives us the wave function. We will examine the stability of interface localization with valence band offset and composition.

BIGGEST PROBLEM: A good bandstructure parameterization. We are looking at a variation using a $k \cdot p$ parameterization which is translated into tight binding parameters.

**CECOM CENTER FOR NIGHT VISION AND ELECTRO-OPTICS
PHOTOREFLECTANCE STUDIES OF GROUP II-VI SYSTEMS**

PHOTOREFLECTANCE STUDIES OF GROUP II-VI SYSTEMS.

PAUL AMIRTHARAJ.

**DECEMBER 7, 1988.
CECOM CENTER FOR NIGHT VISION
AND ELECTRO-OPTICS.**

PHOTOREFLECTANCE CHARACTERIZATION

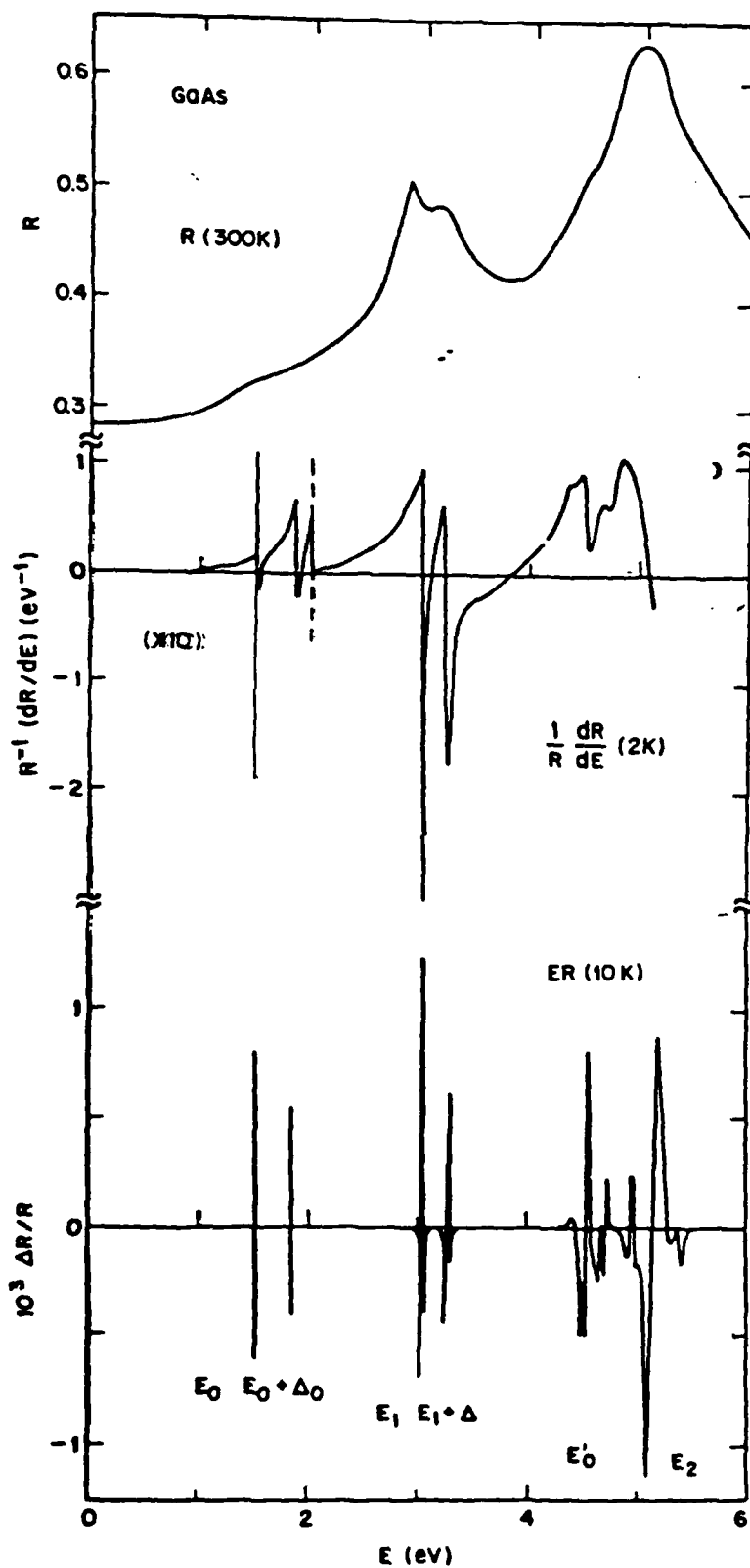
OF

II-VI SEMICONDUCTORS

PAUL AMIRTHANARAJ

NIGHT VISION LAB

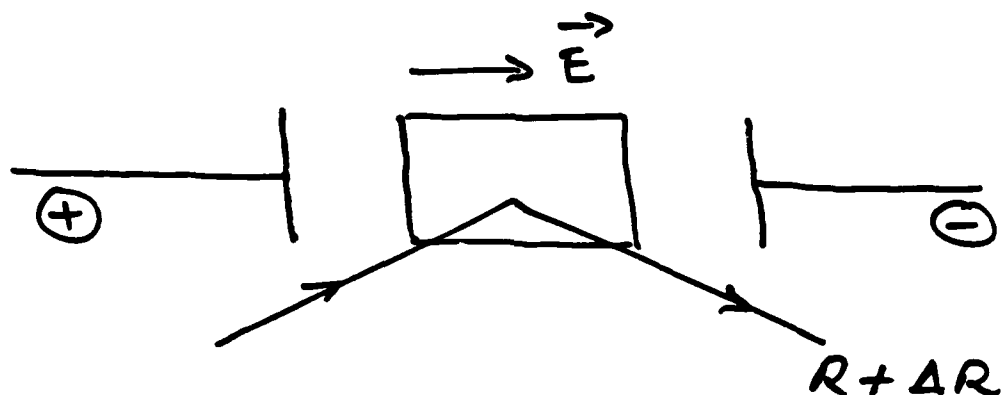
FORT BELVOIR, VA



ASPRIGS,
HANDBOOK OF SEMICONDUCTORS, VOL. 2

PHOTOREFLECTANCE!

CONTACTLESS FORM OF ELECTRIC
FIELD MODULATED REFLECTIVITY
(ELECTROREFLECTANCE)



$$|\vec{E}| \sim 10^3 \text{ to } 10^5 \text{ V/cm}$$

$$\left| \frac{\Delta R}{R} \right| \sim 10^{-3} \text{ to } 10^{-7}$$

LOCK-IN AMPLIFICATION.

ELECTROREFLECTANCE

DRY : MIS, p-n jn., SCHOTTKY
BARRIER, ETC.

WET : ELECTROLYTE ELECTROREFLECTANCE
(USUALLY LIMITED TO
> 150°K)

PHOTOREFLECTANCE

USE PHOTOVOLTAGE AT JUNCTION
TO MODULATE ELECTRICAL FIELD

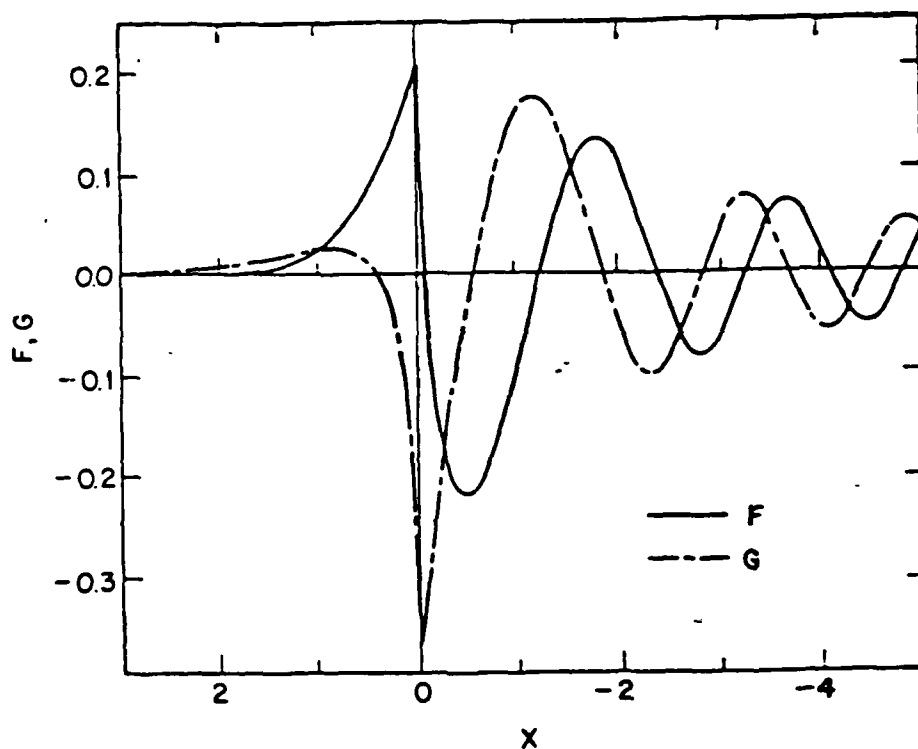


Fig. 12. The Franz-Keldysh lineshapes F and G , plotted with x -axis reversed to simulate electric field modulation of the imaginary and real parts of ϵ of an M_0 critical point plotted against increasing energy.

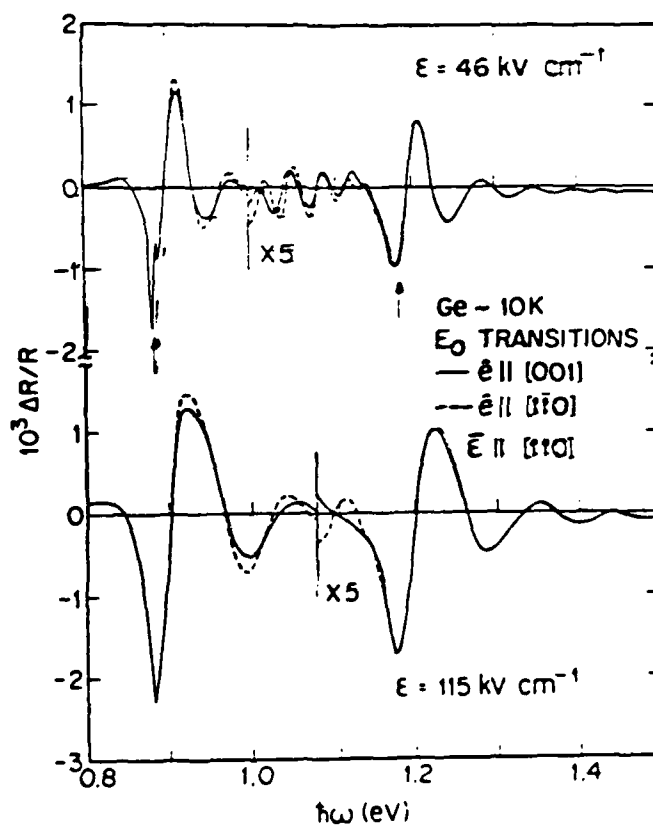
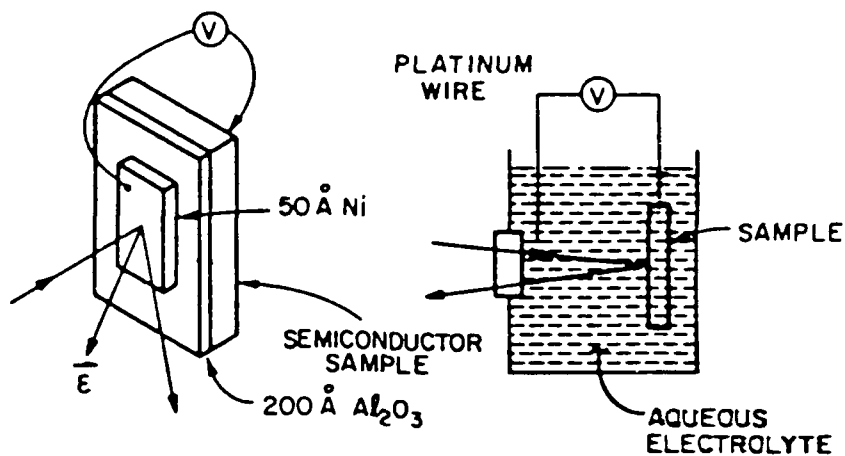


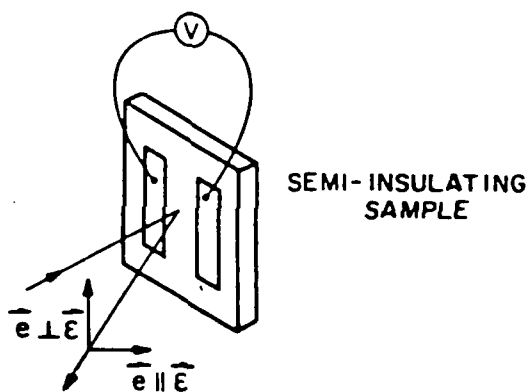
Fig. 13. Electroreflectance lineshapes for Ge for two fields taken under conditions where the Franz-Keldysh theory is applicable (Aspnes 1975).

ASPNES, HANDBOOK OF SEMICONDUCTORS, VOL. 2

ELECTRIC FIELD MODULATION

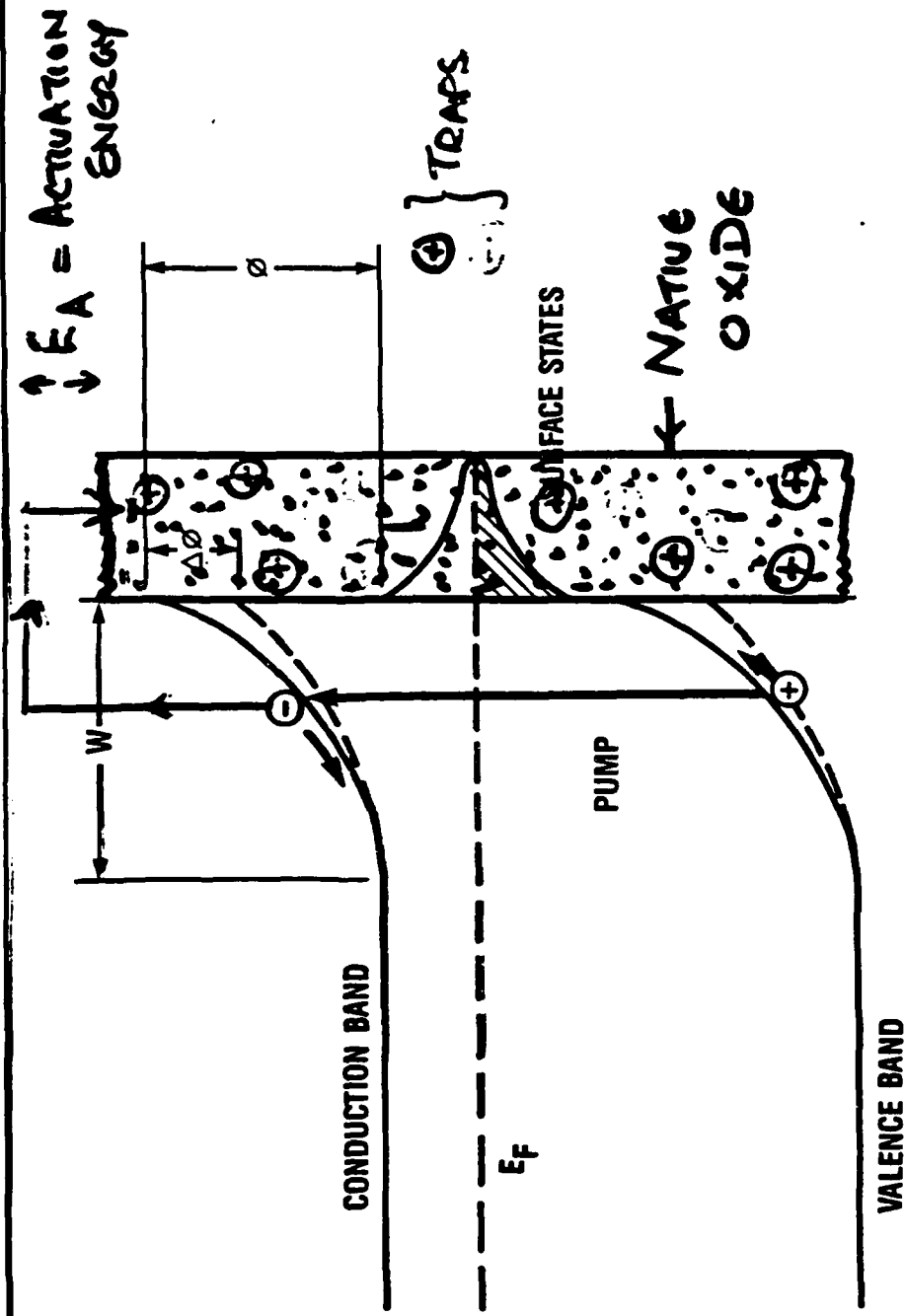


(a) LONGITUDINAL

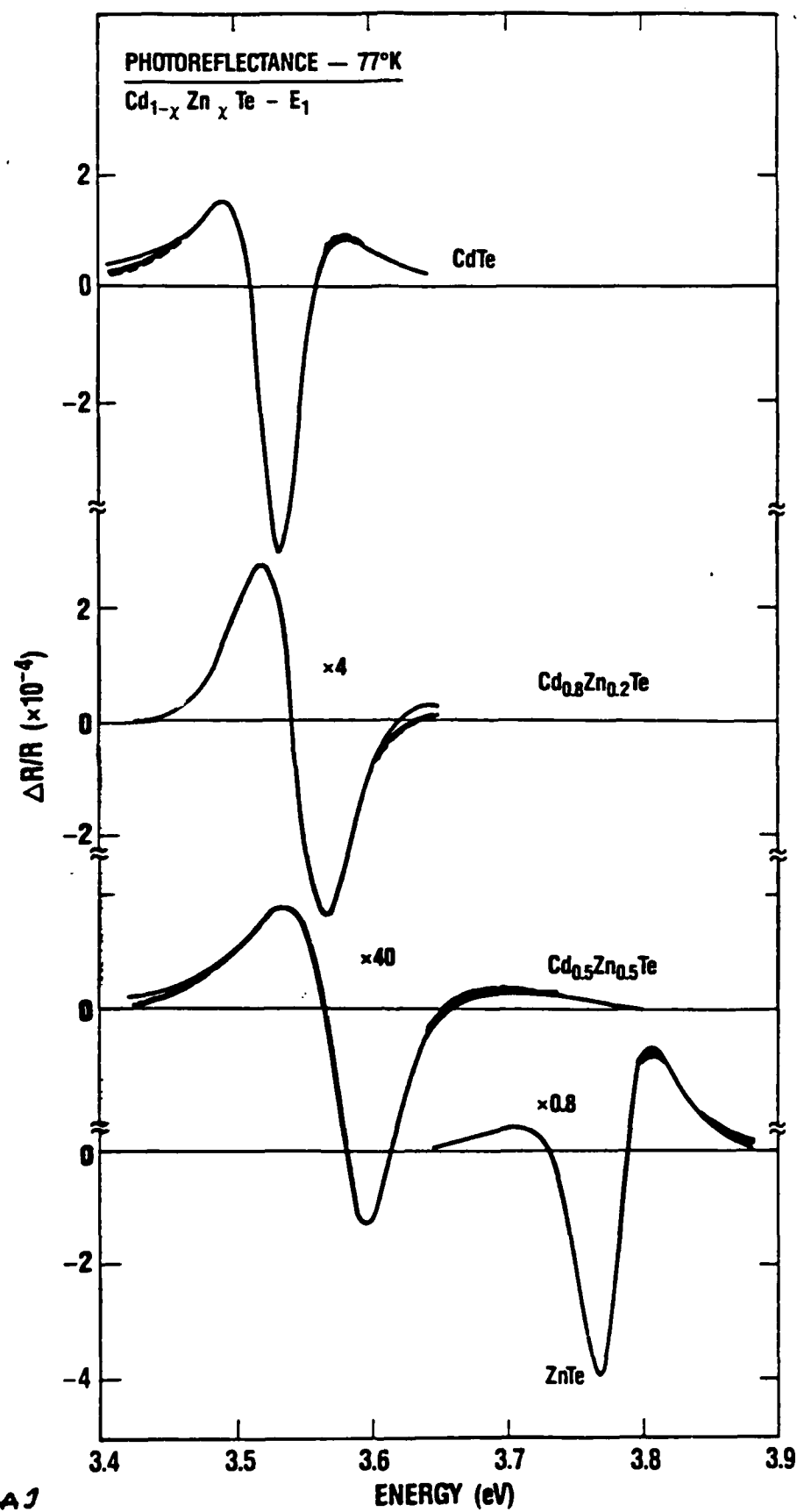


(b) TRANSVERSE

ASPNER, HANDBOOK OF SEMICONDUCTORS, VOL II



NOTE: $\Delta\phi$ CAN BE dc (steady pump) or ac (MODULATED PUMP) CHOSEN TO PUMP INTENSITY (MODULATED PART) CHOSEN TO BE LARGE ENOUGH TO DRIVE BANDS TO FLAT BAND POSITION.



AMIRTHARAJ
 ET AL, JYST A3, 266 (1985)

FIGURE 3

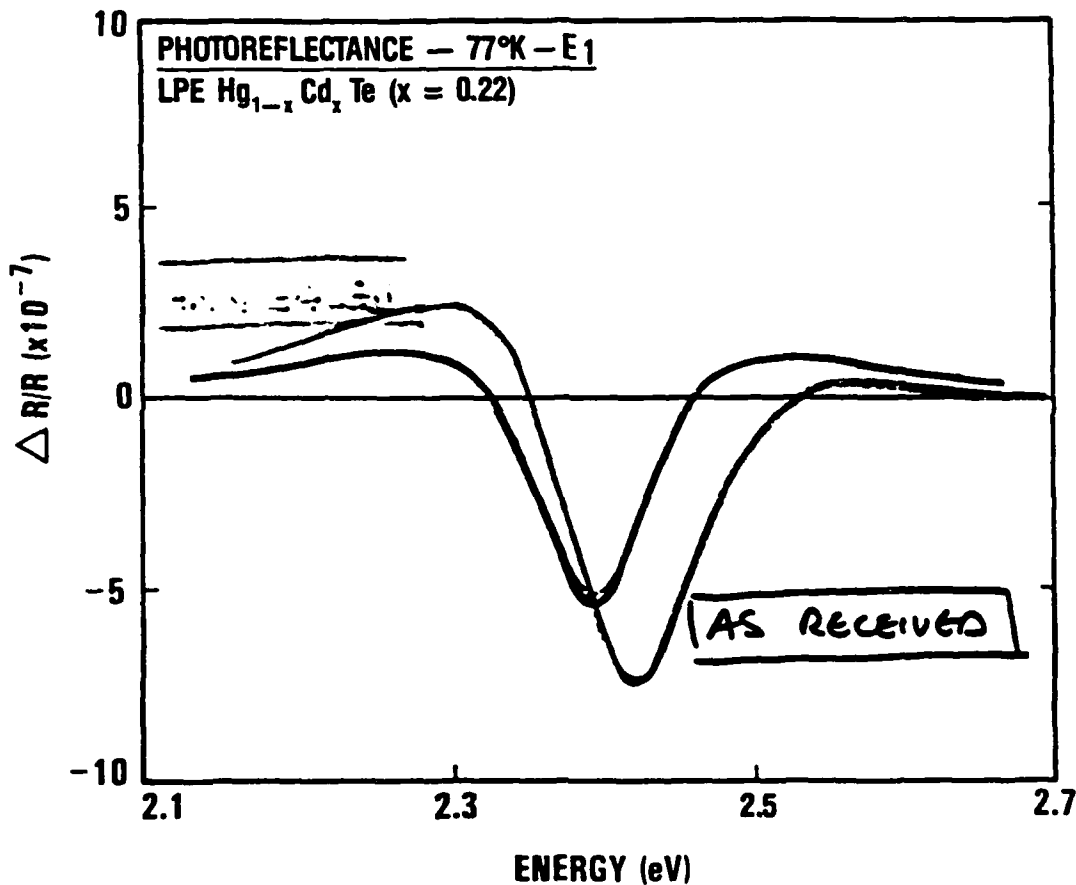
AMIRTHARAJ ETAL, JUST AS,
3184 (1987)

Fit results:

$$E_1 = 2.402 \text{ eV} \Rightarrow x = 0.23$$

$$I_1 = 87 \text{ meV}$$

$$\Delta\sigma^2/(kT)^3 = 0.13 \text{ eV}^{-1} \quad \Delta E_1/(kT)^3 = 0.024 \text{ eV}^{-2}$$

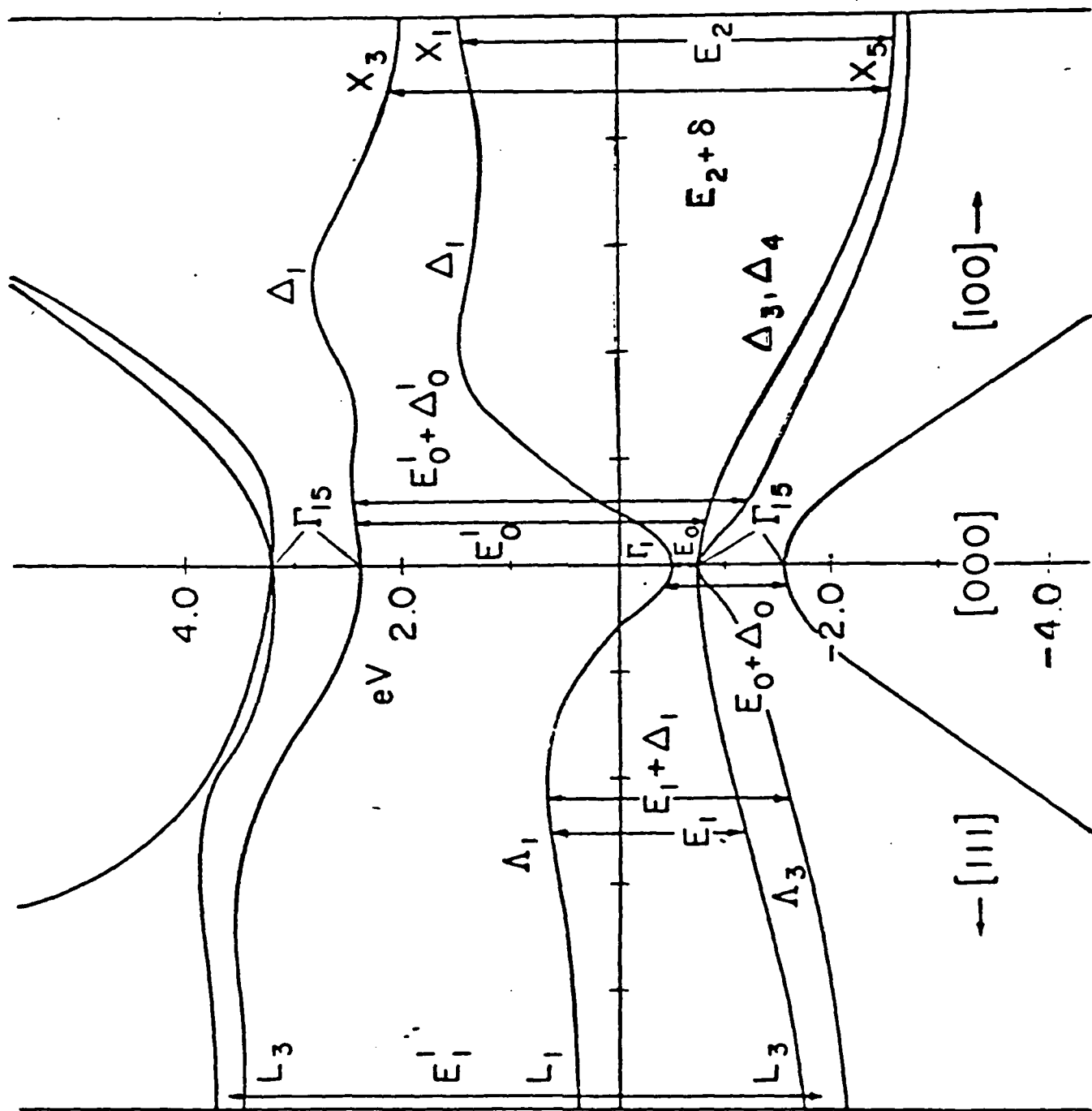


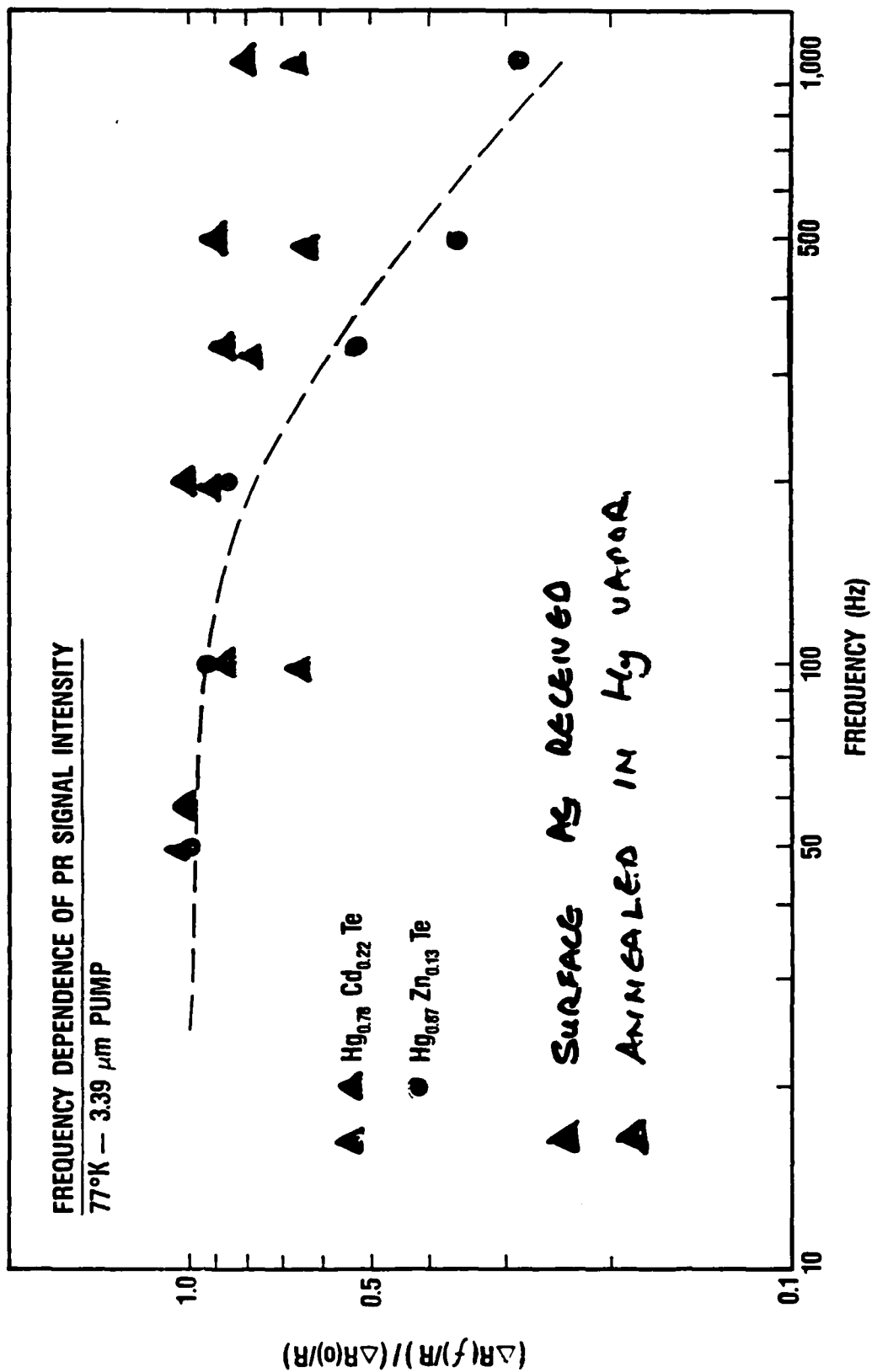
FIT RESULTS.

$$E_1 = 2.427 \text{ eV} \Rightarrow x = 0.251$$

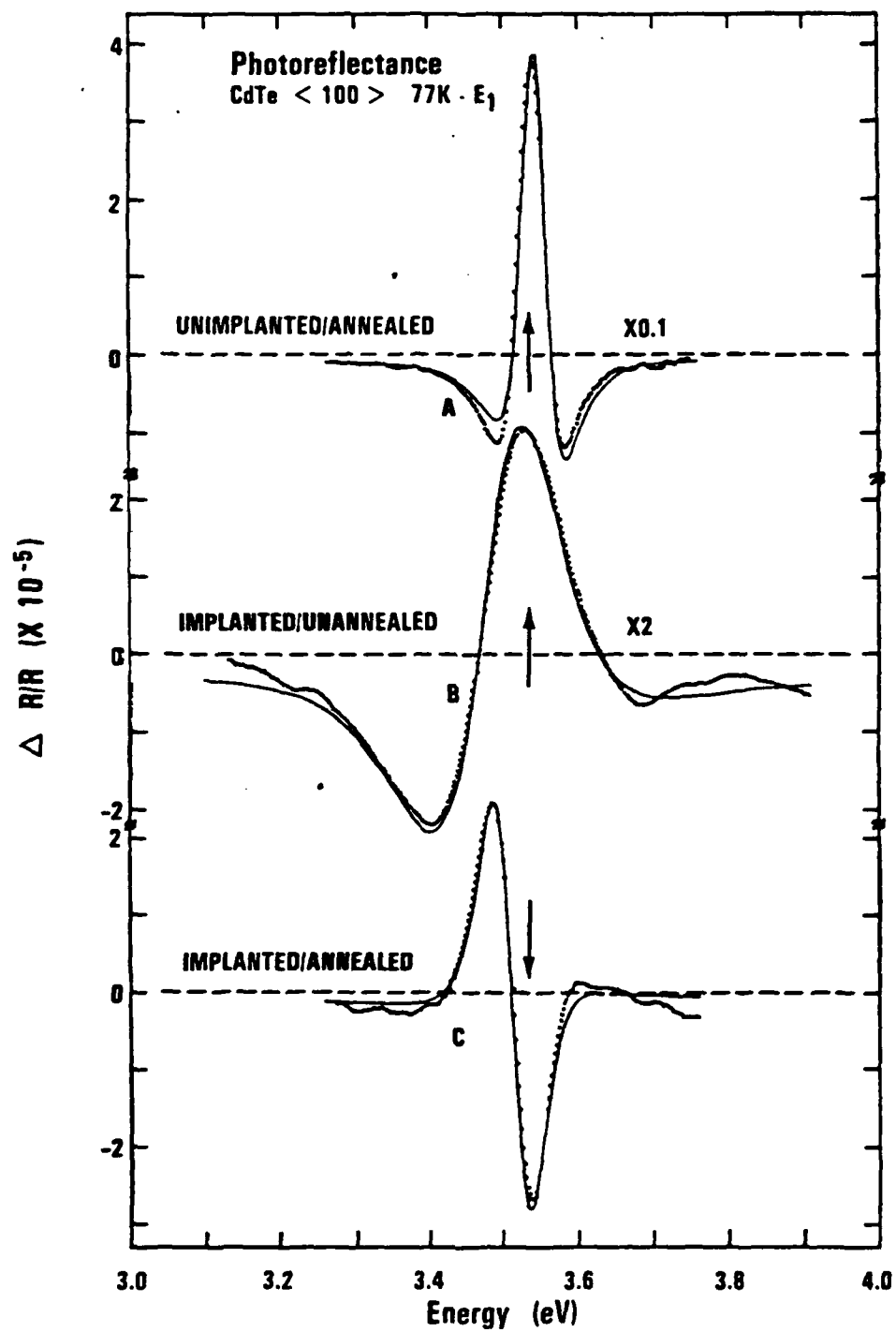
$$I_1 = 96 \text{ meV}$$

$$\Delta\sigma^2/(kT)^3 = 1.28 \text{ eV}^{-1} \quad \Delta E_1/(kT)^3 = 0.054 \text{ eV}^{-2}$$

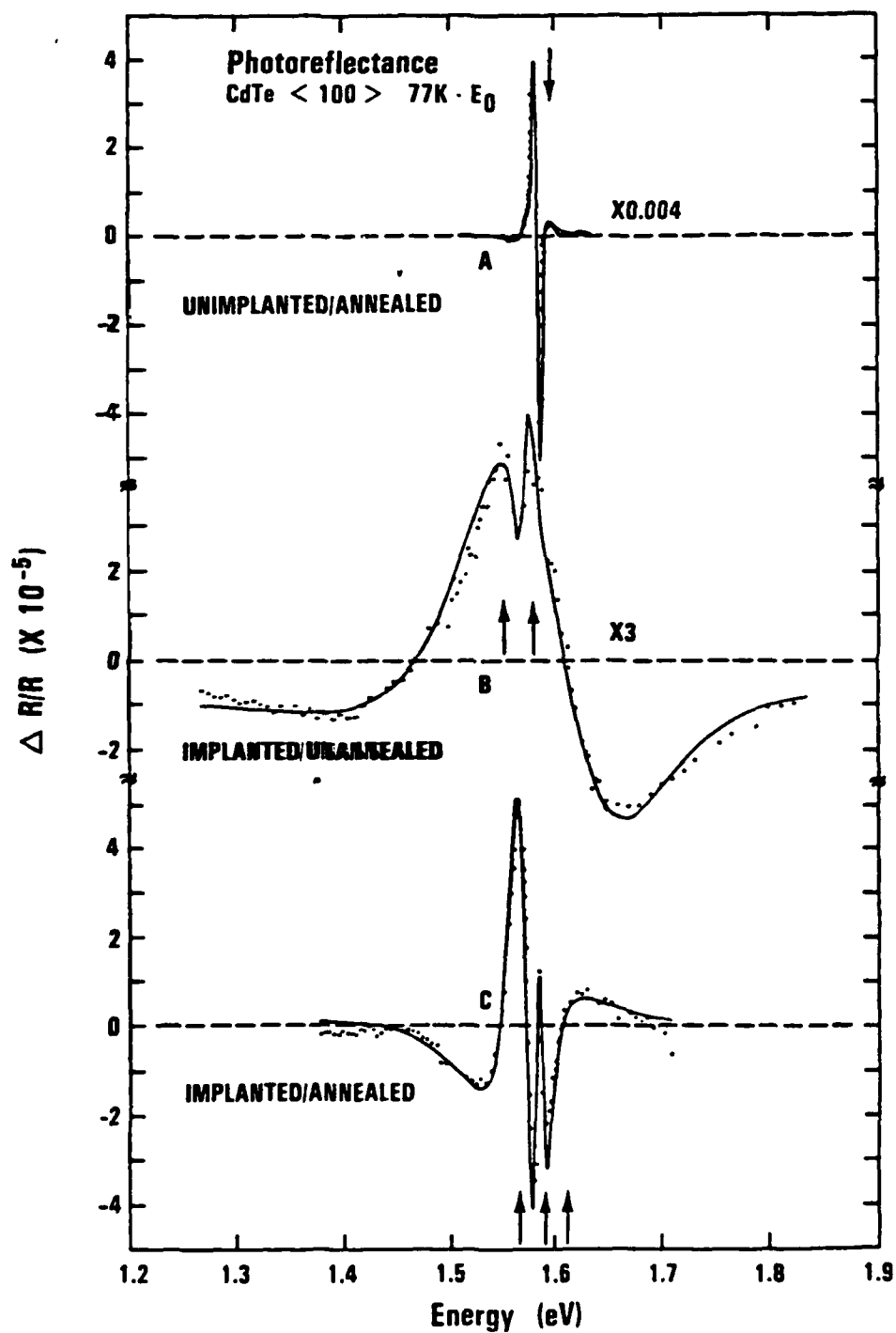




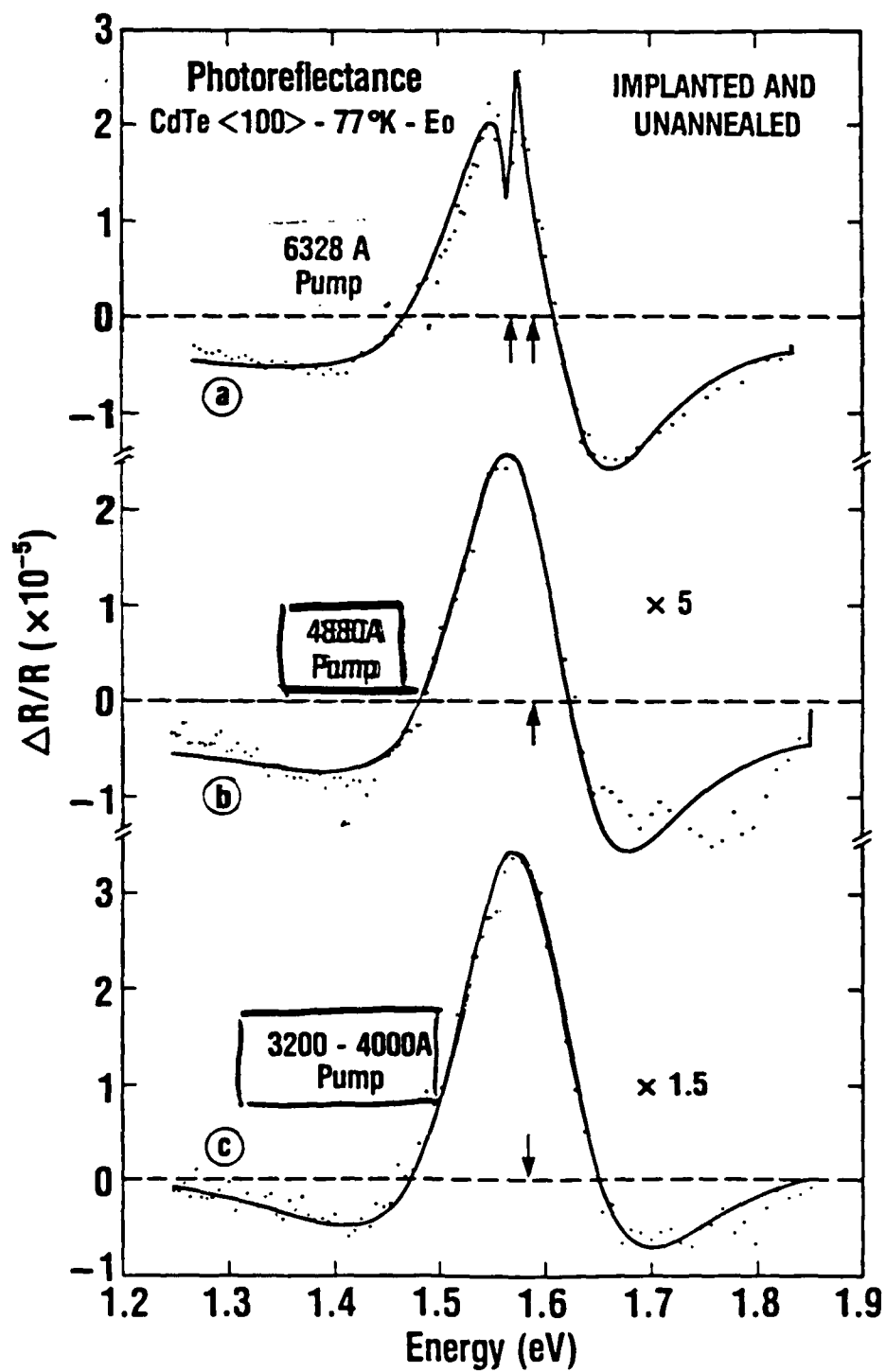
AMIRNARAJ ET AL, JUST AS, 3104 (1967)

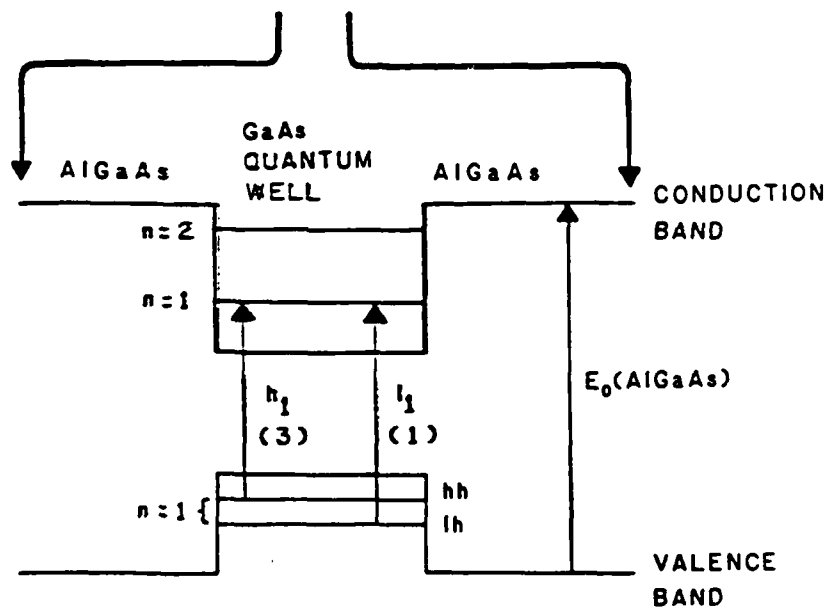
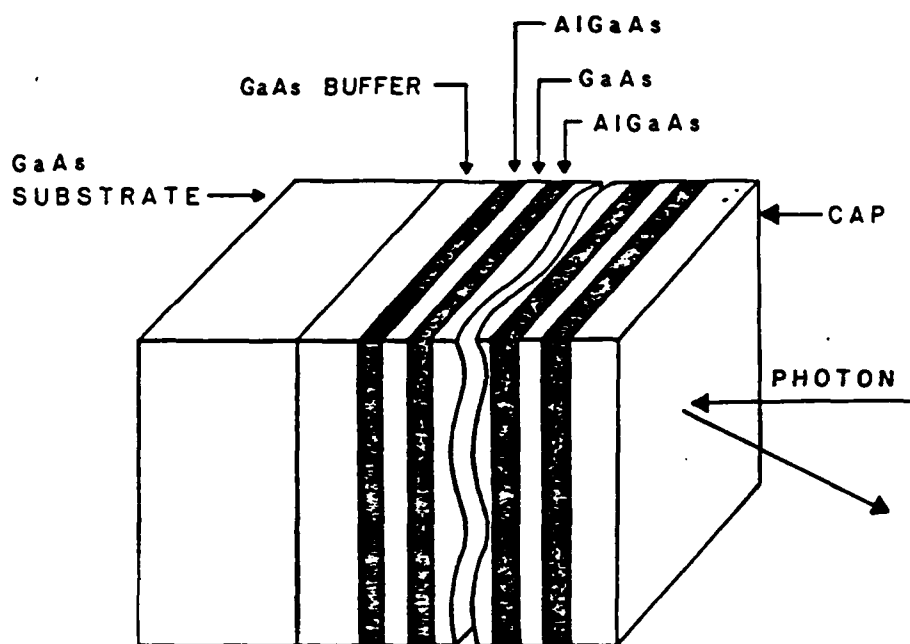


AMIR THARAJ ET AL JUST, MAY/JUNE 88,
SPIE VOL 846

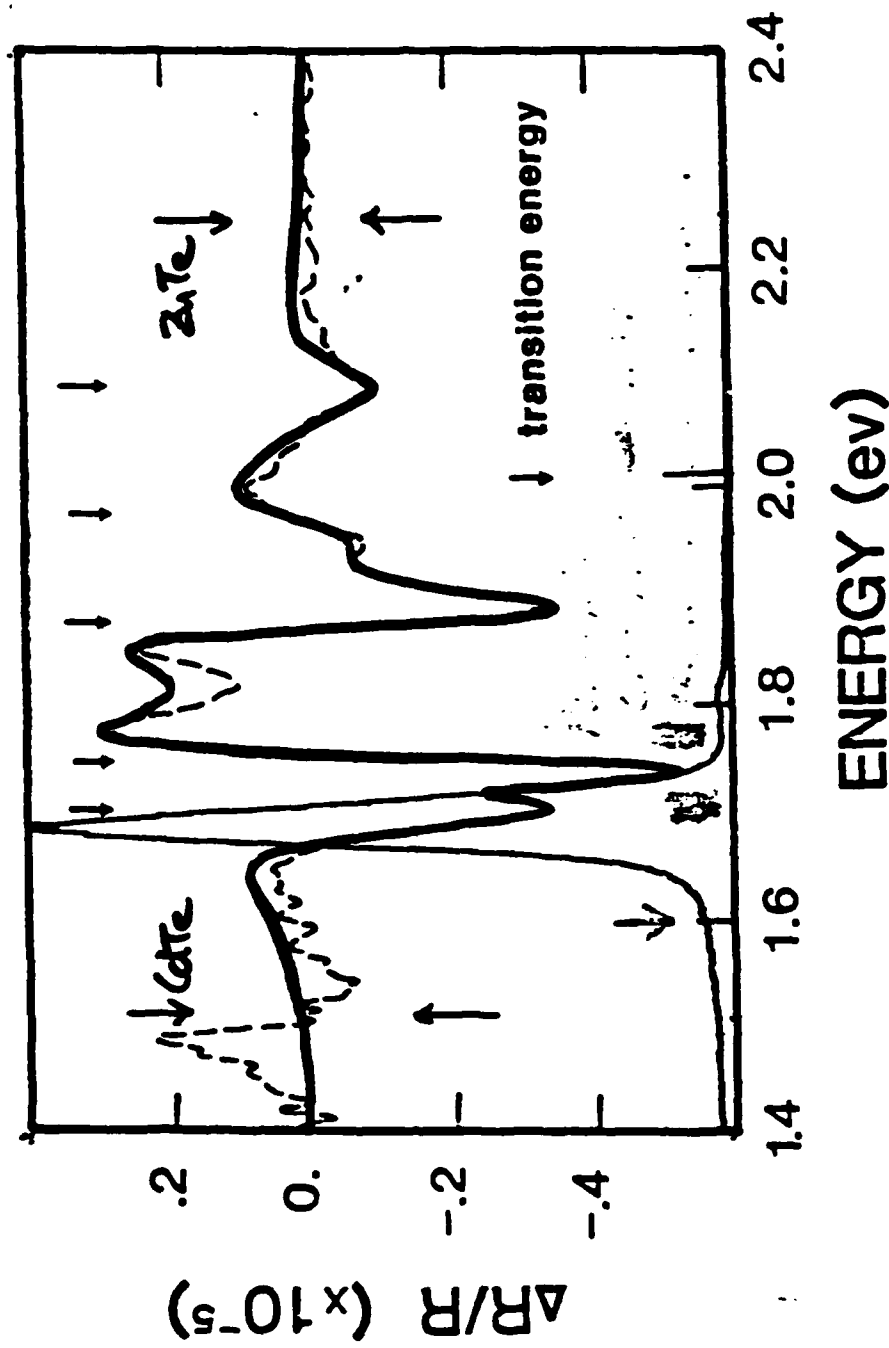


AMIRTHARAS ET AL, JUST MAY/JUNE 88,
SPIE VOL 946

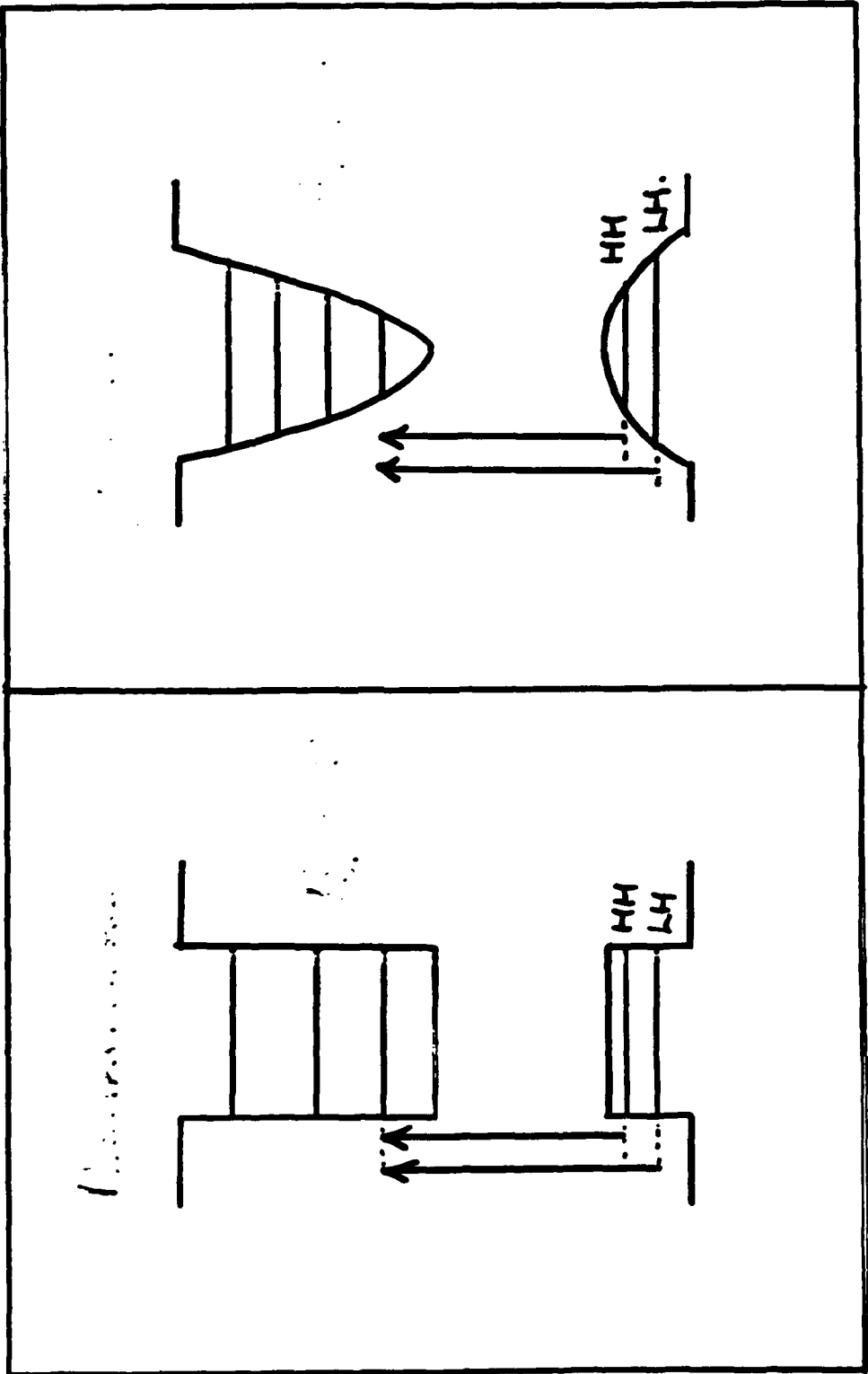




PHOTOREFLECTANCE - 300K - 4416 PUMP 40 PERIODS
 CuTe/ZnTe 50/50



KISKER ET AL, J. Crystal Growth 86, 210 (1988)



CdTe/ZnTe 50/50 SL

Transition	Square	Parabolic*	SL-1	SL-2
E_{1h}	1.61	1.67	1.7	1.65
E_{2h}	1.88	1.82	1.88	1.83
E_{3h}		1.98	1.97	1.92
E_{4h}		2.13	2.09	2.08
E_{1l}	1.65	1.71	1.74	1.74

* 75°A WELL WIDTH.

**CECOM CENTER FOR NIGHT VISION AND ELECTRO-OPTICS
PROPERTIES OF CdTe/InSb INTERLAYERS**

PROPERTIES OF CdTe/InSb INTERLAYERS.

MICHAEL MARTINKA.

DECEMBER 7, 1988.
CECOM CENTER FOR NIGHT VISION
AND ELECTRO-OPTICS.

Molecular Beam Epitaxial Growth and Characterization of In_2Te_3

T.D. Golding†, P.R. Boyd, M. Martinka, P.M. Amirtharaj and J.H. Dinan
U.S. Army Center for Night Vision and Electro-Optics
AMSEL-RD-NV-IT, Fort Belvoir, Virginia 22060-5677, U.S.A.

S.B. Qadri
U.S. Naval Research Laboratories, Washington D.C. 20375, U.S.A.

D.R.T. Zahn
Department of Physics, University College, P.O. Box 78, Cardiff CF1 1XL, U.K.

C.R. Whitehouse
Royal Signals and Radar Establishment, Malvern, Worcestershire, WR14 3PS U.K.

†Permanent address: Cavendish Laboratory, University of Cambridge, Cambridge, U.K.

Abstract

We report studies of the molecular beam epitaxial growth of In_2Te_3 . The unique structure of In_2Te_3 , with 1/3 of the In sublattice sites vacant, is of fundamental interest for molecular beam epitaxial growth dynamics. We show that thin film (500Å-7000Å) single crystal In_2Te_3 can be grown successfully on $\text{InSb}(100)$ homoepitaxial layers at substrate temperatures of 300 - 350°C and Te/In flux ratios of 3/2 - 5/2. Epitaxy has been monitored by reflection high energy electron diffraction and the stoichiometry of the grown layers assessed by Auger spectroscopy and energy dispersive X-ray analysis. Raman studies of the layers are presented and compared with a bulk In_2Te_3 standard. Crystal structure has been determined by X-ray diffraction using Weissenburg and oscillation photographs, confirming that the layers have a f.c.c. crystal structure with a lattice parameter of 18.50Å, in excellent agreement with the bulk value. Bandgap measurements have been performed on the layers by photoreflectance. We report a value for the α - In_2Te_3 bandgap of 1.19 eV and 1.31 eV at 300K and 77K respectively. Molecular beam epitaxial growth of InSb and CdTe on epitaxial In_2Te_3 films for fabrication of $\text{InSb}/\text{In}_2\text{Te}_3/\text{InSb}$ and $\text{InSb}/\text{In}_2\text{Te}_3/\text{CdTe}$ multilayers has been studied. Auger depth profiling of the resulting layers

shows severe intermixing into the In_2Te_3 . These results are supported by thermodynamic considerations of the $\text{InSb-In}_2\text{Te}_3$ interface.

Introduction

In the course of a study into the molecular beam epitaxial growth (MBE) of InSb/CdTe multilayers and superlattices, it has been found^{1,2} that there is a strong chemical reaction at the InSb/CdTe interface during growth at substrate temperatures compatible with the growth of high structural and electronic quality of both InSb and CdTe (275-300 °C).

Recent studies^{3,4,5,6} by soft X-ray photoemission and Raman spectroscopy of the heterojunction formed from the MBE growth of CdTe on InSb under stoichiometric flux conditions and growth temperatures of 200-300°C reveal that the InSb and CdTe react to form a complex interface identified to consist predominantly of In_2Te_3 and elemental Sb .

In_2Te_3 is a defect zinc blende type semiconductor with a bandgap of approximately 1 eV, lying between that of InSb ($E_g=0.18\text{eV}$) and CdTe ($E_g=1.44\text{eV}$). Thermodynamic considerations of the stability of In_2Te_3 with respect to InSb and CdTe ^{7,8} led us to examine the possibility of MBE growth of In_2Te_3 for use as a barrier between the CdTe and InSb to facilitate fabrication of InSb/CdTe multilayers, and the interesting possibility of exploiting the large difference in badgaps between InSb and In_2Te_3 to grow $\text{InSb/In}_2\text{Te}_3$ multilayers for novel quantum well structures.

In this paper we present results of the study of the MBE growth of In_2Te_3 and characterization of the grown layers. We show that thin film single crystal In_2Te_3 can be grown on InSb (100) homoepitaxial layers. Reflection high-energy electron diffraction (RHEED) was used to monitor growth of the In_2Te_3 , and stoichiometry of the grown layers was assessed by Auger spectroscopy and energy dispersive X-ray analysis. Raman

spectroscopy of the In_2Te_3 MBE grown layer was compared with a In_2Te_3 bulk sample to verify chemical composition. The crystal structure of the In_2Te_3 layers was determined by X-ray diffraction techniques, confirming a f.c.c. structure with a lattice parameter of 18.50\AA , indicating that the MBE grown In_2Te_3 is in the alpha phase ($\alpha\text{-In}_2\text{Te}_3$)⁹ where the In sublattice vacancies are ordered. The bandgap of the In_2Te_3 layers has been determined by photoreflectance, yielding a value of 1.2eV at 300K and 1.31eV at 77K . As a preliminary investigation into $\text{InSb}/\text{In}_2\text{Te}_3/\text{CdTe}$ and $\text{InSb}/\text{In}_2\text{Te}_3$ multilayer structures, we have studied the MBE growth of InSb and CdTe on 500\AA thick In_2Te_3 epilayers. Auger depth profiling has been used to examine the layers and their interfaces. Results show a severe intermixing of both the CdTe and InSb into the In_2Te_3 layers. The experimental results are supported by thermodynamic considerations of the $\text{InSb-In}_2\text{Te}_3$ interface. Points of interest are discussed.

Experimental

The In_2Te_3 , InSb and CdTe layers were grown in a Varian 360 MBE system equipped with a quadrupole mass analyzer and *in situ* RHEED and flux monitoring facilities. Base pressure during growth was below 5×10^{-10} Torr. The $\text{InSb}(100)$ substrates were solvent cleaned and mounted onto molybdenum heating blocks using a colloidal suspension of graphite in alcohol. Immediately before growth the native oxide was removed from the substrate surfaces by heating at 410°C in an Sb_4 flux. A 1000\AA InSb buffer was grown on all substrates to ensure a consistent high quality $\text{InSb}(100)$ surface present for the growth of the Indium telluride.

Separate effusion cells containing high purity In, Sb, CdTe , Cd and Te were used for the growth of the InSb , CdTe and In_2Te_3 layers. A relative measure of the flux from a given cell was obtained by interposing an ion gauge flux monitor into the molecular beam and

relating the measured beam equivalent pressure to the cell temperature, molecular weight and ionization efficiency of the beam species.

Indium telluride growth was studied for substrate temperatures, T_s , within the range $300 \leq T_s < 350^\circ\text{C}$ and Te/In flux ratios ($J_{\text{Te}}/J_{\text{In}}$) between $1 < J_{\text{Te}}/J_{\text{In}} < 5/2$. The Te/In flux ratio range was restricted to help avoid the possibility of growth of the compounds InTe and In_2Te_5 . The In cell setting was kept constant throughout. Growth rates were estimated to be $0.2 \mu\text{m/hr}$ as calculated from the measured In flux, assuming a unity sticking coefficient for the In.

Following growth the samples were analyzed by Auger spectroscopy, and the atomic and weight percentages of the layers were assessed by energy dispersive X-ray analysis (EDX) using a standard facility with an accelerating voltage of 15 KV and a beam current of approximately 8×10^{-10} amps. All layers examined by EDX were $\approx 7000 \text{\AA}$ thick to ensure there would be no contributions from the InSb substrate appearing in the EDX spectra. A sample of bulk In_2Te_3 supplied by CERAC/PURE Inc was used for standardization purposes for both the Auger and EDX analysis. Selected layers were further characterized and studied by Raman spectroscopy, X-ray diffraction techniques and photoreflectance. During the course of our studies, it became apparent that the In_2Te_3 was oxidizing over a period of time when exposed to atmosphere. To avoid oxidation during transportation for the Raman studies, a 50\AA Sb cap layer was deposited at room temperature on the In_2Te_3 . It has been reported that Sb deposited under these conditions may be either amorphous or crystalline, dependant on the substrate and thickness¹⁰. RHEED studies during deposition of the Sb indicated that the Sb was amorphous. The Raman studies employed an Argon ion laser as an exciting source ($\lambda = 514.5 \text{ nm}$, $P = 40 \text{ mW}$) with the spectra taken in a back scattering geometry. A bulk In_2Te_3 sample⁴ grown by the horizontal Bridgeman technique at UC Cardiff was used as a standard for comparison. X-ray analysis of the layers used a single crystal diffractometer together with Weissenberg and oscillation photographs

utilizing Cu K α radiation. Photoreflectance measurements were used to measure the band-gap and were performed with a standard facility¹¹ that used a Ge or Si detector and a 6328Å He-Ne pump beam to produce the electric field modulation. Measurements were conducted at 300 and 77K in the vicinity of the direct gap, E_g .

InSb and CdTe were grown by MBE on thin film (500Å) In₂Te₃ epilayers at 300°C. The InSb and CdTe growth, together with the experimental details of the Auger depth profiling, has been described elsewhere¹.

Results

Initiating growth of the Indium telluride resulted in an immediate conversion from the Sb stabilized (2X2) InSb RHEED pattern¹² to a characteristic streaked pattern shown in Figure 1. For flux ratios $J_{Te}/J_{In} < 3/2$ this pattern became spotted and eventually vanished, indicative of a disordered growth, after approximately 300Å growth for all substrate temperatures studied. For growth with flux ratios $J_{Te}/J_{In} \geq 3/2$ and a substrate temperature of 300°C, the pattern remained streaked throughout the entire growth. Growth at substrate temperatures greater than 300°C required Te/In flux ratios greater than 3/2 to preserve the streaked two-dimensional growth pattern.

Energy dispersive X-ray spectra of samples grown at $T_s = 300^\circ\text{C}$ and flux ratios, $J_{Te}/J_{In} < 3/2$ and $J_{Te}/J_{In} \geq 3/2$ (Figure 2, (a) and (b) respectively) are compared with the spectrum obtained from a bulk In₂Te₃ reference standard. The spectra for layers grown at 300°C and flux ratios $J_{Te}/J_{In} \geq 3/2$ were identical to that obtained from the bulk In₂Te₃ standard, indicating that the stoichiometry of these layers was identical to that of the In₂Te₃ bulk standard. Layers grown with flux ratios $J_{Te}/J_{In} < 3/2$ were identified to be In rich.

Auger spectra of the MBE grown layers were compared with the Auger spectrum obtained for the In_2Te_3 bulk standard. The spectra obtained from samples grown at 300°C with flux ratios $J_{\text{Te}}/J_{\text{In}} \geq 3/2$ matched the spectrum obtained from the bulk standard. Samples grown with flux ratios $J_{\text{Te}}/J_{\text{In}} < 3/2$ were identified as In rich, correlating and supporting the results obtained from the EDX studies. An Auger spectrum from a stoichiometric In_2Te_3 layer is shown in Fig 3. High magnification SEM imaging of the samples showed a clear distinction between the stoichiometric and non-stoichiometric layers. The stoichiometric layers had a smooth surface morphology whilst non-stoichiometric layers were rough and structured with island-type precipitates. Further examination by EDX identified these precipitates as indium.

Raman studies of an 1100\AA thick MBE layer grown under $J_{\text{Te}}/J_{\text{In}} > 3/2$ and $T_s = 300^\circ\text{C}$ growth conditions were compared with the spectrum obtained from a bulk In_2Te_3 sample. Although the optical constants of In_2Te_3 are not well documented, the penetration depth of the laser light used in the studies was considered to be less than 1100\AA , ensuring that there would be no contributions from the InSb buffer and substrate appearing in the Raman spectrum. The spectra obtained for the MBE layer and In_2Te_3 bulk are shown in Fig. 4(a) and (b) respectively. Both spectra exhibit prominent peaks labeled A,B,C and D for the In_2Te_3 layer and A',B',C' and D' for the bulk material. The position of these features are in excellent agreement. Slight interference with A,B and C is caused by an additional background from the amorphous Sb, which has a characteristic broad band which peaks at 152 cm^{-1} ¹³. Additional features at 70 cm^{-1} can also be seen, although difficult to separate from the increasing background due to Rayleigh scattering from a slightly rough sample surface. Whilst little is known about the Raman spectrum of many of the indium tellurides, InTe has been reported¹⁴, and the spectrum differs substantially from Fig. 4 (a) and (b).

Further characterization of the MBE grown indium telluride and analysis of the crystal structure were obtained from X-ray diffraction, Weissenberg and oscillation photographs. Fig 5(a) and (b) show 2θ diffractometer traces of a 1100Å thick In_2Te_3 layer grown on an $\text{InSb}(100)$ substrate for $\text{InSb}(200)$ and $\text{InSb}(400)$ reflections respectively. $\text{In}_2\text{Te}_3(600)$ and $\text{In}_2\text{Te}_3(12,00)$ reflections are observed in these traces suggesting that $\text{In}_2\text{Te}_3\langle 100 \rangle$ lies along $\text{InSb}\langle 100 \rangle$ direction with an out of plane lattice parameter of 18.50Å. This lattice parameter is in good agreement with a value of 18.486 reported⁹ for bulk In_2Te_3 . To confirm that the periodicity was 18.50Å in the plane of the epitaxial film, Weissenberg and oscillation photographs were taken. Figure 6 shows the oscillation photographs of $\text{In}_2\text{Te}_3/\text{InSb}(100)$ taken about $(01\bar{1})$ oscillation axis. First and second layers of InSb are observed with a repeat distance of 4.58Å ($6.48/\sqrt{2}$ Å). Weak and medium intensity layers are seen for In_2Te_3 . Zero to sixth layers are identifiable with a repeat distance of 13.08 Å ($18.50/\sqrt{2}$ Å), suggesting that the in plane lattice parameter of the film is 18.50Å. All the reflections can be indexed based on a f.c.c. lattice with lattice parameter of 18.50Å.

Photoreflectance spectra, measured in the vicinity of E_g are presented in Fig 7. The line shapes are qualitatively similar to those observed in other semiconductors¹¹ with a sharp oscillation near the transition energy; the broad feature below it is most likely due to absorption modulation of the light that is transmitted through the film and reflected from the $\text{In}_2\text{Te}_3/\text{InSb}$ interface¹⁵. The maximum in the spectrum is assumed to represent the transition energy and found to be 1.19 ± 0.02 eV and 1.31 ± 0.015 eV, at 300 and 77K respectively.

The ability to grow thin film In_2Te_3 made it possible to study the subsequent growth of InSb and CdTe on these layers. An Auger depth profile of a 500Å In_2Te_3 layer grown on a InSb homoepitaxial layer is shown in Fig. 8. The interface is seen to be abrupt and estimated to be less than 100Å, with no evidence of intermixing between the InSb and In_2Te_3 layers. A 800-s InSb growth was attempted on a 500Å In_2Te_3 layer with $T_s=300$

°C and a growth rate of 0.6 Å/s to give a nominal growth of 500 Å. The RHEED pattern showed no change from the characteristic In_2Te_3 pattern (Fig. 1) upon initiating, and during growth of the InSb . The Auger depth profile of the resulting layer is shown in Fig. 9(a). There is no evidence of InSb layer growth. Comparison with Fig. 8 indicates that the layer is In rich with respect to In_2Te_3 and the interface broader. A 300-s CdTe growth was attempted on a 500 Å In_2Te_3 layer at $T_s=300^\circ\text{C}$ under stoichiometric flux conditions ($J_{\text{Cd}}/J_{\text{Te}}=1$) and nominal growth rate of 1.85 Å/s. The RHEED pattern remained unchanged from the In_2Te_3 pattern during growth of the CdTe . The resulting Auger depth profile is shown in Figure 9(b). No CdTe layer growth is evident. However, Cd has been incorporated through approximately 400 Å of the indium telluride layer, suggesting the formation of an alloy. A similar CdTe growth was attempted, with a Cd/Te flux ratio $J_{\text{Cd}}/J_{\text{Te}}=3/1$. The RHEED pattern remained unchanged from the In_2Te_3 pattern during growth. The resulting profile is shown in Fig. 9(c). In this case the Cd has mixed uniformly throughout the indium telluride layer. Initial analyses of the Auger data using sensitivity factors suggest that the resulting layer has ratios Cd:In:Te of 1:2:4

Discussion

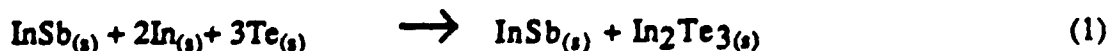
We have shown that single crystal In_2Te_3 can be grown epitaxially on $\text{InSb}(100)$ at substrate temperatures $300 \leq T_s \leq 350$ and flux ratios $3/2 \leq J_{\text{Te}}/J_{\text{In}} < 5/2$. For a given growth temperature, there is a minimum Te/In flux ratio required for epitaxial growth (3/2 at 300°C), below which the layers are non-epitaxial and indium rich. The minimum Te/In flux ratio increases as the growth temperature is increased, suggesting that the ratio in the Te/In sticking coefficients decrease with increasing growth temperature.

The Weissenberg and oscillation photographs indicate that the In_2Te_3 layers are in the α -phase, where the cation vacancies are distributed uniformly throughout the In sublattice. It

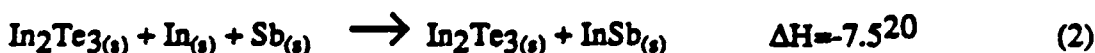
is of fundamental interest for MBE growth dynamics to ascertain whether the ordered vacancy structure is formed on the growth surface during epitaxy, or if the vacancy distribution on the growth surface is random and there is a subsequent rearrangement of the In sublattice within the layer. A detailed analysis of the RHEED pattern during growth may help to clarify these points.

We report a value for the bandgap of the α -phase of In_2Te_3 to be $1.19 \pm 0.02 \text{ eV}$ and $1.31 \pm 0.015 \text{ eV}$, at 300 and 77K, respectively as measured by photoreflectance. As far as we are aware, this is the first direct measurement of the band-gap of $\alpha\text{-In}_2\text{Te}_3$. A value of 1.12 eV has been deduced from electrical measurements¹⁶. Other 300K band gap values reported range from 1.01 eV for the β -phase, determined from absorption measurements¹⁷, to 1.2 eV determined from the reflectivity¹⁸; pseudopotential calculations yield a band gap of 1.3 eV for the β -phase¹⁹.

We have shown that an attempt to grow an epitaxial layer of either InSb or CdTe on In_2Te_3 layers at growth temperatures compatible with InSb/ In_2Te_3 and CdTe/ In_2Te_3 /InSb multilayer growth (300°C) results in severe intermixing in the In_2Te_3 layer with no InSb or CdTe layer growth. RHEED studies indicate that the layers formed are crystalline. For InSb growth on In_2Te_3 Auger depth studies show In incorporation into the In_2Te_3 layer. In contrast an abrupt interface is observed for the growth of In_2Te_3 on InSb. Consideration of the thermodynamics of the In_2Te_3 -InSb interface can help to explain the heterogeneity of the two growths. For this, we ignore the fact the reactants may be dimers or tetramers (i.e. Te_2 , Sb_4), assuming that the molecular beam species degenerate into the monomer upon contact with the growth surface. As such the deduced change in enthalpy should only be considered approximate. For the growth of In_2Te_3 on InSb we can consider the following reaction where In and Te are present on an InSb surface.



for which the change in enthalpy ΔH is -45.8 kcal^{20} . Our growth conditions were carefully controlled by tailoring $J_{\text{Te}}/J_{\text{In}}$ to ensure In_2Te_3 formation rather than InTe or In_2Te_5 , and we will not consider these other possible reactions here. For the growth of InSb on In_2Te_3 we consider In and Sb present on an In_2Te_3 surface.



where the In and Sb react to form InSb . However, if the Sb has a short residence lifetime with respect to the In , the growth surface may be Sb deficient and we should consider the following possible reactions.



For reactions (3) and (4) the elemental In converts In_2Te_3 to InTe or In_2Te respectively. The experimental results indicating the inability to grow InSb on In_2Te_3 , with the incorporation of In into the In_2Te_3 layer suggests that the MBE growth of InSb on In_2Te_3 may be described by a reaction such as (3) or (4).

Whilst these thermodynamic considerations are non-rigorous, they suggest that InSb growth may be possible on In_2Te_3 if sufficient Sb is present on the In_2Te_3 growth surface to bond with the available In . Once InSb growth has been initiated on the In_2Te_3 , the resulting interface should be stable, since no chemical equation with a negative change in enthalpy can be written with InSb and In_2Te_3 as the reactants. This thermodynamic consideration is supported by the abrupt interface observed for the growth of In_2Te_3 on InSb (Figure 8).

For CdTe growth on In_2Te_3 there is severe Cd interdiffusion. Increasing the Cd flux results in a uniform incorporation of the Cd throughout the indium telluride layer. Preliminary Auger data suggests that the layer so formed may be a ternary alloy such as CdIn_2Te_4 . Further analysis by Raman and X-ray will help to clarify these points. The

readiness of Cd to interdiffuse into the In_2Te_3 layer supports the notion that the interfacial layer formed during growth of CdTe on InSb under conventional MBE growth conditions is complex and is unlikely to consist of merely a thin layer of In_2Te_3 and elemental Sb.

While these studies suggest that the successful growth of InSb/ In_2Te_3 and CdTe/ In_2Te_3 multilayers is unlikely, the results shed additional insight into the MBE growth of mixed systems. Recent studies^{1,8} of the growth of CdTe on InSb have shown that simple thermodynamic considerations⁸ are applicable to the MBE growth of this II-VI/III-V mixed system. The results presented in this paper also suggest that simple thermodynamic concepts can be successfully applied to the MBE growth of a mixed III-V/III-VI system. We believe that these thermodynamic concepts combined with considerations of the surface residence lifetimes of the incident beam species will prove to be of fundamental importance in predicting and optimizing growth conditions for the MBE of other mixed multilayer systems.

Acknowledgments

The authors are grateful to J. Branton for technical support and K.J. Mackey for many helpful discussions. T.D. Golding would like to thank Prof. M. Pepper for assistance, and acknowledges a CASE award with the GEC Hirst Research Centre, London.

References

- 1 T.D. Golding, M.Martinka, and J.H.Dinan, J.Appl.Phys. 64 1873 (1988).
- 2 T.D.Golding, J.H.Dinan, M.Martinka, A.G.Cullis, G.M.Williams, S.Barrat, C.F.McConville, C.R.Whitehouse, J.E.Macdonald and K.M.Conway, to be published.
- 3 K.J.Mackey, P.M.G.Allen, W.G.Herrenden-Harker, R.H.Williams, C.R.Whitehouse and G.M.Williams, Appl.Phys.Lett 49 (6) 354 (1986).
- 4 D.R.T.Zahn, K.J.Mackey, R.H.Williams, H.Münder, J.Geurts and W.Richter, Appl.Phys.Lett. 50 742 (1987).
- 5 D.R.T. Zahn, T.D.Golding, K.J.Mackey, W.Richter, M. Martinka, J.H. Dinan and R.H.Williams, to be published.
- 6 D.R.T.Zahn, T.D.Golding, K.J.Mackey, T.Eickhoff, J.Geurts, W.Richter, M. Martinka, J.H.Dinan and R.H.Williams, to be published.
- 7 B.Legendre, B.Gather, and R.Blachnik, Z.Metallkd. 71, 588 (1980)
- 8 K.J.Mackey, D.R.T.Zahn, P.M.G.Allen, R.H.Williams, W.Richter and R.S.Williams, J.Vac.Sci.Technol. B5,1233 (1987).
- 9 B.Grzeta-Plenkovic, S.Popovic, B.Celustka, Z.Ruzic-Toros, B.Santic and D.Soldo, J.Appl.Cryst. (1983) 16, 415.
- 10 D.R.T. Zahn, N.Esser, W.Pletschen, J.Geurts and W.Richter, Surf. Sci 168, 823 (1986).
- 11 D.E. Aspnes, Handbook on Semiconductors, Vol.II, ed. M.Balkanski (North-Holland, New York, 1980), p.109.
- 12 A.J. Noreika, M.H. Francombe and C.E.C. Wood, J.Appl.Phys. 52 7416 (1981).
- 13 M.Wihl, P.J. Stiles and J. Tauc, Proc. 11th Intern. Conf. on the Physics of Semiconductors, Warsaw 1972, p.484.
- 14 M.A. Nizametdinova, Phys. Status Solidi b 97, K9 (1980).
- 15 C. Vazquez-Lopez, H. Navarro, R. Aceves, M.C. Vargas and C.A. Menezes, J.Appl.Phys. 58, 2066 (1985).
- 16 V.P. Zhuze, A.I. Zaslavaskii, V.A. Petrusevic, V.M. Sergeiva and A.I. Slelykh, Proc. Int. Conf. on the Physics of Semiconductors, Prague, 1960, p.871.
- 17 S.Sen and D.N. Bose, Solid State Commun. 50, 39 (1984).
- 18 D.L. Greenaway and M. Cardona, Proc. Int. Conf. Physics of Semiconductors, Exeter, 1962, p.666.
- 19 G.Guizzetti, F.Meloni and A.Baldereschi, J.Phys.Soc.Japan 49 19809 Suppl. A p93-96.

20 Change of enthalpy calculated from heats of formation obtained from Ref.7

Fig. 1

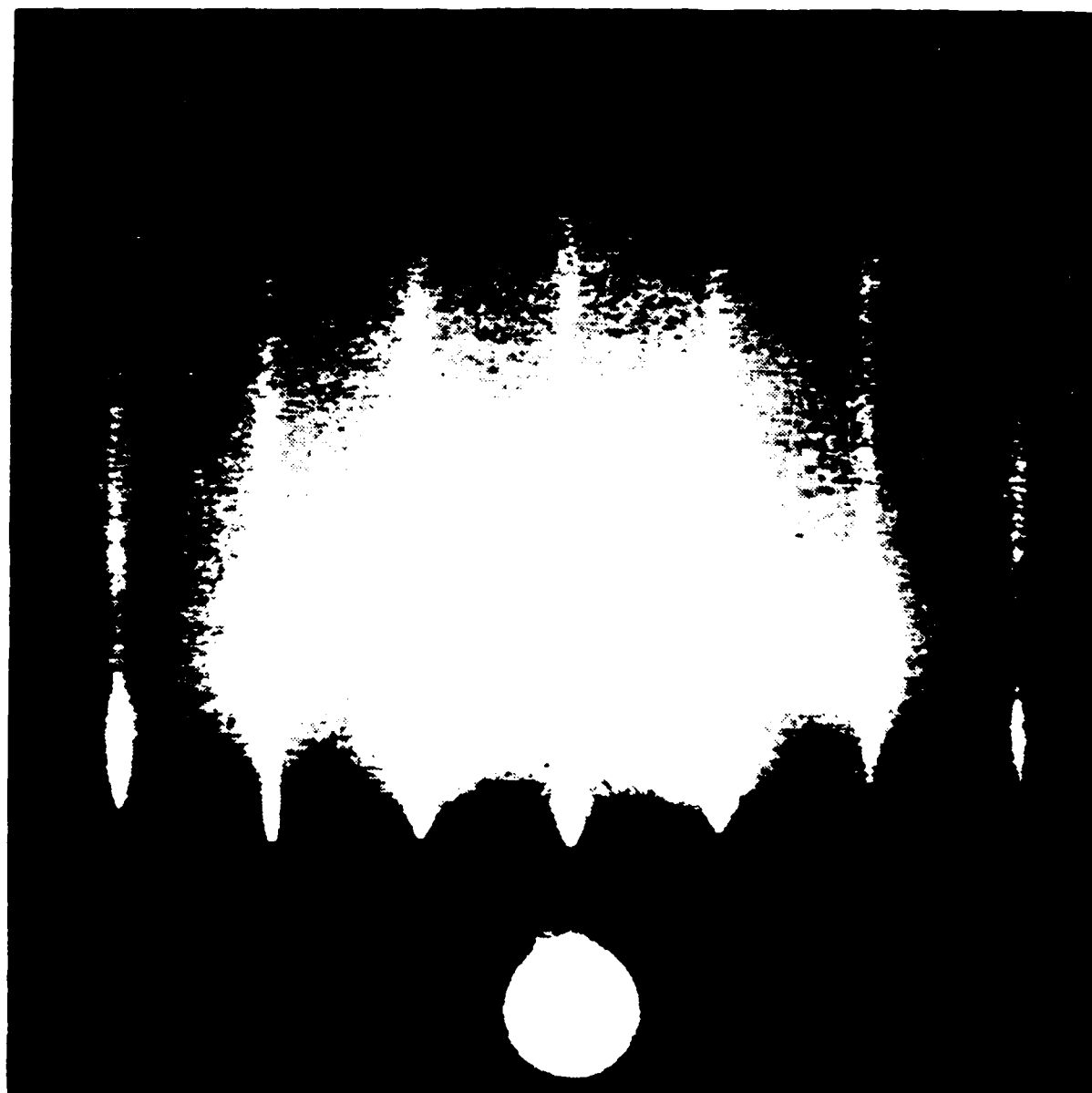


Figure captions

Figure 1

Reflection high energy electron diffraction pattern observed along [011] azimuth during growth of In_2Te_3 with $T_s=300^\circ\text{C}$ and $J_{\text{Te}}/J_{\text{In}} = 3/2$.

Figure 2

Energy dispersive X-ray spectra of 7000Å thick indium telluride layers grown by MBE at a growth temperature of 300°C and with flux ratios (a) $J_{\text{Te}}/J_{\text{In}} < 3/2$ and (b) $J_{\text{Te}}/J_{\text{In}} \geq 3/2$. The spectra are compared with the spectrum obtained from a In_2Te_3 bulk standard.

Figure 3

Auger spectrum of MBE grown In_2Te_3 layer.

Figure 4

Raman spectra ($\lambda=514.5\text{nm}$, $T=80\text{K}$) of (a) 1100Å thick In_2Te_3 layer capped with 50Å of Sb. (b) In_2Te_3 bulk standard.

Figure 5

Diffraction traces of 1100Å thick In_2Te_3 layer grown on $\text{InSb}(100)$ substrate for (a) $\text{InSb}(200)$ reflection. (b) $\text{InSb}(400)$ reflection.

Figure 6

Oscillation pattern of $\text{In}_2\text{Te}_3/\text{InSb}(100)$ taken about (011) oscillation axis. All reflections can be indexed based on a f.c.c. lattice with lattice parameter of 18.50Å.

Figure 7

Photoreflectance spectra of 1100Å In_2Te_3 layer. The transition energy is $1.19 \pm 0.02\text{eV}$ and $1.31 \pm 0.015\text{eV}$, at 300K and 77K respectively.

Figure 8

Auger depth profile of 500Å In_2Te_3 layer grown on an InSb homoepitaxial layer.

Figure 9

Auger depth profiles of the attempted growth at 300°C of (a) InSb , (b) CdTe with $J_{\text{Cd}}/J_{\text{Te}} = 1$, (c) CdTe with $J_{\text{Cd}}/J_{\text{Te}} = 3$, on 500Å thick In_2Te_3 layers. The estimated nominal thickness of the InSb and CdTe growths was 500Å.

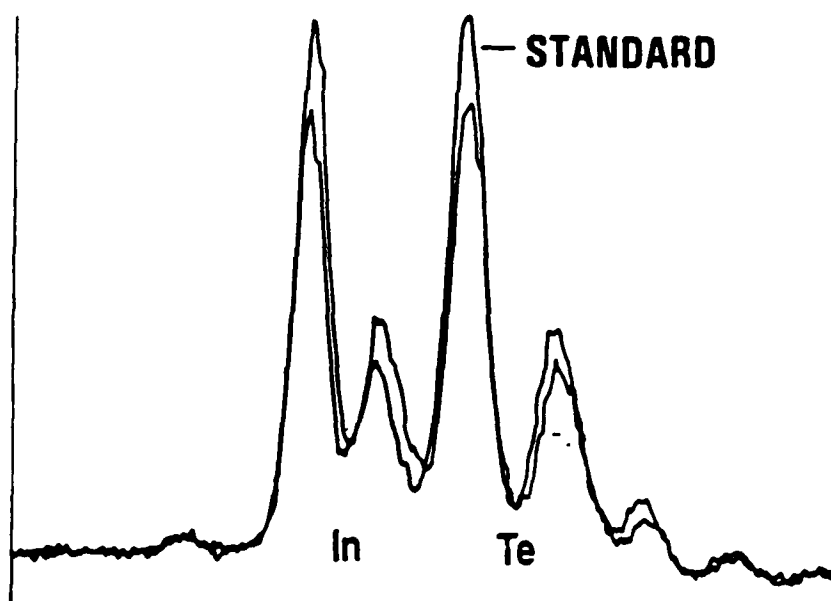
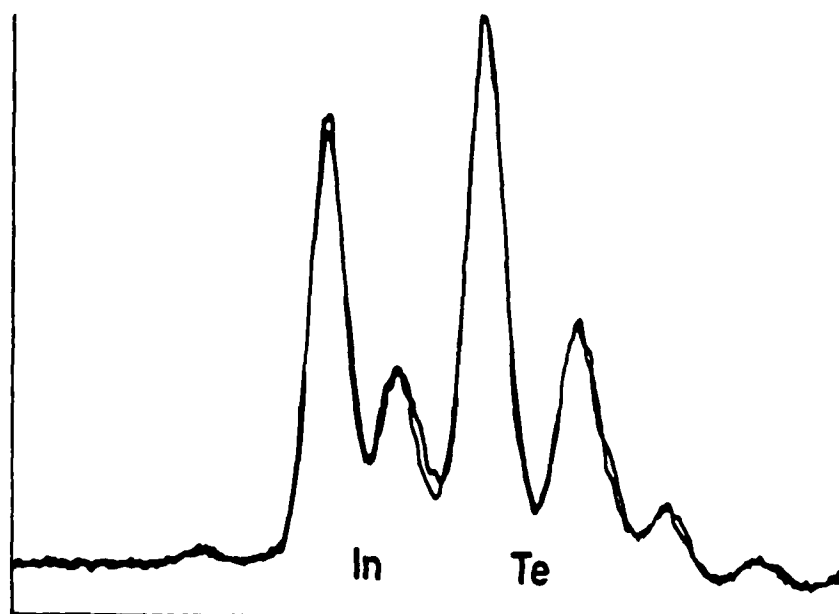
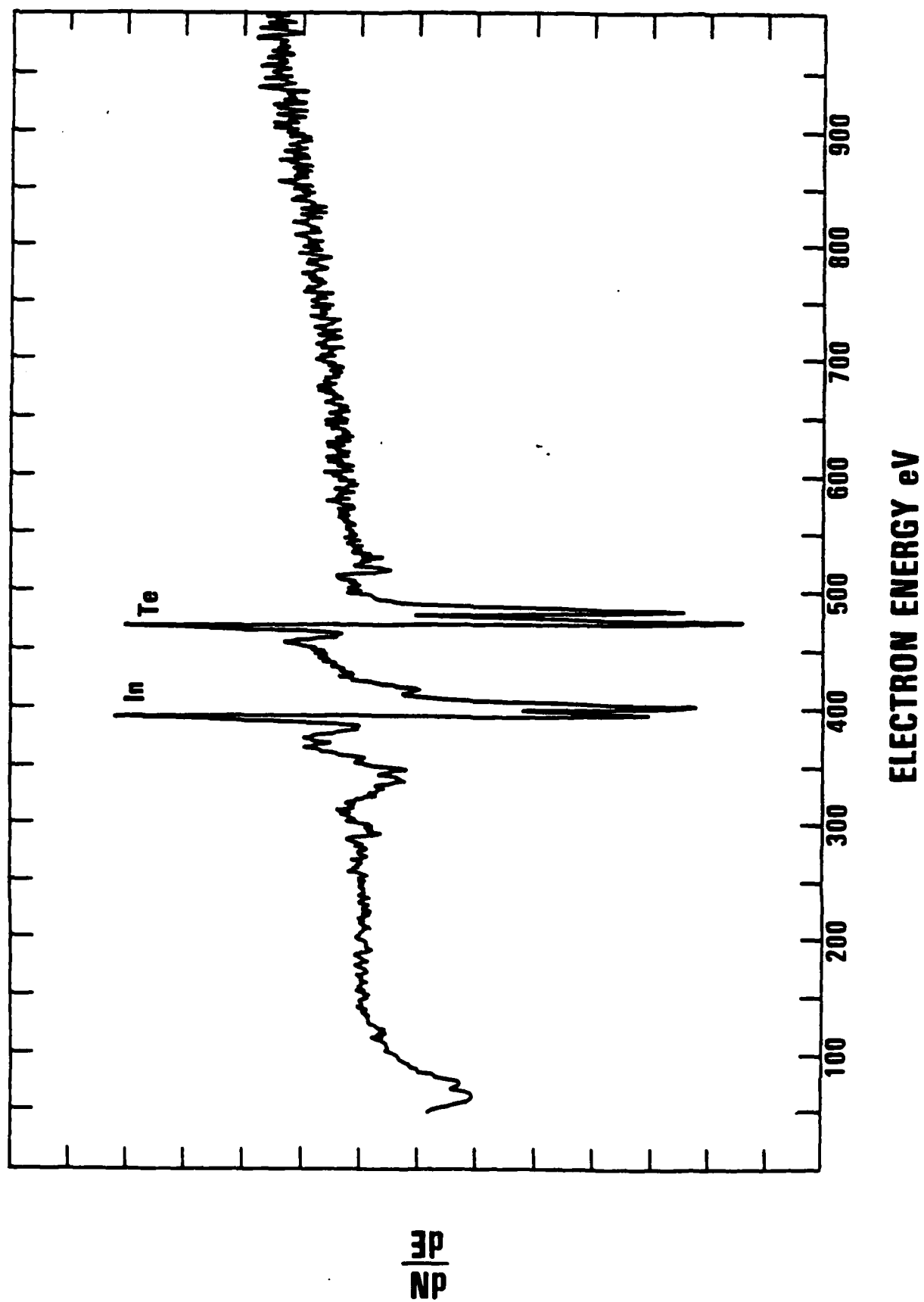
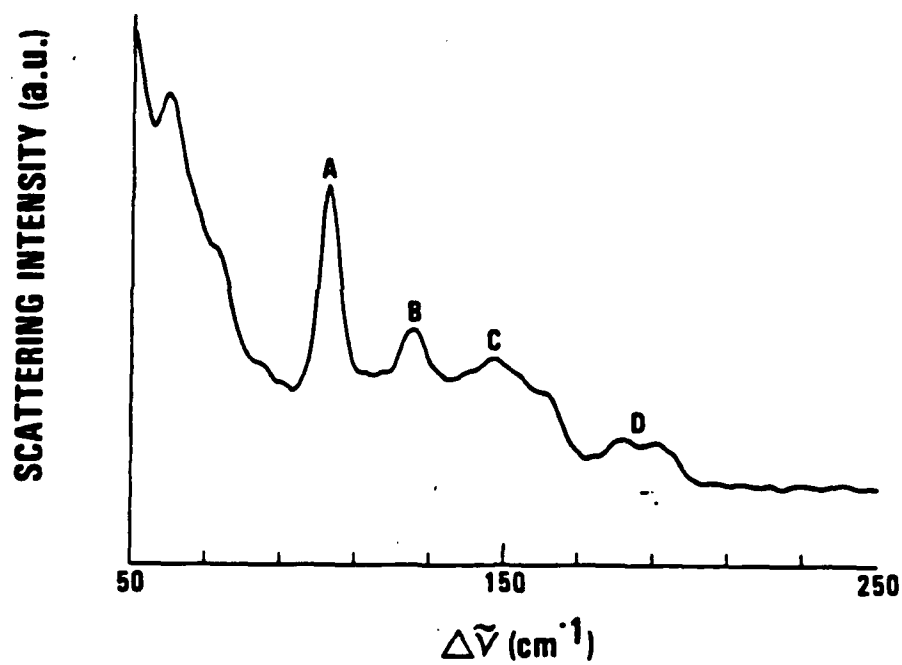
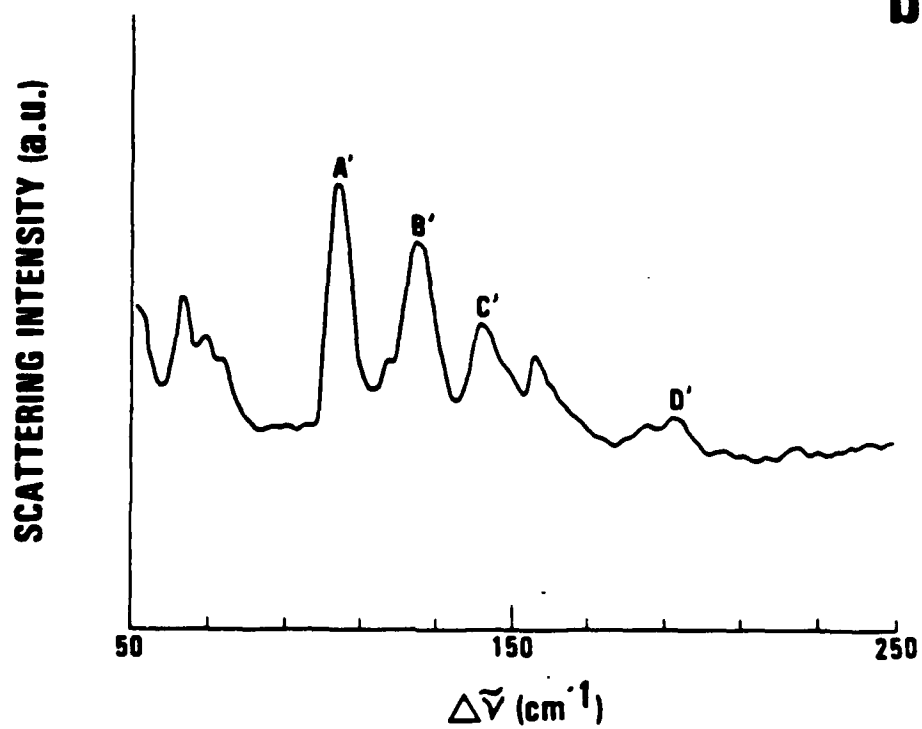
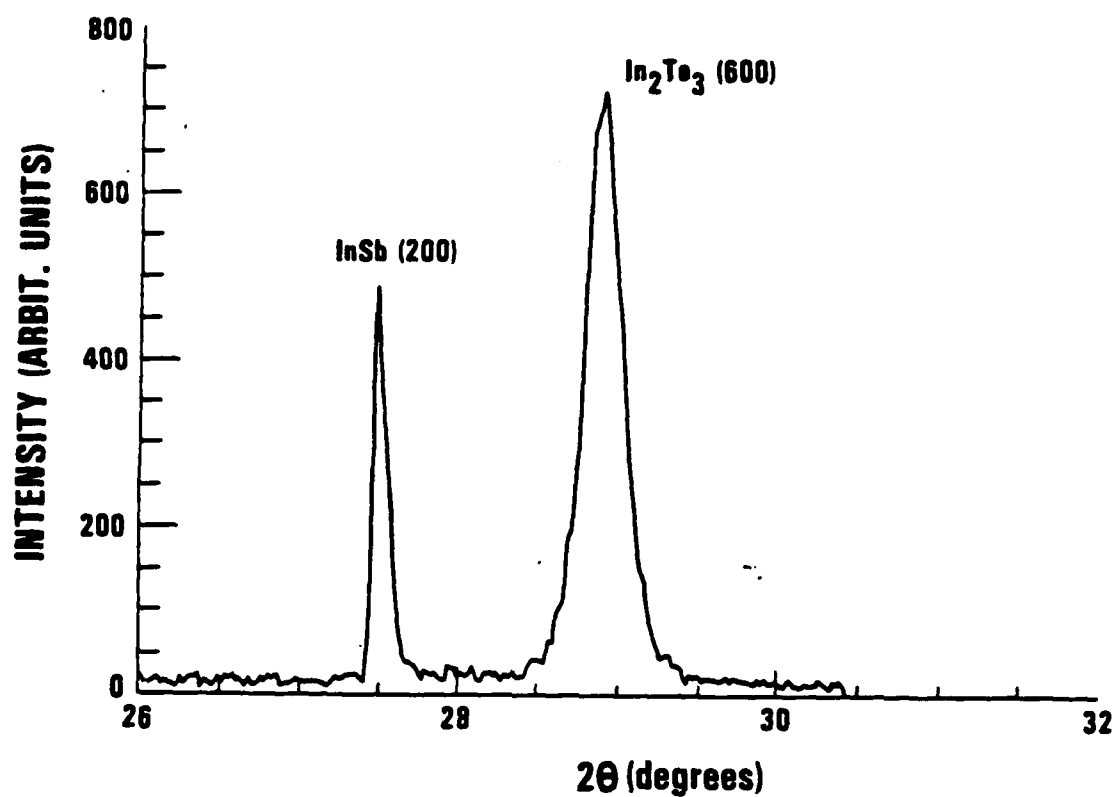
a**b**

Fig 3

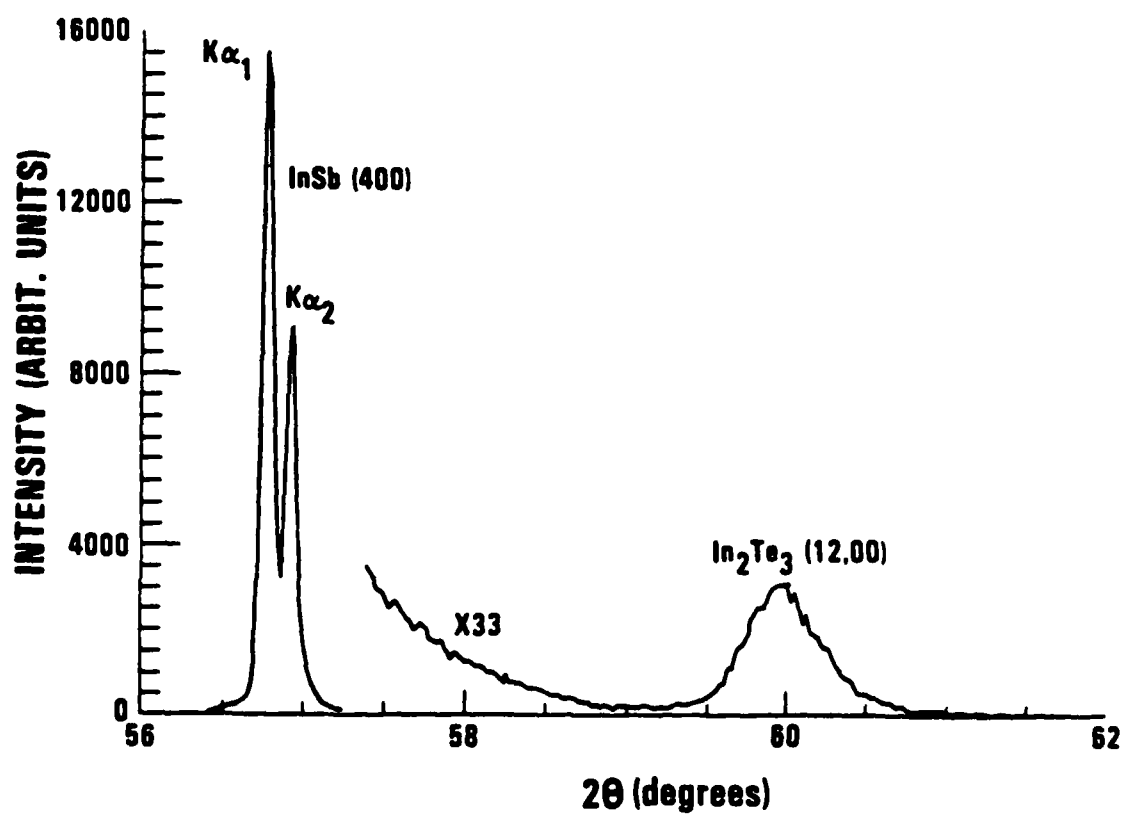


a**b**

a



b



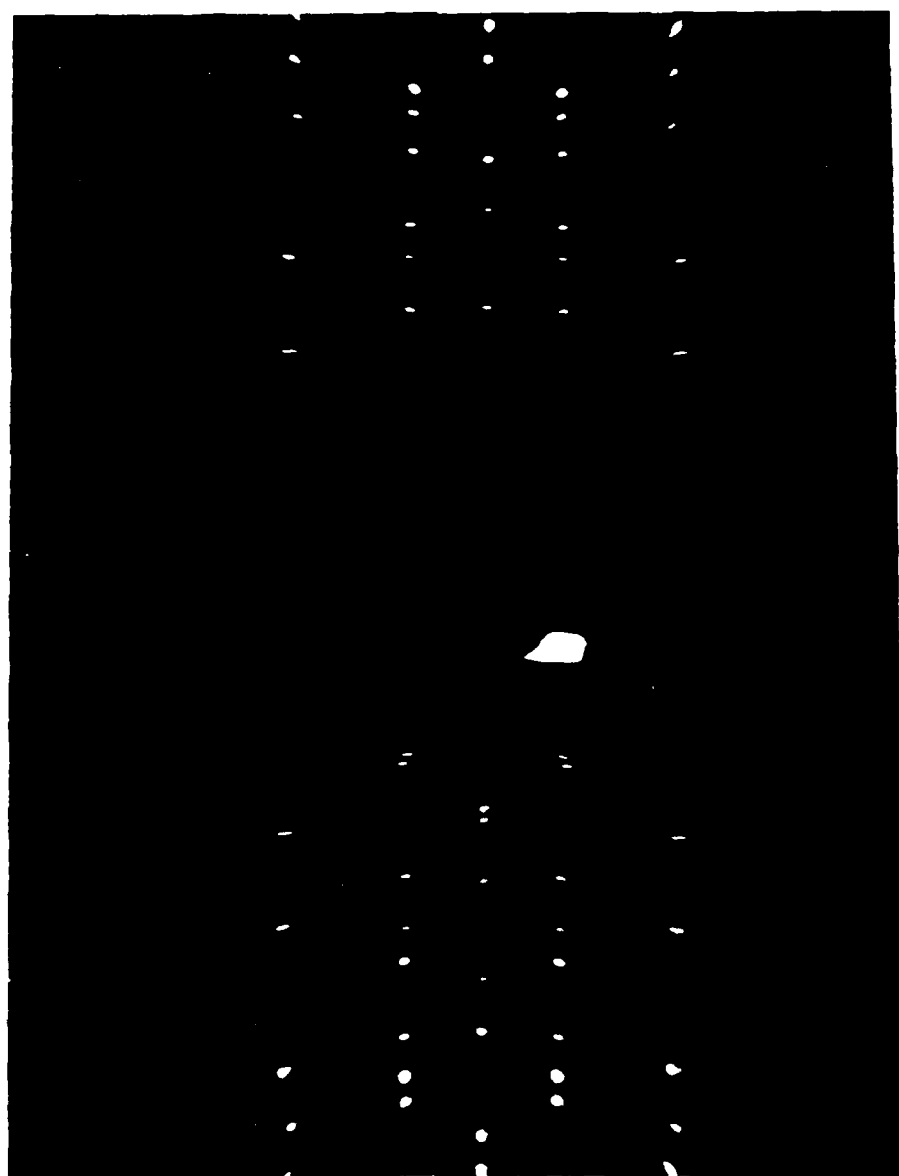
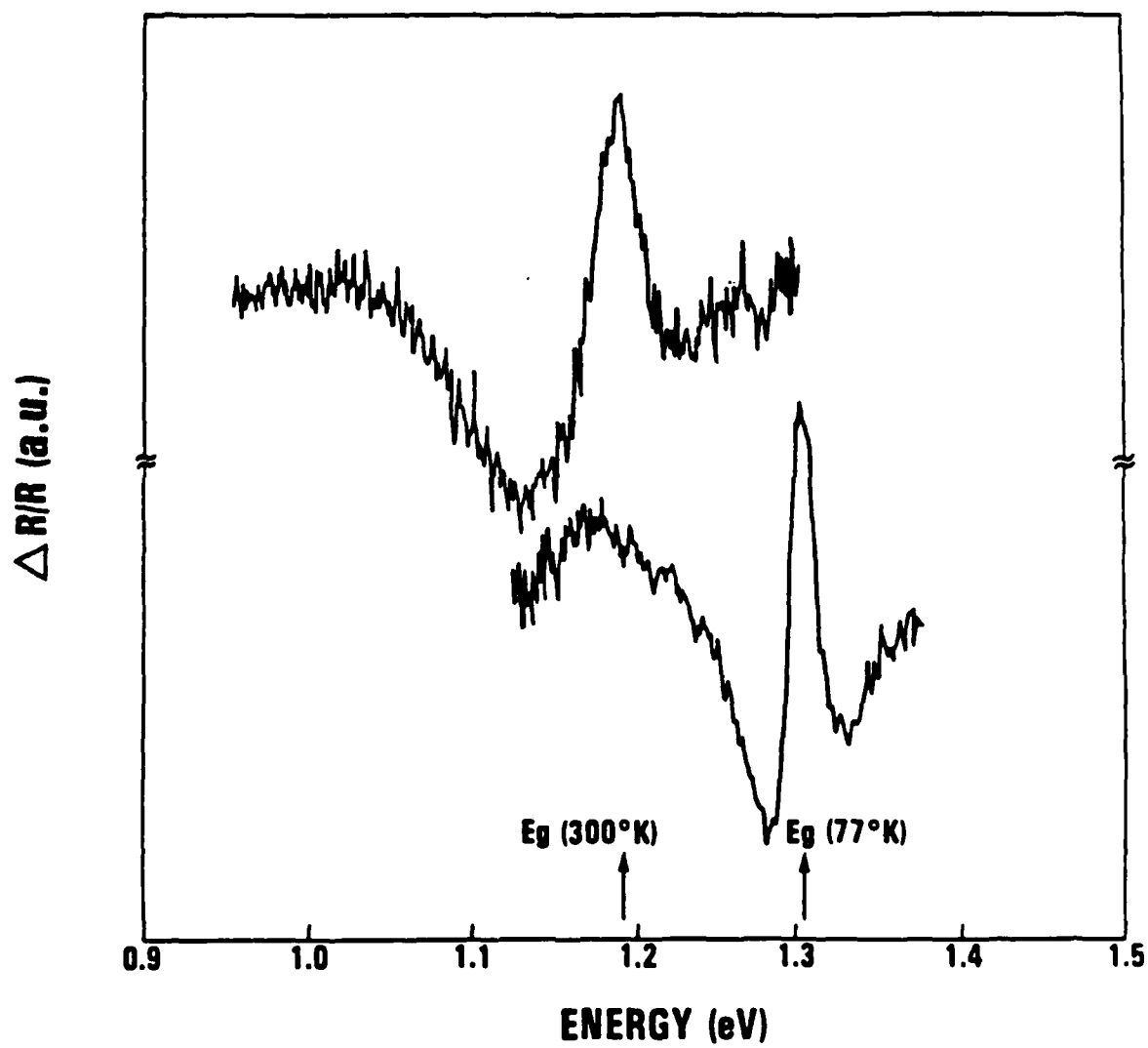
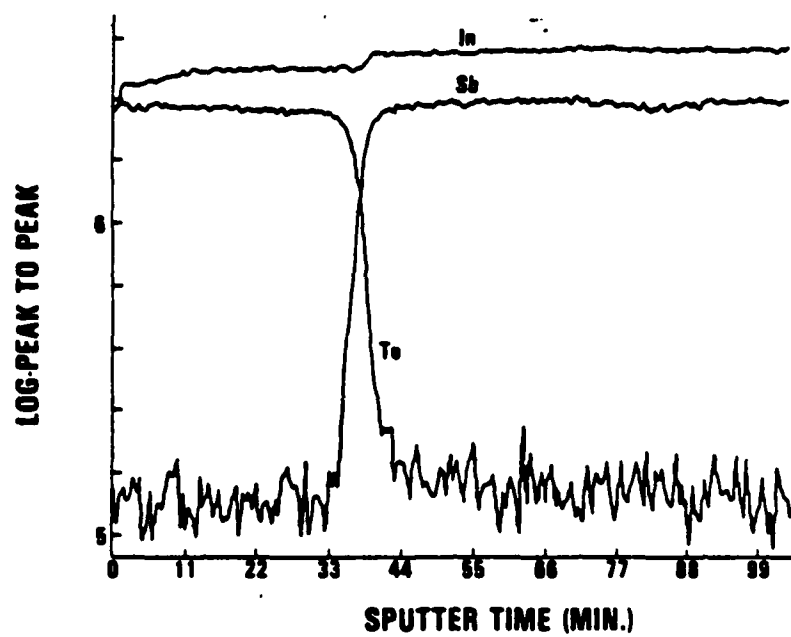
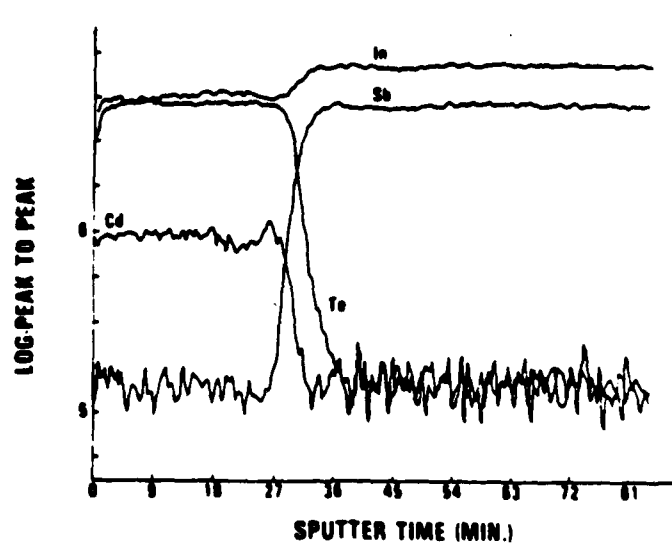
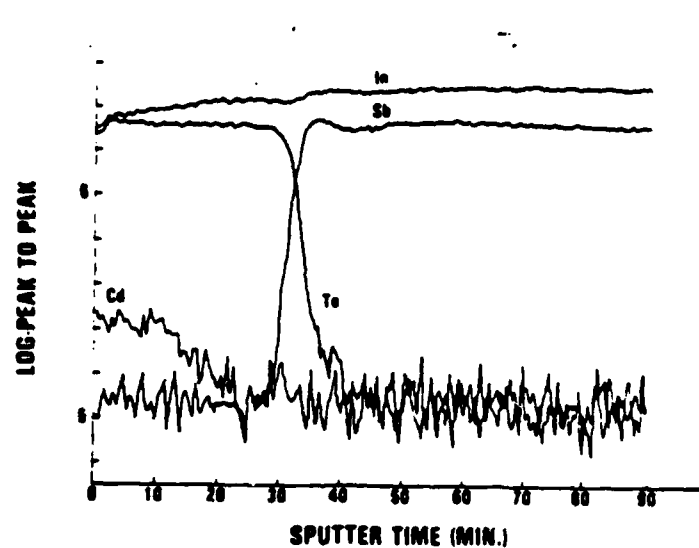
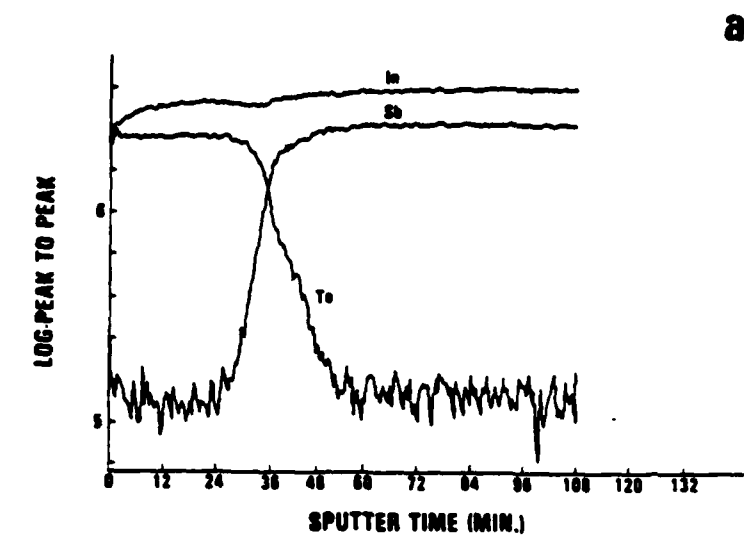


Fig. 7







Molecular-beam epitaxial growth of InSb/CdTe heterojunctions for multilayer structures

T. D. Golding,^{a)} M. Martinka, and J. H. Dinan

U. S. Army Center for Night Vision and Electro-Optics, AMSEL-RD-NV-IT, Fort Belvoir, Virginia 22060-3677

(Received 10 March 1988; accepted for publication 27 April 1988)

We have used the technique of molecular-beam epitaxy to grow layers of CdTe on InSb and InSb on CdTe and have performed a detailed analysis of the layers and their interfaces using Auger depth profiling and reflection high-energy electron diffraction. We show that significant improvements in interfacial quality can be obtained by the proper choice of fluxes during growth. The use of a Cd/Te flux ratio of 3:1 ($J_{\text{Cd}}/J_{\text{Te}} = 3$) during the growth of CdTe has enabled epitaxy at a substrate temperature of 300 °C. Interfaces formed with this flux ratio are abrupt, in sharp contrast to those formed under stoichiometric flux conditions ($J_{\text{Cd}}/J_{\text{Te}} = 1$). Subsequent growth of InSb at a substrate temperature of 300 °C on thin CdTe epilayers (400 and 800 Å) is examined as a function of the InSb growth rate and Sb/In flux ratio. Quality of the interfaces shows a progressive improvement with increasing InSb growth rate.

I. INTRODUCTION

There is at present considerable interest in the InSb/CdTe material system. The mixed III-V/II-VI heterostructure has a near perfect lattice match ($\Delta a/a < 0.05\%$), which, combined with the large difference in band gaps between CdTe ($E_g = 1.44$ eV) and InSb ($E_g = 0.18$ eV), offers great potential for the fabrication of quantum-well lasers and detectors spanning the photon energy range 0.2–0.5 eV (2.5–6 μm). The small effective mass of electrons in InSb promises low-temperature HEMT structures with exceptionally high electron mobilities¹ and should allow quantization effects to be seen in significantly wider wells than with the more familiar material systems.

Attempts at experimental realization of multilayer structures have met with only limited success. Although good structural properties have been reported for CdTe layers grown by molecular-beam epitaxy (MBE) on InSb substrates^{2,3} and homoepitaxial layers⁴ and for InSb layers grown by MBE on (100) oriented CdTe substrates,⁵ recent studies^{6,11} of the growth of CdTe on InSb under typical MBE growth conditions have shown that the interfaces are complex due to a chemical reaction between InSb and CdTe. A study of the growth of InSb/CdTe multilayers has been reported,⁷ where reflection high-energy electron diffraction (RHEED) patterns indicated that individual layers grown at a substrate temperature of 220–240 °C were ordered. Although structurally good InSb epilayers have been reported⁵ for substrate temperatures in the range 225–275 °C, electrically active layers have only been reported⁸ for substrate temperatures in excess of 270 °C. To be useful for electronic device applications which involve tunneling, the thickness of individual layers of a multilayer device must be limited to several hundred angstroms. To facilitate growth, a substrate temperature must be found which results in high structural and electronic quality of both CdTe and InSb.

In this paper, we present results of a study of the MBE

growth of CdTe on InSb homoepitaxial layers, and of InSb on CdTe epilayers for potential applications in two-dimensional electron gas (2DEG) and electron tunneling devices. Auger depth profiling has been used to examine the layers and their interfaces. We show that significant improvements in interfacial quality can be obtained by the proper choice of fluxes during growth. CdTe layers have been grown on InSb for substrate temperatures of 200 and 300 °C under stoichiometric ($J_{\text{Cd}}/J_{\text{Te}} = 1$) and Cd-enhanced ($J_{\text{Cd}}/J_{\text{Te}} = 3$) flux conditions. The use of an enhanced Cd flux has enabled epitaxy of CdTe on InSb at 300 °C, a temperature which is compatible with the subsequent growth of electrically active InSb. Growth of InSb epilayers on thin layers (400 and 800 Å) of CdTe at a substrate temperature of 300 °C is examined as a function of InSb growth rate and Sb/In flux ratio. Interfaces are intermixed, but show a progressive improvement with increasing InSb growth rates.

II. EXPERIMENT

CdTe and InSb epitaxial layers were grown in a Varian 360 MBE system equipped with a quadrupole mass analyzer and *in situ* RHEED and flux monitoring facilities. Base pressure during growth was below 5×10^{-10} Torr. Prior to loading, InSb (100) substrates were solvent cleaned and mounted onto molybdenum support blocks using a colloidal suspension of graphite in alcohol. Immediately before growth the native oxide was removed from substrate surfaces by heating at 410 °C in an Sb₄ flux. A single effusion cell containing high-purity CdTe was used to provide a stoichiometric beam of Cd and Te, (Ref. 2) and was supplemented by a cell containing Cd for Cd-enhanced ($J_{\text{Cd}}/J_{\text{Te}} > 1$) studies. A relative measure of the flux from a given cell was obtained by interposing an ion gauge flux monitor into the molecular beam and relating the measured beam equivalent pressure to the cell temperature, molecular weight, and ionization efficiency of the beam species. Normal settings for the CdTe cell gave a total flux of 2.4×10^{14} atoms/cm²/s which corresponded to a homoepitaxial growth rate at $T_s = 220$ °C

^{a)} Permanent address: Cavendish Laboratory, University of Cambridge, Cambridge, England.

of approximately 1.7 \AA/s ($0.6 \mu\text{m/h}$). The Cd cell was set to supply its maximum safe flux of $2.6 \times 10^{14} \text{ atoms/cm}^2/\text{s}$ giving a flux ratio value $J_{\text{Cd}}/J_{\text{Te}} = 3$ during the Cd-enhanced growth experiments. Separate effusion cells containing high-purity In and Sb were used for growth of InSb. All InSb homoepitaxial and heteroepitaxial layers were grown at $T_s = 300^\circ\text{C}$ with growth rates in the range $0.3\text{--}2.0 \text{ \AA/s}$ ($0.1\text{--}0.7 \mu\text{m/h}$). Practical considerations related to the In cell temperature prevented growth of InSb with rates in excess of $0.7 \mu\text{m/h}$. $J_{\text{Sb}}/J_{\text{In}}$ was kept in the range $1.1\text{--}3.5$ to keep within the (2×2) Sb-stabilized surface reconstruction⁹ as indicated by RHEED.

Immediately following growth, each sample was transferred in air to a Physical Electronics 560 scanning Auger microscope configured with a double pass cylindrical-mirror analyzer and a differentially pumped and gettered argon ion gun. Depth profiles of the constituent species, as well as of carbon and oxygen, were obtained by alternate sputtering and data acquisition periods of 30 and 80 s, respectively. No carbon or oxygen recontamination was seen within the layers during the profile. To reduce artificial broadening of the growth interface, the sputter beam of 4-kV argon ions was incident at 40° from the sample surface normal with the sputter rate reduced to $20\text{--}30 \text{ \AA/min}$ by expanding to a $6 \times 6 \text{ mm}$ raster. The growths and sputter depths were limited to a few thin compositional periods to reduce roughness due to preferential ion etching of (100) InSb as observed in electron micrographs. The electron beam was used in spot mode and incident on the surface at 40° from the surface normal. An electron energy of 3 kV was used with a moderate and constant current of $0.16 \mu\text{A}$. Auger peaks overlapping the MNN transitions were minimized by collecting high energy resolution, $\Delta E/E = 0.4\%$, pulse count data from selectively contracted energy "windows."

The Auger analysis was calibrated in the usual manner. The analyzer energy scale was referenced to the known energy, 2 keV, of electrons backscattered from a sample surface while at its focal point, and the beam current was measured from the sample stage while biased to $+130 \text{ V}$. The current density of the argon beam was $600 \mu\text{A/cm}^2$ with FWHM of $550 \mu\text{m}$ and the sputter rates were referenced to thin-film standards and to bulk (110) CdTe. These agree well with our known MBE growth rates. Finally, Auger signal strengths from bulk (100) InSb and (111) CdTe were used to judge stoichiometric conditions within the MBE layers.

III. RESULTS

Auger depth profiles of 300-s growths of CdTe under stoichiometric beam conditions ($J_{\text{Cd}}/J_{\text{Te}} = 1$) on 1000- \AA InSb homoepitaxial layers at substrate temperatures $T_s = 200$ and 300°C are shown in Fig. 1. For growth at $T_s = 200^\circ\text{C}$, the (2×2) InSb RHEED pattern converted to a streaked (2×1) CdTe pattern immediately after CdTe growth was initiated. The epilayer is stoichiometric with a thickness of approximately 500 \AA which corresponds closely to that calculated from flux measurements. Width of the interface is estimated to be $120\text{--}180 \text{ \AA}$, a value which is near the Auger resolution limit. For growth at $T_s = 300^\circ\text{C}$, the

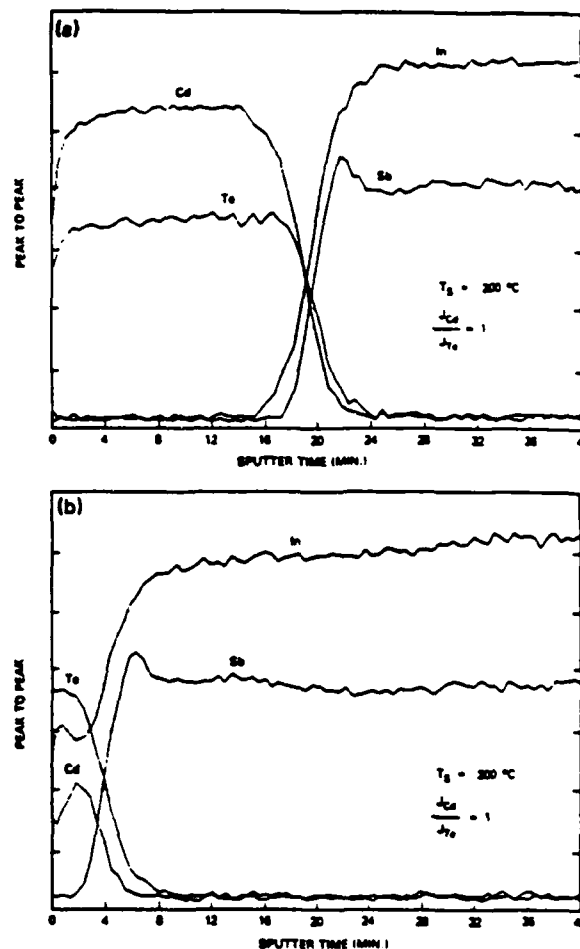


FIG. 1. Auger depth profiles of 300-s growths of CdTe on InSb homoepitaxial layers with $J_{\text{Cd}}/J_{\text{Te}} = 1$ for substrate temperatures of (a) 200 and (b) 300°C .

(2×2) InSb RHEED pattern vanished immediately after CdTe growth was initiated, indicating a disordered growth. The resulting layer is deficient in Cd and rich in In and Te. Layer thickness is estimated to be 150 \AA . These results are similar to those recently reported by Mackey *et al.*,⁶ where indium telluride compounds were identified at the InSb/CdTe interface. It has been suggested that the lack of Cd incorporation in layers grown at 300°C may be attributed to a Cd deficiency on the growth surface, thereby allowing Te to react with the InSb. To overcome this Cd deficiency we grew layers of CdTe on InSb using an enhanced Cd flux. For $T_s = 300^\circ\text{C}$, the additional Cd flux has a dramatic effect on the quality of layers and interfaces. An Auger depth profile of a 300-s growth of CdTe using Cd-enhanced flux conditions ($J_{\text{Cd}}/J_{\text{Te}} = 3$) is shown in Fig. 2(a). The (2×2) InSb RHEED pattern converted to a streaked (2×1) pattern immediately after CdTe growth was initiated. The depth profiles show that the interfacial width for this sample is as abrupt as that grown under stoichiometric flux conditions at $T_s = 200^\circ\text{C}$. To establish that the high-quality epitaxy of thin CdTe layers grown at elevated temperatures is due to the enhanced Cd flux and not to the total Cd flux or growth rate, the temperature of the CdTe cell was set to give a Cd

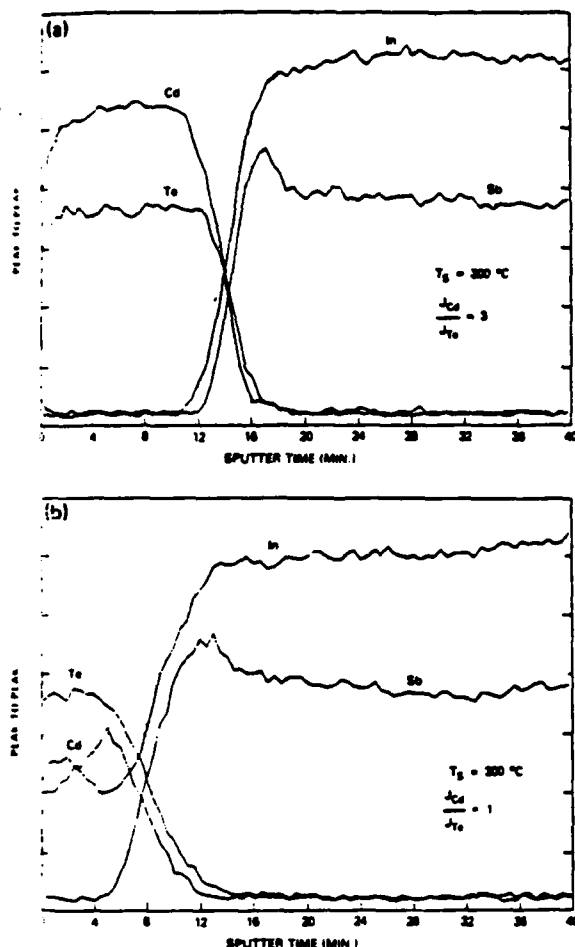


FIG. 2. Auger depth profiles of 300-s growths of CdTe on InSb homoepitaxial layers with substrate temperature of 300 °C for (a) $J_{Cd}/J_{Te} = 3$ and (b) $J_{Cd}/J_{Te} = 1$, with CdTe flux adjusted to give a Cd component equal to the total Cd flux in (a).

component equal to the total Cd flux used during the Cd-enhanced growth. An Auger depth profile of a 300-s growth of CdTe at $T_s = 300$ °C with $J_{Cd}/J_{Te} = 1$ and total flux of 7.2×10^{14} atoms/cm²/s (corresponding to a growth rate of 1.5 $\mu\text{m/h}$) is shown in Fig. 2(b). Again, the layer formed is rich in In and Te with severely degraded interfacial quality.

The ability to grow thin layers of CdTe on InSb at $T_s = 300$ °C made it possible to study the subsequent growth of InSb on these layers. Layer and interface quality of the films grown was examined as a function of the InSb growth rate and Sb/In flux ratio. Epitaxy of InSb on CdTe epilayers was not achieved for growth rates less than 0.15 $\mu\text{m/h}$ for J_{Sb}/J_{In} in the range 1.1–3.5. Immediately after initiation of growth of InSb, the streaked (2×1) CdTe RHEED pattern became spotty, an indication of three-dimensional nucleation. This spotted pattern remained unchanged throughout the growth period. Auger depth analysis revealed complete degradation of the 400-Å CdTe underlayer with severe intermixing throughout. For growth rates of 0.2 $\mu\text{m/h}$ or higher, the (2×1) CdTe RHEED pattern immediately became spotty, but gradually changed to the (2×2) Sb-stabilized pattern characteristic of homoepitaxial InSb. The time taken for the RHEED pattern to evolve was approximately 3, 2,

and 1 min for growth rates of 0.2, 0.4, and 0.7 $\mu\text{m/h}$, respectively. Auger analysis reveals that the degree of intermixing is independent of J_{Sb}/J_{In} but dependent on the InSb growth rate, with the highest growth rate resulting in the least intermixing. The decrease in In and Sb in the CdTe underlayer as the InSb growth rate is increased is evident in Fig. 3. For all growth rates, however, In and Sb are present throughout the 400-Å CdTe layer leading to a deterioration and broadening of the initial (CdTe on InSb) interface. To prevent this broadening of the initial interface, an 800-Å CdTe layer was grown. The depth profile of this structure, grown with our maximum InSb growth rate of 0.7 $\mu\text{m/h}$, is shown in Fig. 4. There is a distinct asymmetry between the first and second interfaces. Growth of the InSb epilayer has induced a Cd loss resulting in an In- and Te-rich interfacial region and incorporation of In and Sb throughout the CdTe layer. In a separate study, small shifts in energy and shape of Auger peaks

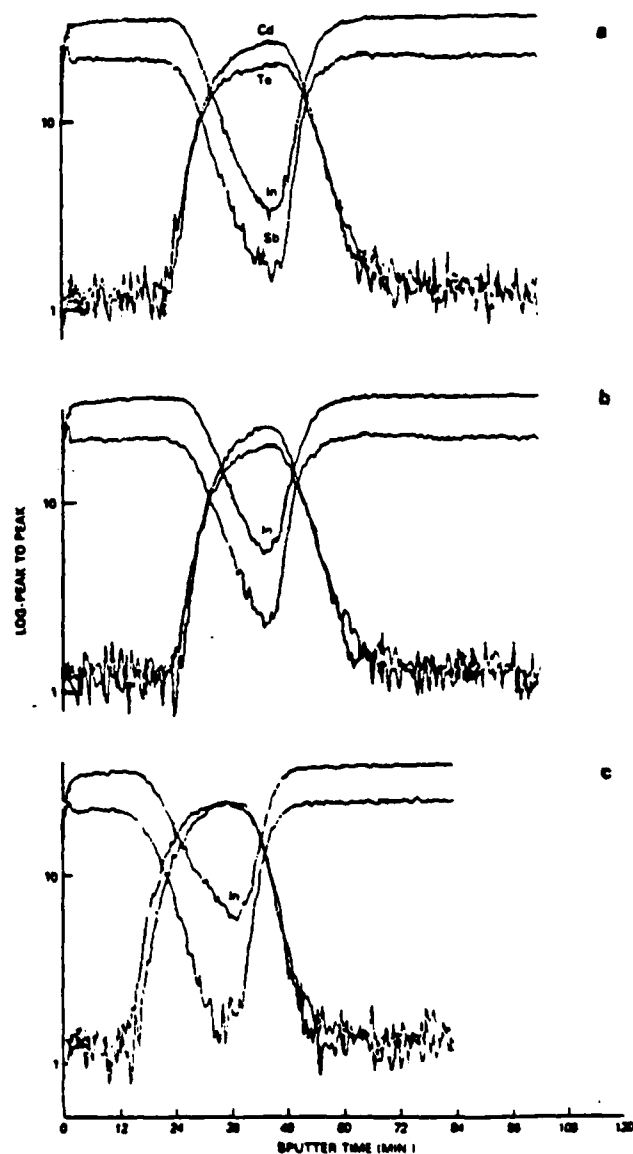


FIG. 3. Auger depth profile of an InSb epilayer grown with a substrate temperature of 300 °C on a 400-Å-thick CdTe layer with In and Sb fluxes corresponding to growth rates of (a) 0.7, (b) 0.4, and (c) 0.2 $\mu\text{m/h}$.

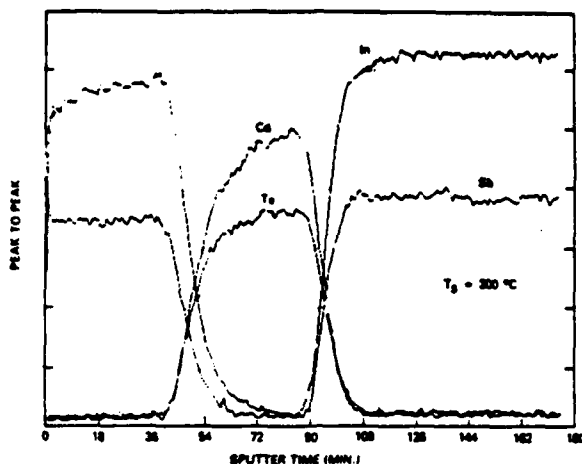
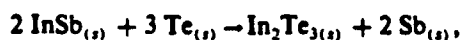


FIG. 4. Auger depth profile of an InSb/CdTe/InSb structure grown at a substrate temperature of 300 °C with an equivalent growth rate for InSb of 0.7 $\mu\text{m/h}$. The CdTe layer was grown to a thickness of ≈ 800 Å under Cd-enhanced flux conditions ($J_{\text{Cd}}/J_{\text{Te}} = 3$).

for the elements at each interface indicated similar electronic environments at each interface and the presence of excess antimony.

IV. DISCUSSION

We have shown that an attempt to grow CdTe on InSb at $T_s = 300$ °C under stoichiometric flux conditions results in a severely intermixed and disordered layer. The use of an enhanced Cd flux during growth has a dramatic effect, resulting in a CdTe layer which is epitaxial and an interface which is abrupt. This suggests that the residence time of Cd on the InSb surface is less than that of Te, resulting in a Cd deficiency at the growth surface and allowing Te to react with InSb to form indium telluride compounds, as suggested by



for which the change in enthalpy ΔH is -30.9 kcal. Use of an enhanced Cd flux clearly reduces or eliminates the Cd deficiency, ensuring that sufficient Cd is available on the InSb growth surface to bond with the incident Te and inhibit access of Te to the In. Thus, perhaps, the enhanced Cd flux need only be applied during the initial stages of growth to allow nucleation of the CdTe, after which the growth can be continued under stoichiometric beam conditions.

We believe that our data for growth at $T_s = 300$ °C of CdTe on InSb have implications for growth at 200 °C. Comparison of the interfacial width of layers grown on InSb at 200 °C with and without enhanced Cd flux indicates that an enhanced flux improves interfacial quality at this "typical" MBE growth temperature. We speculate that the formation of In_2Te_3 , seen⁶ in samples grown under similar conditions is reduced or eliminated by use of enhanced Cd flux during growth. The relatively low mobilities reported¹⁰ for a 2DEG at an InSb/CdTe interface may result from indium loss within the InSb due to indium telluride compound formation at the interface. Samples have been grown at $T_s = 200$ °C using an enhanced Cd flux and magnetotransport measurements

are in progress to assess the 2DEG transport characteristics. It would be of interest to extend our growth studies to include higher values of $J_{\text{Cd}}/J_{\text{Te}}$. The ability to grow CdTe layers on InSb at 200 °C with $J_{\text{Cd}}/J_{\text{Te}} = 3$ clearly suggests that higher flux ratios could be beneficial at higher growth temperatures.

For the growth of InSb on CdTe, the dependence of interfacial abruptness and epitaxy on the InSb growth rate suggests a competitive process between the intermixing and deterioration in the CdTe and the nucleation and growth of InSb. It is possible that broadening of the interface profile is caused by nonuniform sputtering of the InSb; however, the observed Cd deficiency indicates that deterioration of the CdTe has occurred during the InSb growth, most likely due to formation of indium telluride compounds. Results similar to those in Fig. 4 have also been obtained for a structure grown at 275 °C, indicating that atomically abrupt interfaces may not be obtainable for values of T_s compatible with growth of electrically active InSb.

V. CONCLUSION

In conclusion, we have found evidence of a strong chemical reaction which occurs at the CdTe/InSb interface during MBE growth at a substrate temperature of 300 °C. For growth of CdTe on InSb, we have presented a technique for suppressing this reaction by use of Cd-enhanced flux conditions. For growth of InSb on CdTe layers at a substrate temperature of 300 °C, we have found that epitaxy is strongly dependent on the InSb growth rate. Our results extend the substrate temperature range to $225 < T_s < 300$ °C, within which single-crystal layers of both CdTe and InSb can be grown at a fixed substrate temperature. We have shown that multilayer growth is possible at substrate temperatures compatible with electrically active InSb, but that thin period (200 Å) InSb/CdTe structures for tunneling devices may not be feasible due to breakdown of the CdTe barrier. However, the question of whether the chemical profiles presented are adequate for 2DEG or tunneling devices can be answered only after electrical transport measurements have been made.

ACKNOWLEDGMENTS

The authors are grateful to P. Boyd for electron microscopy studies, J. Bratton for technical support, and S. Greene and Dr. M. Pepper for assistance and discussions. T. D. Golding acknowledges a CASE award with the GEC Hirst Research Centre, London.

¹R. G. vanWeizenis and B. K. Ridley, *Solid State Electron.* 27, 113 (1984).

²R. F. C. Farrow, G. R. Jones, G. M. Williams, and I. M. Young, *Appl. Phys. Lett.* 39, 954 (1981).

³T. H. Myers, Yawcheng Lo, J. F. Schetzina, and S. R. Jost, *J. Appl. Phys.* 53, 9232 (1982).

⁴S. Wood, J. Gregg, R. F. C. Farrow, W. J. Takei, F. A. Shirland, and A. J. Noreika, *J. Appl. Phys.* 55, 4225 (1984).

⁵K. Sugiyama, *J. Cryst. Growth* 60, 450 (1982).

⁶K. J. Mackey, D. R. T. Zahn, P. M. G. Allen, R. H. Williams, W. Richter,

- and R. S. Williams, *J. Vac. Sci. Technol. B* 5, 1233 (1987).
- ¹⁰M. Kimata, A. Ryoji, and T. Aoki, *J. Cryst. Growth* 81, 508 (1987).
- ¹¹G. M. Williams, C. R. Whitehouse, T. Martin, N. G. Chew, A. G. Cullis, T. Ashley, D. E. Sykes, and K. Mackey, presented at 4th MBE International Conference, York, England, 1986 (unpublished).
- ¹²A. J. Noreika, M. H. Francombe, and C. E. C. Wood, *J. Appl. Phys.* 52, 7416 (1981).
- ¹³Y. D. Zheng, Y. H. Chang, B. D. McCombe, R. F. C. Farrow, T. Temo-fonte, and F. A. Shirland, *Appl. Phys. Lett.* 49, 1187 (1986).
- ¹⁴G. M. Williams, C. R. Whitehouse, N. G. Chew, G. W. Blackmore, and A. G. Cullis, *J. Vac. Sci. Technol. B* 3, 704 (1985).

**CECOM CENTER FOR NIGHT VISION AND ELECTRO-OPTICS
NON-LINEAR OPTICAL PROPERTIES**

NON-LINEAR OPTICAL PROPERTIES.

GARY WOOD.

DECEMBER 7, 1988.
CECOM CENTER FOR NIGHT VISION
AND ELECTRO-OPTICS.



SC4466T

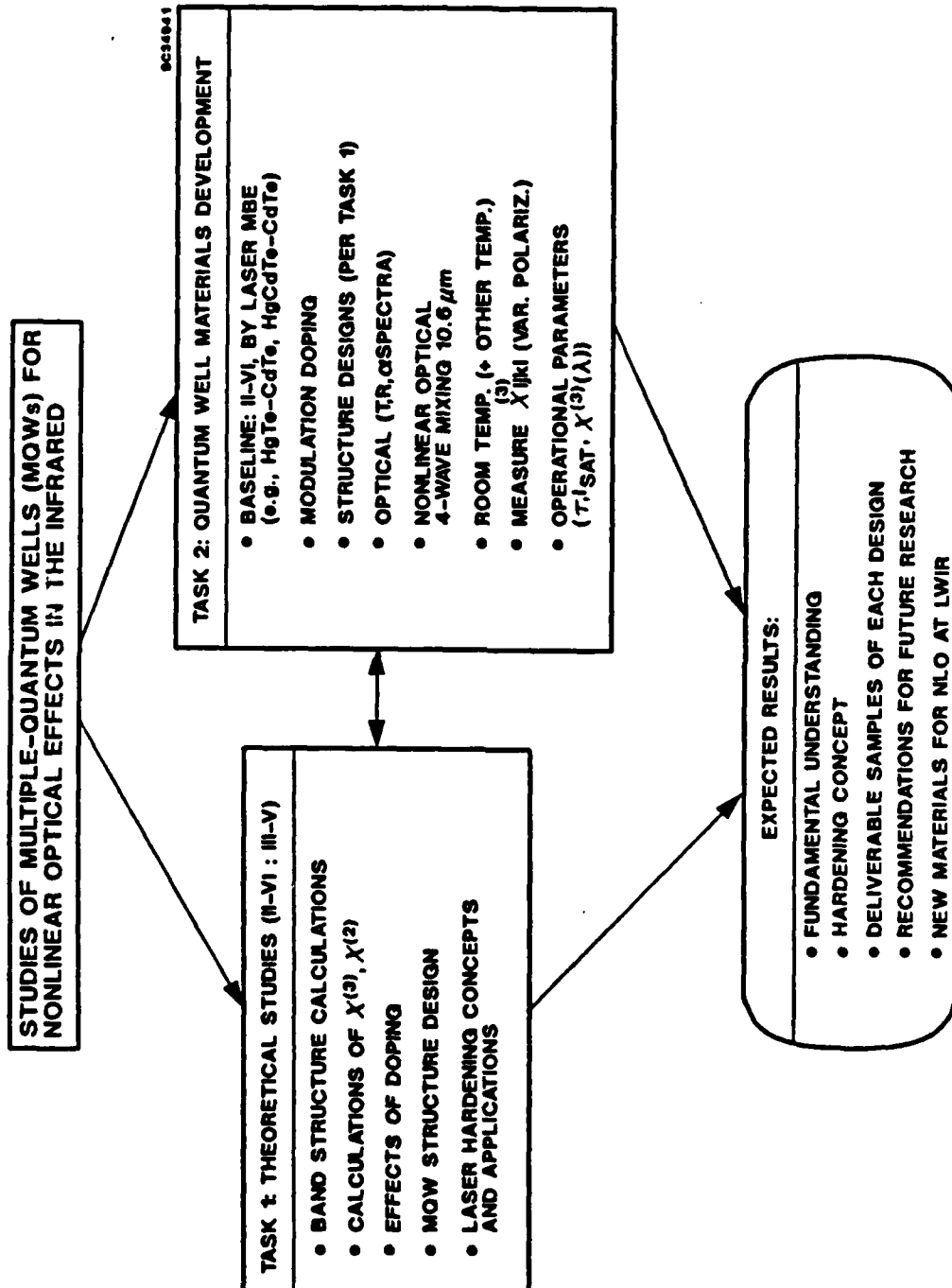


Fig. 1-1. Roadmap of the proposed program.

TECHNICAL CONTRIBUTORS

THEORY AND MODELING (III-V; II-VI)

- Y.C. CHANG (U. OF ILLINOIS)
 - FUNDAMENTAL PROPERTIES
 - PROPOSED STRUCTURES
(COMPOSITION, SL PARAMETERS, DOPING)
- POCHI YEH (DEVICE CONCEPTS)

STRUCTURE GROWTH (II-VI BASELINE)

- J. CHEUNG (LMBE)
- J. ARIAS AND S. SHIN (MBE)

NLO CHARACTERIZATION

- A. CHION, M. KHOSHNEVISAN (ROCKWELL)
- NVEOL FEEDBACK



Rockwell International
Science Center

MECHANISMS THAT CONTRIBUTE TO $\chi^{(3)}$ IN SEMICONDUCTOR BULKS AND MQWs

• BAND-NONPARABOLICITY (NONRESONANT)

• PHOTO-EXCITED PLASMA

• EXCITONIC ABSORPTION

• INTER-SUBBAND TRANSITION

(RESONANT)



Rockwell International
Science Center

BAND NON-PARABOLICITY

AN IMPORTANT MECHANISM FOR $h\nu < E_g$

$$\bullet \chi^{(3)}(\omega_1, \omega_2, \omega_3) = \frac{N_0 e^4 \langle \epsilon^{(4)} \rangle}{24 \omega_1 \omega_2 \omega_3 h^4 (\omega_1 + \omega_2 + \omega_3)},$$

N_0 : CARRIER DENSITY

$$\epsilon^{(4)} = (\partial/\partial k_z)^4 \epsilon(\vec{k})$$

$\langle \rangle$: AVERAGE OVER THE CARRIER DISTRIBUTION
AT THERMAL EQUILIBRIUM

FROM {S.S. JHA AND N. BLOEMBERGEN,
PHYS. REV. 171, 891 (1968)}

- RESPONSE TIME $\tau \sim 10^{-15}$ sec
- ABSORPTION COEFFICIENT $\alpha \sim 1$ TO 10^2 cm^{-1}



Rockwell International
Science Center

$\chi^{(3)}$ DUE TO BAND NON-PARABOLICITY

(A) BULK SEMICONDUCTORS

- VALENCE BAND ~ PARABOLIC
 \therefore p-TYPE ≈ 0
- CONDUCTION BAND: SIGNIFICANT NON-PARABOLICITY
 \therefore n-TYPE: SIGNIFICANT
- $\chi^{(3)} \propto (1/E_g)^3$
 \therefore FAVOR SMALL GAP MATERIALS SUCH AS InSb, InAs, HgCdTe

EXAMPLE

FOR InSb WITH $N_0 \approx 10^{16} \text{ cm}^{-3}$
AT $\hbar\omega_1 = \hbar\omega_2 = 0.117 \text{ eV}$ (10.6 μm)
 $\hbar\omega_3 = -0.335 \text{ eV}$
 $\chi^{(3)} \approx 10^{-9} \text{ esu}$



Rockwell International
Science Center

$\chi^{(3)}$ DUE TO BAND NON-PARABOLICITY (B) MQW

- n-TYPE (CONDUCTION BAND NON-PARABOLICITY)
- REQUIRE Z-POLARIZATION
- FOR GaAs

$$\chi^{(3)} \text{ (MQW)} \approx 30 \times \chi^{(3)} \text{ (BULK)}$$

- FOR HgCdTe

NO ADVANTAGE

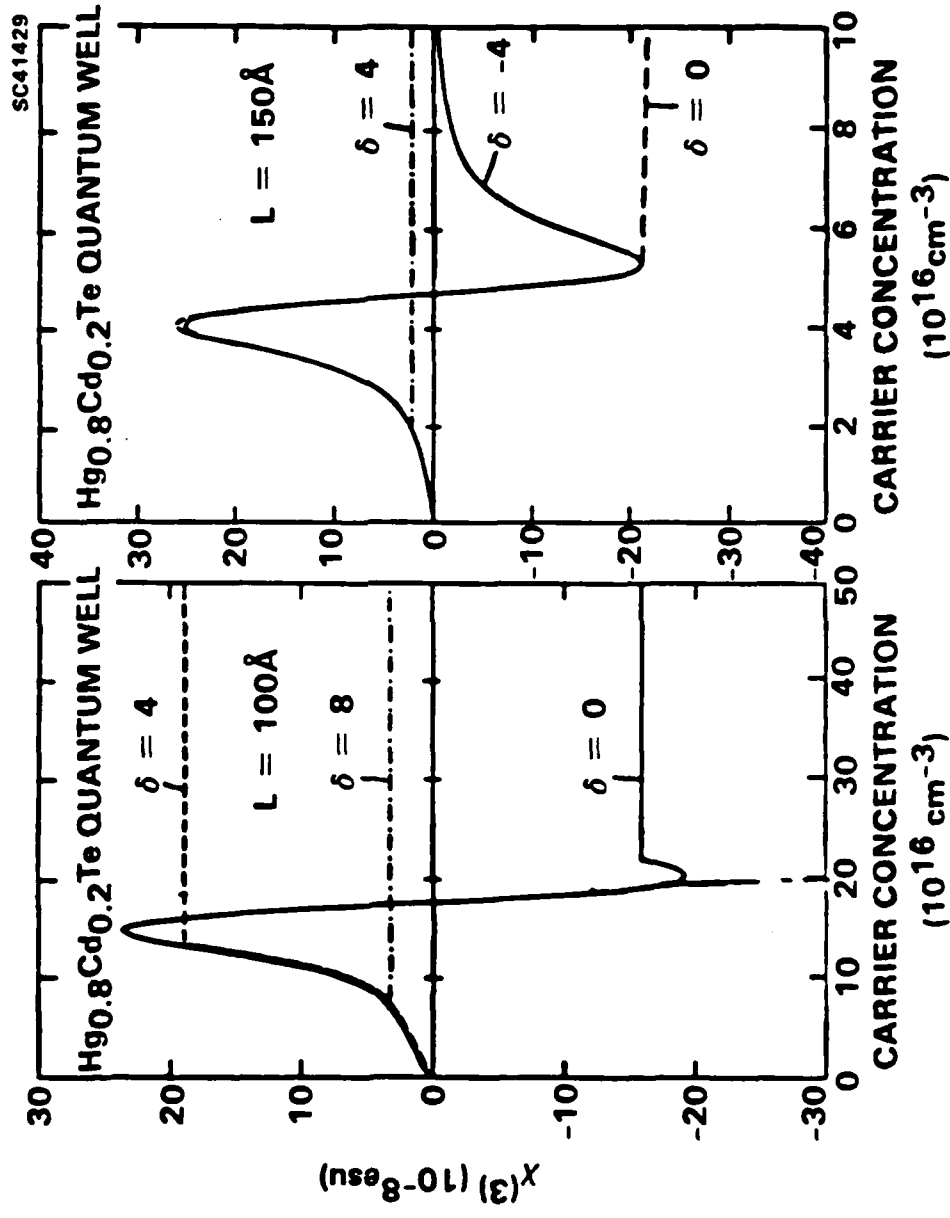
- p-TYPE (VALANCE BAND NON-PARABOLICITY)
- REQUIRE X-Y POLARIZATION
- $\chi^{(3)} \sim 10^{-6}$ esu

$$[\chi^{(3)} \text{ (p-TYPE MQW)} \approx 10^2 \times \chi^{(3)} \text{ (n-TYPE BULK)}]$$



Rockwell International
Science Center

$\chi^{(3)}$ DUE TO VALENCE BAND NONPARABOLICITY



δ = UNIAXIAL STRESS PARAMETER



Rockwell International
Science Center

PHOTO-EXCITED PLASMA

(DOMINANT FOR $h\nu \approx E_g$)

- ASSOCIATE WITH STRONG ABSORPTION,

$$\alpha \sim 10^4 \text{ cm}^{-1}$$

- $\tau \sim 1 \text{ nsec}$

- $\chi^{(3)} \sim 1 \text{ esu}$ AT $\lambda = 5.3 \mu\text{m}$ FOR InSb AT 77°K
(ABSORPTION EDGE)

- BULK VERSUS Q.W: SAME ORDER OF MAGNITUDE

*A. MILLER, D.A.B. MILLER AND S.D. SMITH,
ADV. PHYS. 30, 697 (1981)



Rockwell International
Science Center

EXCITONIC TRANSITIONS

SIMILAR TO PHOTO-EXCITED PLASMA WITH

- LARGER $\chi^{(3)}$
- LARGER α
- τ : ABOUT THE SAME ORDER

Q.W. VERSUS BULK

- LARGER $\chi^{(3)}$
- LARGER α



Rockwell International
Science Center

INTER-SUBBAND TRANSITIONS

(A) BULK SEMICONDUCTOR

- p-TYPE (HEAVY AND LIGHT HOLES IN VALANCE BAND)

$$\chi^{(3)} \sim 10^{-5} \text{ e.s.u.}$$

$$\alpha \sim 10^2 \text{ cm}^{-1}$$

$$\tau \sim 10^{-12} \text{ sec}$$

$$I_s \sim 1 \text{ mW/cm}^2$$

e.g., Ge AT 10.6 μm

- n-TYPE

NO SUBBANDS IN THE CONDUCTION BAND



Rockwell International
Science Center

INTER-SUBBAND TRANSITIONS (B) MQW

- n-TYPE REQUIRE Z-POLARIZATION
- p-TYPE (X-Y) OR Z POLARIZATION

- FOR p-TYPE $\text{GaAs-Al}_x\text{Ga}_{1-x}\text{As}$ MQW

$$I_s (\text{MQW}) \sim 1/10 I_s (\text{BULK})$$

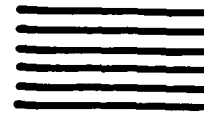
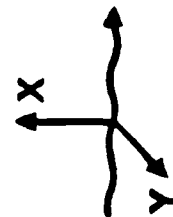
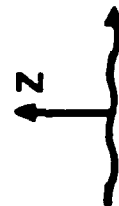
$$\chi^{(3)} (\text{MQW}) \sim 10 \chi^{(3)} (\text{BULK})$$



Rockwell International
Science Center

SUMMARY

MECHANISMS	$\chi^{(3)}$ (esu)	α (cm ⁻¹)	RESPONSE TIME (SEC)	OPTICAL POLARIZATION
CB NON-PARABOLICITY	$10^{-9} \sim 10^{-7}$	1 TO 10^2	10^{-15}	Z
VB NON-PARABOLICITY	$10^{-8} \sim 10^{-6}$	1 TO 10^2	10^{-15}	(X, Y)
PHOTO-EXCITED PLASMA	1	10^4	$10^{-6} \sim 10^{-9}$	(X, Y OR Z)
INTER-SUBBAND TRANSITIONS (CONDUCTION BAND)	$10^{-7} \sim 10^{-5}$	$10^3 \sim 10^5$	10^{-12}	Z
INTER-SUBBAND TRANSITIONS (VALANCE BAND)	$10^{-7} \sim 10^{-5}$	$10^2 \sim 10^4$	10^{-12}	(X, Y OR Z)



Z-POLARIZATION

(X-Y)-POLARIZATION

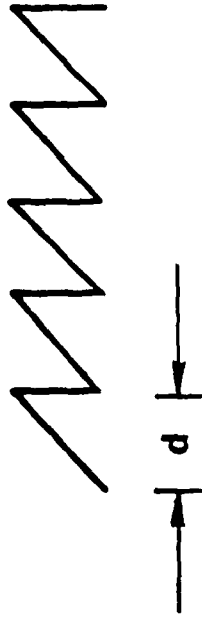


Rockwell International
Science Center

MQW DESIGN PARAMETERS (EXAMPLE)

SC41426

- TWO SAMPLE STRUCTURES FOR $\text{Hg}_{1-x}\text{Cd}_x\text{Te}$ WITH SAWTOOTH PROFILE



- $x = 0.08-0.3$ $d \approx 258\text{\AA}$ (85 MONOLAYERS)
- TRANSITION WAVELENGTH $\approx 10.6\text{ }\mu\text{m}$
- $\chi^{(3)} > 1\text{ esu}$
- $\alpha \sim 10^4\text{ cm}^{-1}$
- RELAXATION TIME $\tau \sim 10^{-12}\text{ s}$ (PHONON-ASSISTED)
- TURN ON TIME $\tau_1 \sim 10^{-9}\text{ s}$ (DEPENDS ON OPTICAL INTENSITY)



Rockwell International
Science Center

SAMPLE DESCRIPTION

300°K

77°K

SAMPLE	THICKNESS (μm)	$n(\text{cm}^{-3})$	$\mu(\text{V-S}/\text{cm}^2)$	TYPE	$N(\text{cm}^{-3})$	$\mu(\text{V-S}/\text{cm}^2)$	TYPE
12-17(6)*	3.7	1.7×10^{16}	5×10^3	N	7×10^{15}	1.3×10^4	N
12-16(6)**	2.5	3×10^{16}	6.7×10^3	N	1×10^{16}	2.2×10^4	N
6-23(7)***	3.6	2×10^{17}	4×10^3	N	1×10^{17}	370	MIXED

*: $X = 0.24$, CONSTANT COMPSITION ALLOY ON (100) CdTe

** : $X_1 = 0.27$, $X_2 = 0.23$, SINUSOIDAL SL ON (100) CdTe

***: $X_1 = 0.43$, $X_2 = 0.05$, SAWTOOTH SL ON (110) CdTe



Rockwell International
Science Center

**CECOM CENTER FOR NIGHT VISION AND ELECTRO-OPTICS
LASER DIODE ARRAYS**

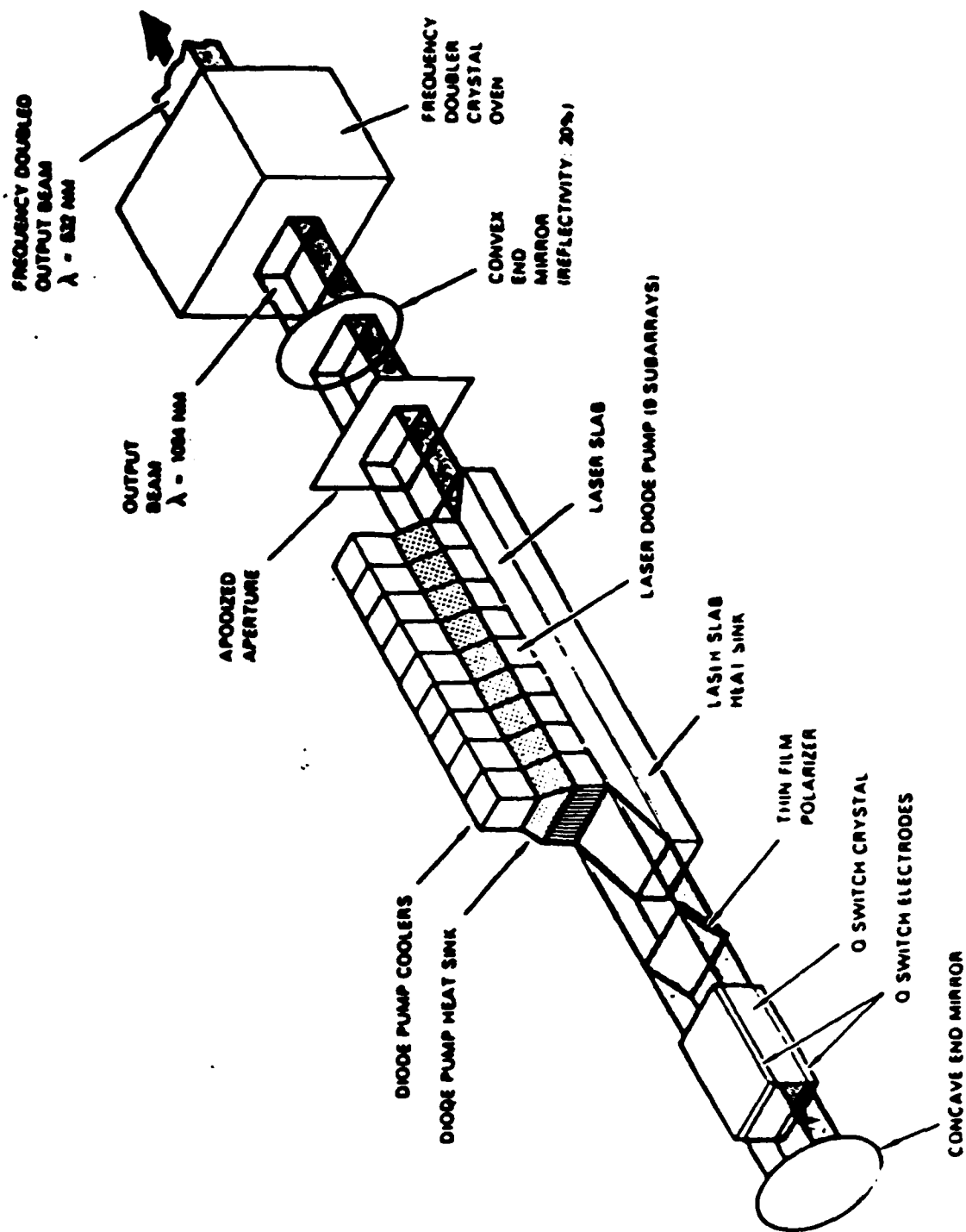
LASER DIODE ARRAYS.

DAVID CAFFEY

DECEMBER 7, 1988.
CECOM CENTER FOR NIGHT VISION
AND ELECTRO-OPTICS.

DIODE PUMPED SLAB LASER

10-0018

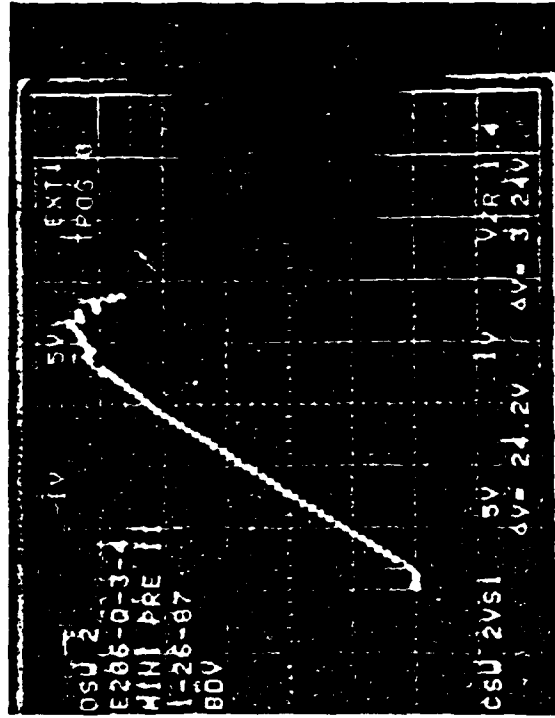


UNCLASSIFIED

M19-01741

VERY HIGH PEAK POWER DEMONSTRATED

- 114 W/cm
- 150 μ SEC PULSES, 20Hz
- 0.24cm MINI-BAR
- MULTIPLE BARS TESTED



5 W/DIV

8.6 A/DIV

EQUIVALENT TO
3600 W/cm²

UNCLASSIFIED

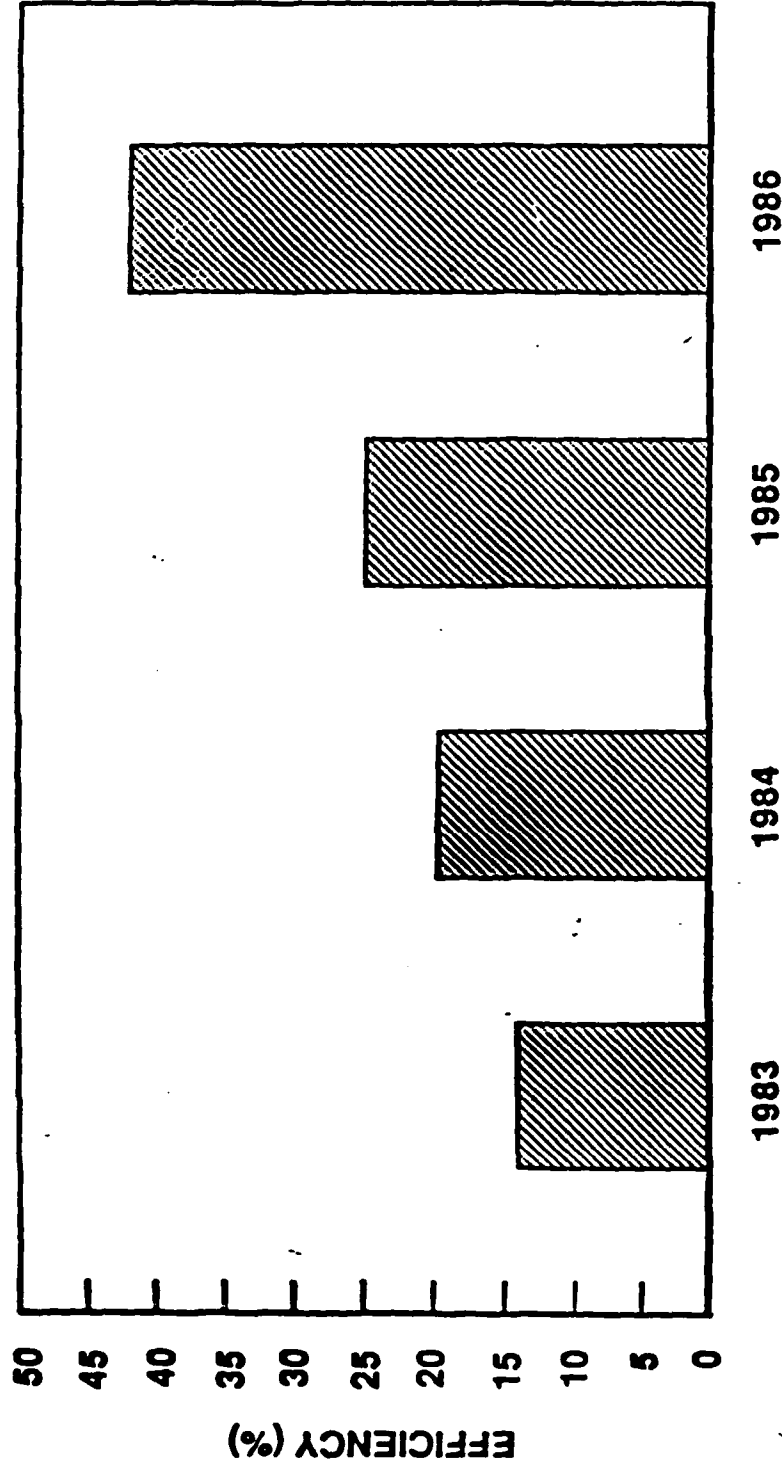
McDonnell Douglas Astronautics Company - St. Louis

UNCLASSIFIED

M10-14517

LASER DIODE ARRAY EFFICIENCY* PROGRESS

*ELECTRICAL POWER IN TO OPTICAL POWER
OUT OF ARRAY AT OPERATIONAL CURRENT



UNCLASSIFIED

58

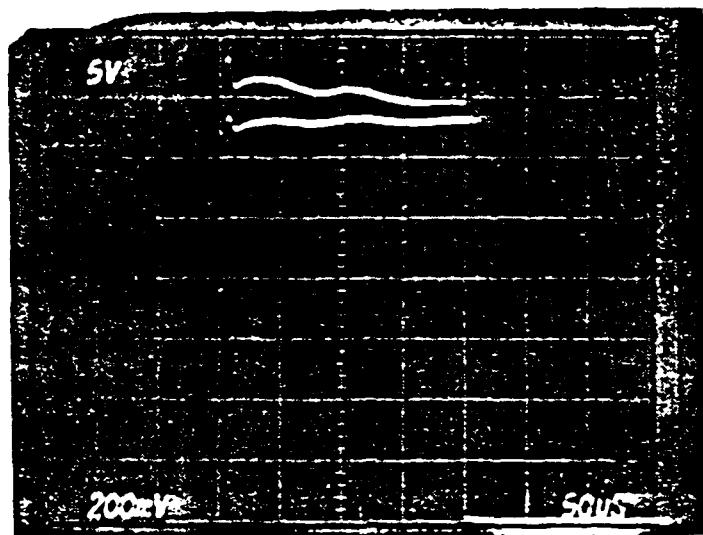


Figure 18. Oscilloscope trace of the pump power at 10 watts per division. The signal is a wavy line, indicating a wavy pump power.

The pump power is a wavy line, indicating a wavy pump power. The signal is a wavy line, indicating a wavy pump power.

Figure 19. Primary array optical output. The signal is a wavy line, indicating a wavy pump power.

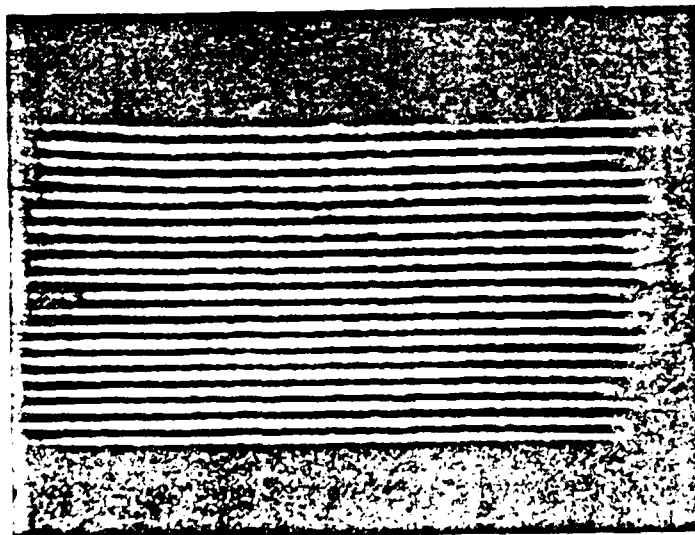
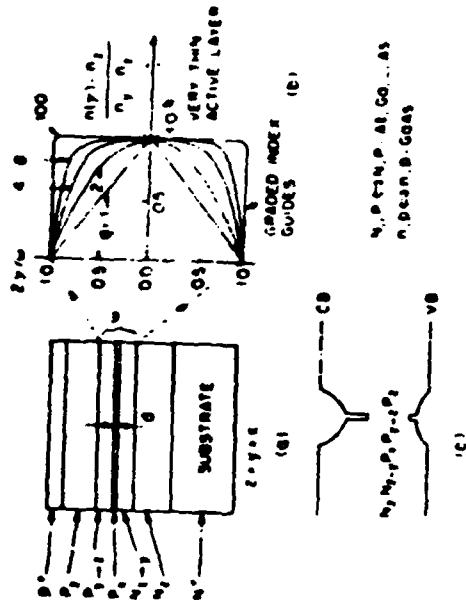
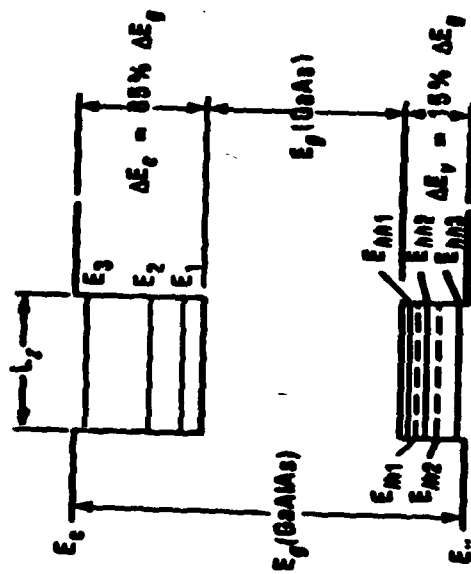
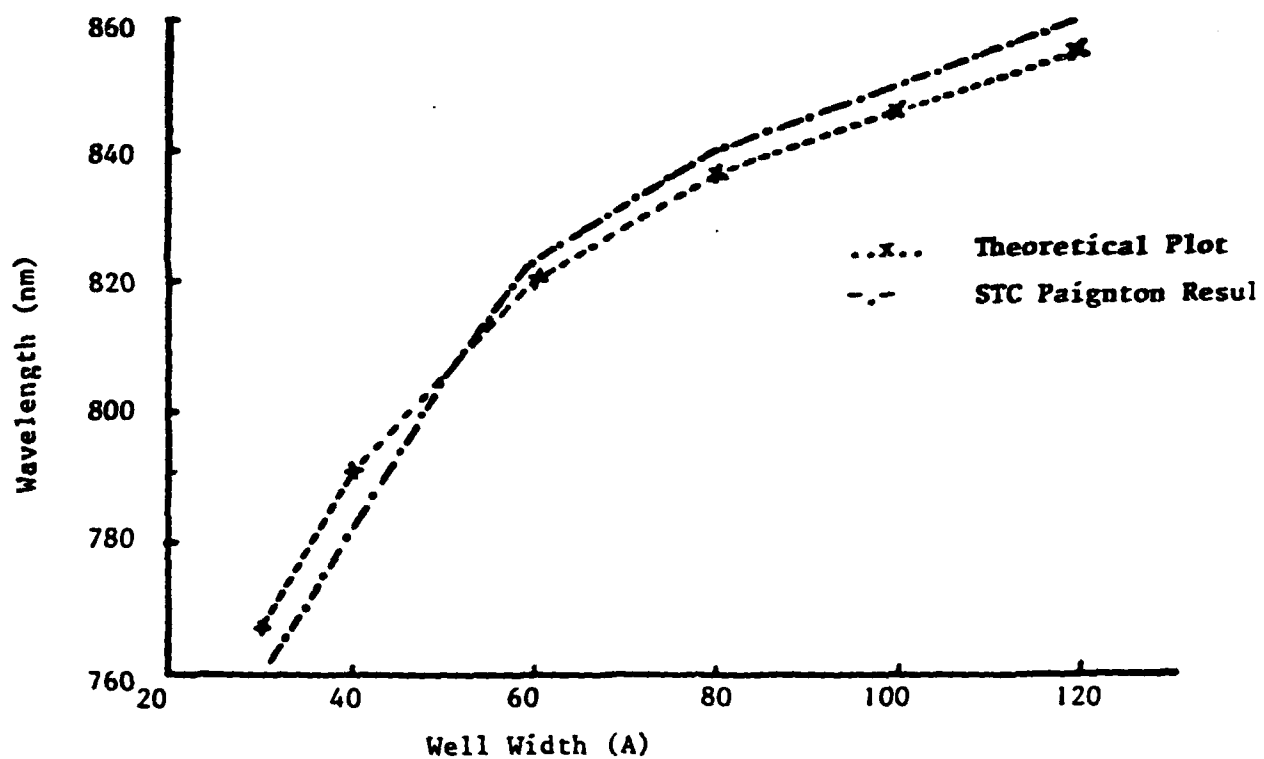


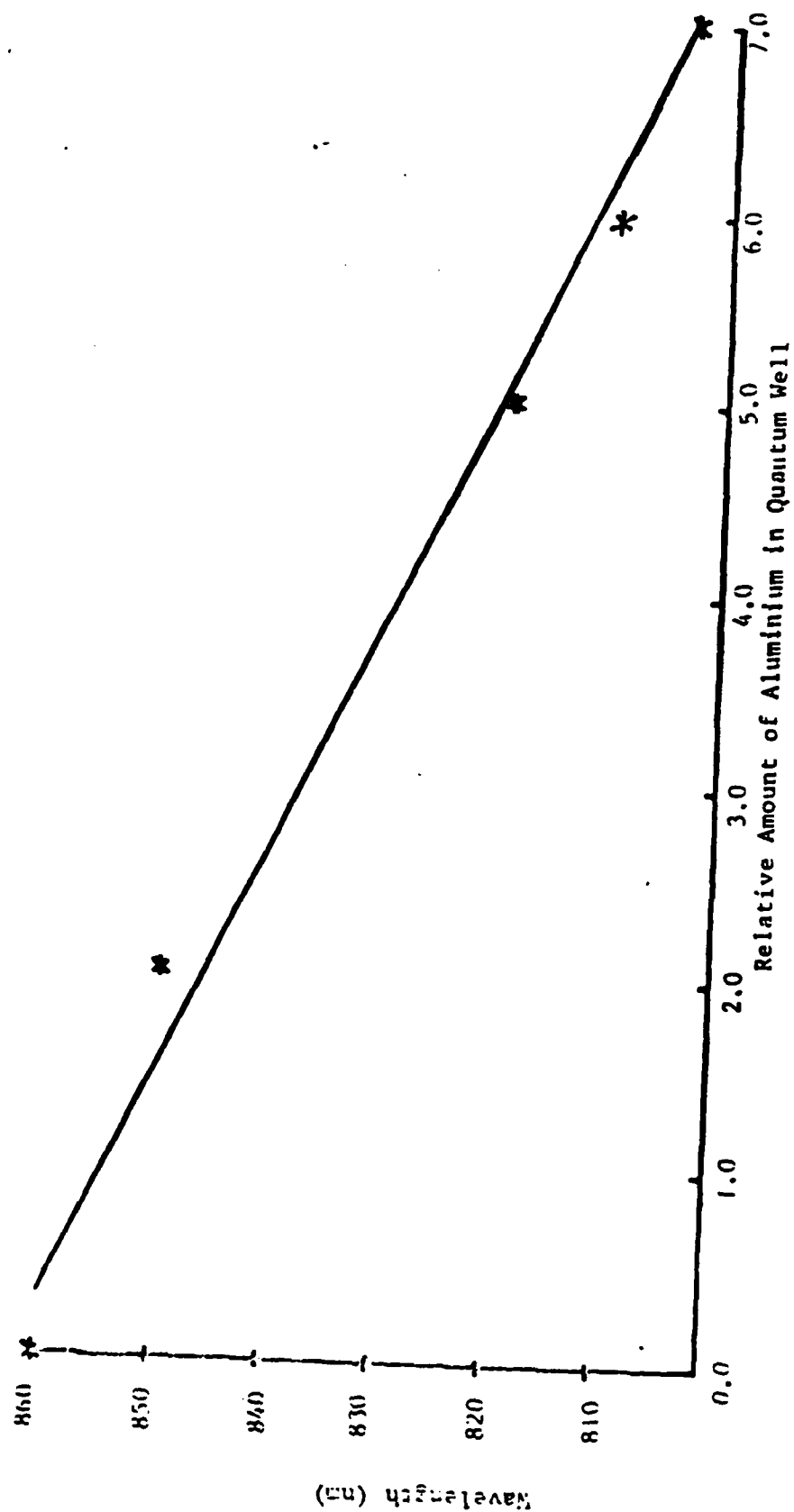
Figure 19. Primary array optical output.



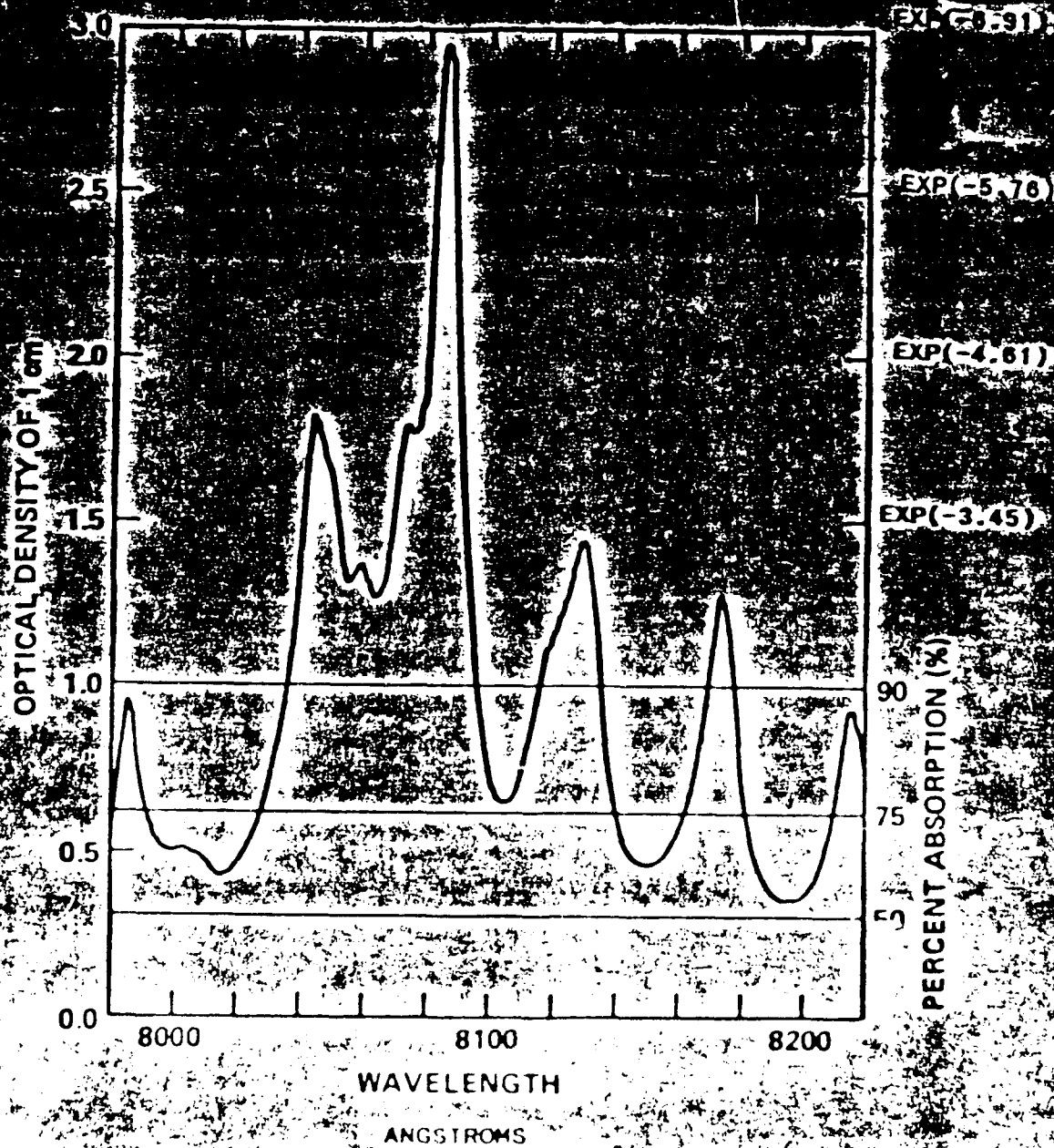
$N_A, P, \text{etc. at } 0.01 \text{ as } n, \text{ etc. at } 0.02$



Shift in Emitted Wavelength as a Function
of Quantum Well Thickness, L_z

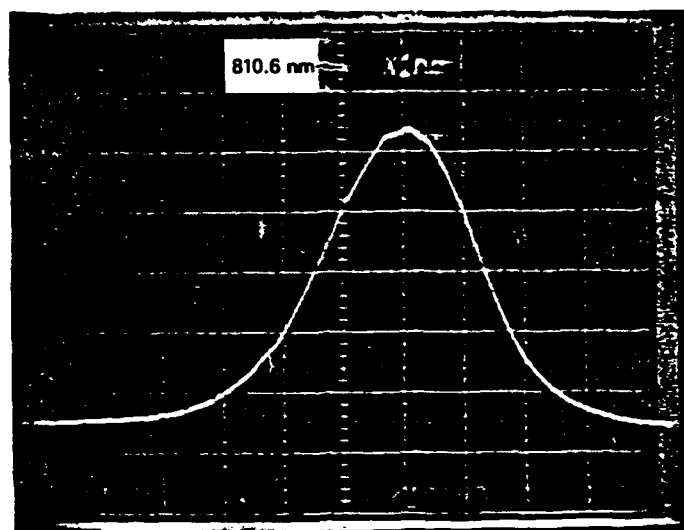


Shift in Emitted Wavelength as a Function of Aluminum Concentration in the Quantum Well



ABSORPTION OF 1% Nd:YAG

10-12998



- 50 AMPERE PULSES, 100 μ sec DURATION, 10 pps
- HEAT SINK TEMPERATURE = 25.9°C
- HORIZONTAL SCALE 1 nm PER DIVISION

Figure 14. Primary array wavelength

10-12999

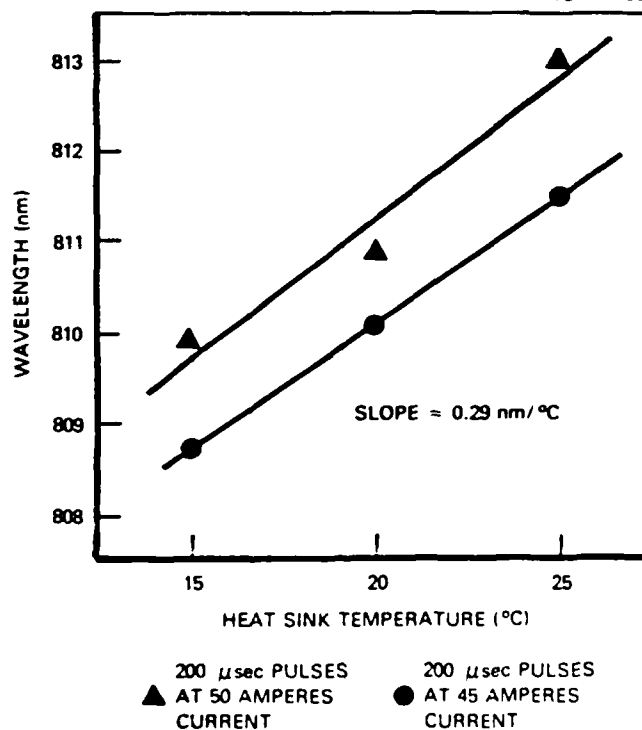
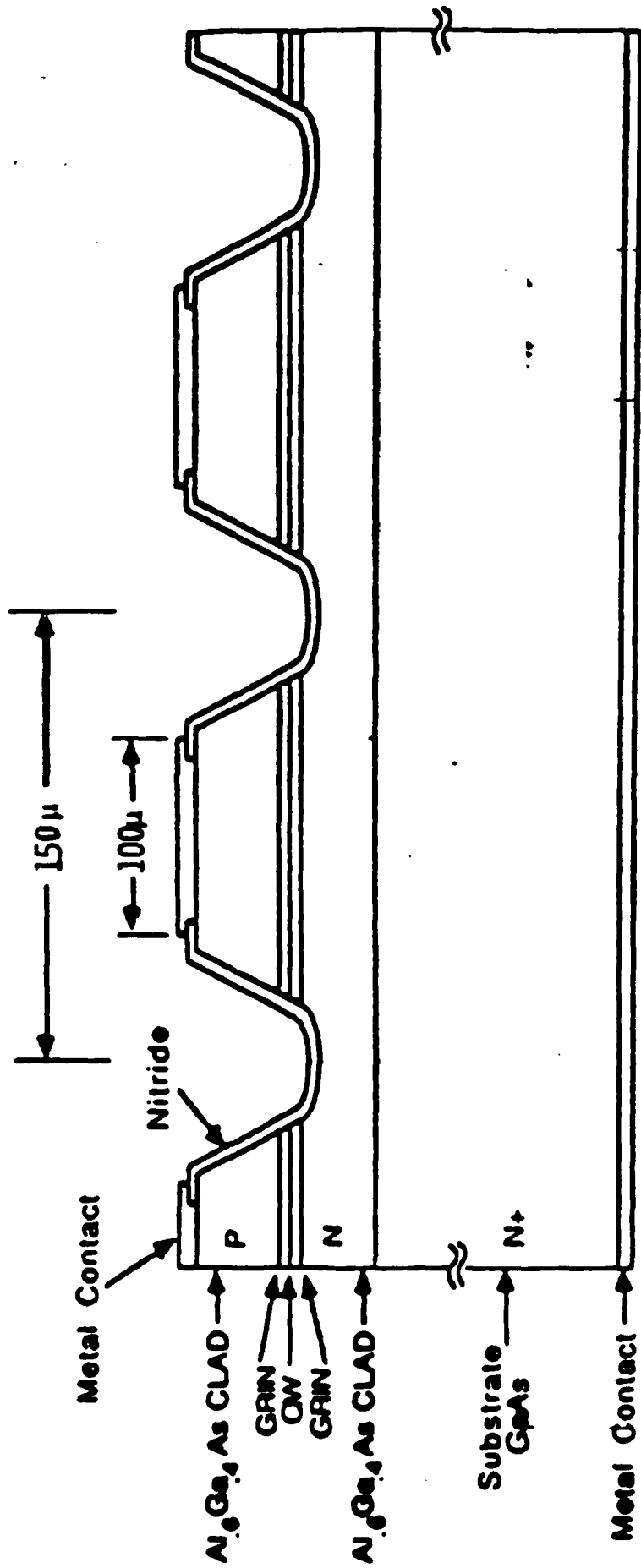


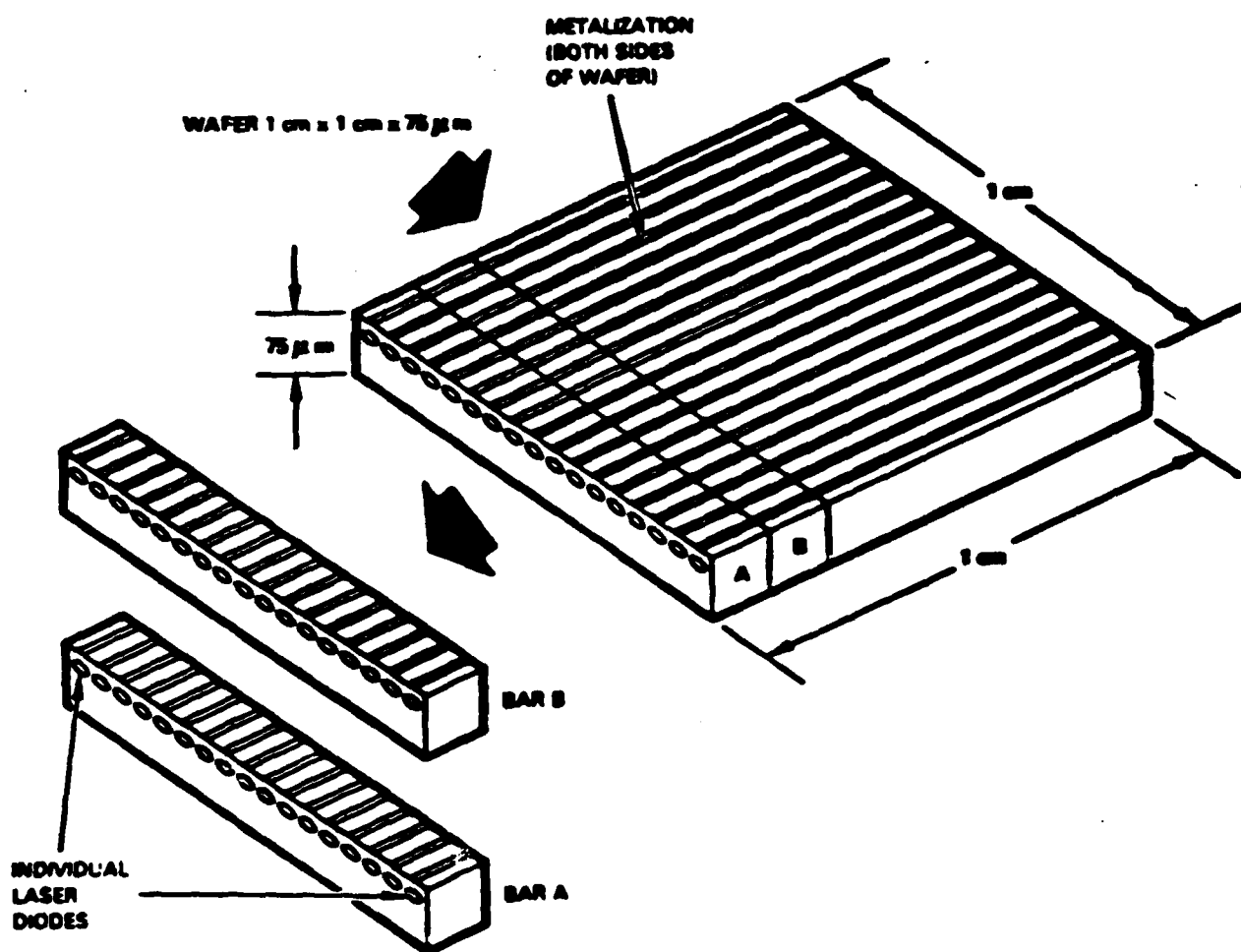
Figure 15. Primary array wavelength versus heat sink temperature

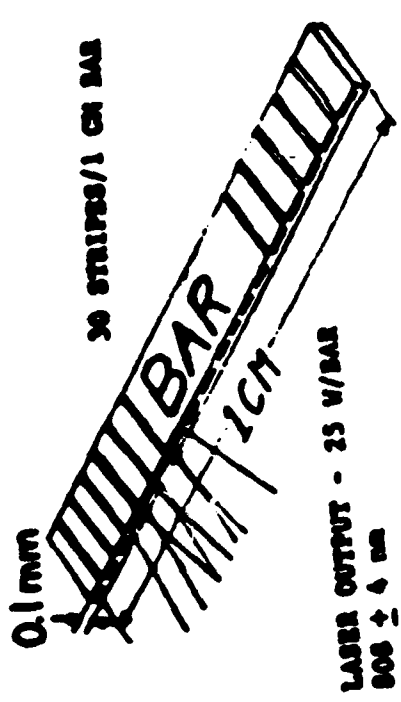


GaAs Quantum Well Linear Array Laser Structure

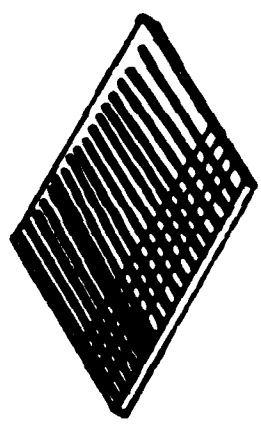
PSL J/27/01
ELECTRONICS
LABORATORY
SYRACUSE, NEW YORK



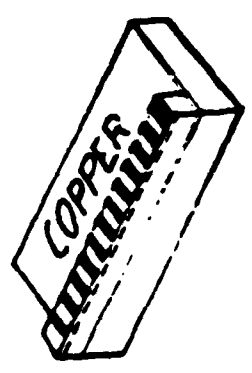
DIODE BAR FABRICATION



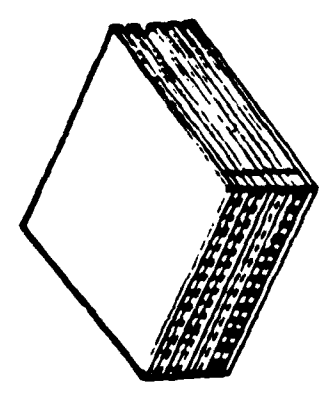
OXIDE REFINED STRIPE LASERS



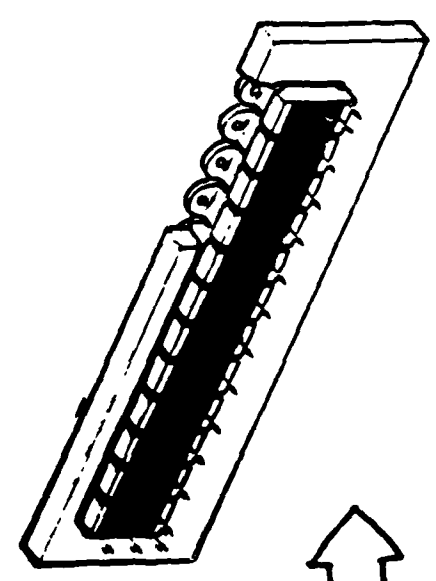
WAFERS ARE CLEAVED
TO FORM BARS



BARS ARE BONDED
TO COPPER HEATSINKS

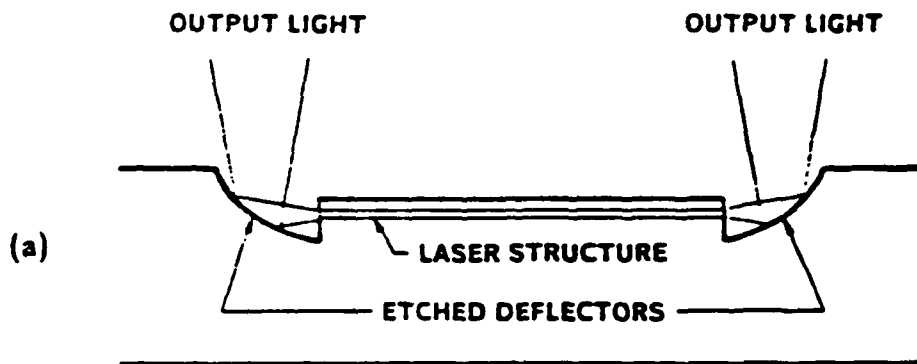


40 MOUNTED BARS ARE STACKED
TO FORM A 1 KW SUBARRAY

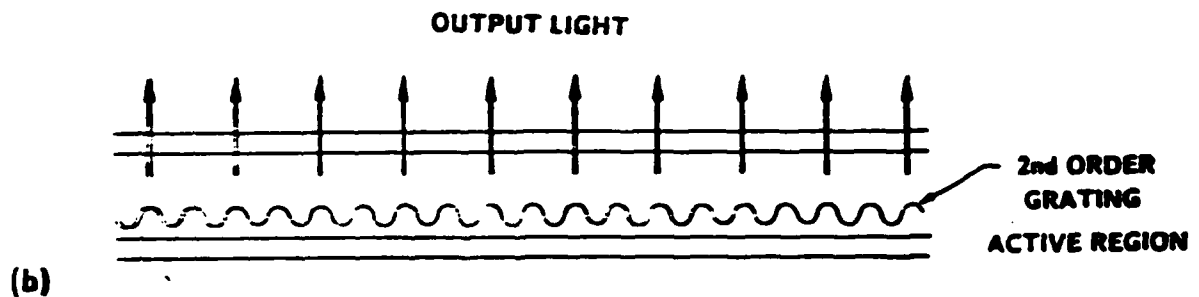


12 SUBARRAYS ARE COMBINED TO
FORM A 12 KW LASER DIODE PUMP

**TYPE I SURFACE EMITTERS WITH LASING
PARALLEL TO THE SURFACE**



LASER WITH ETCHED DEFLECTORS FOR OUTPUT COUPLING

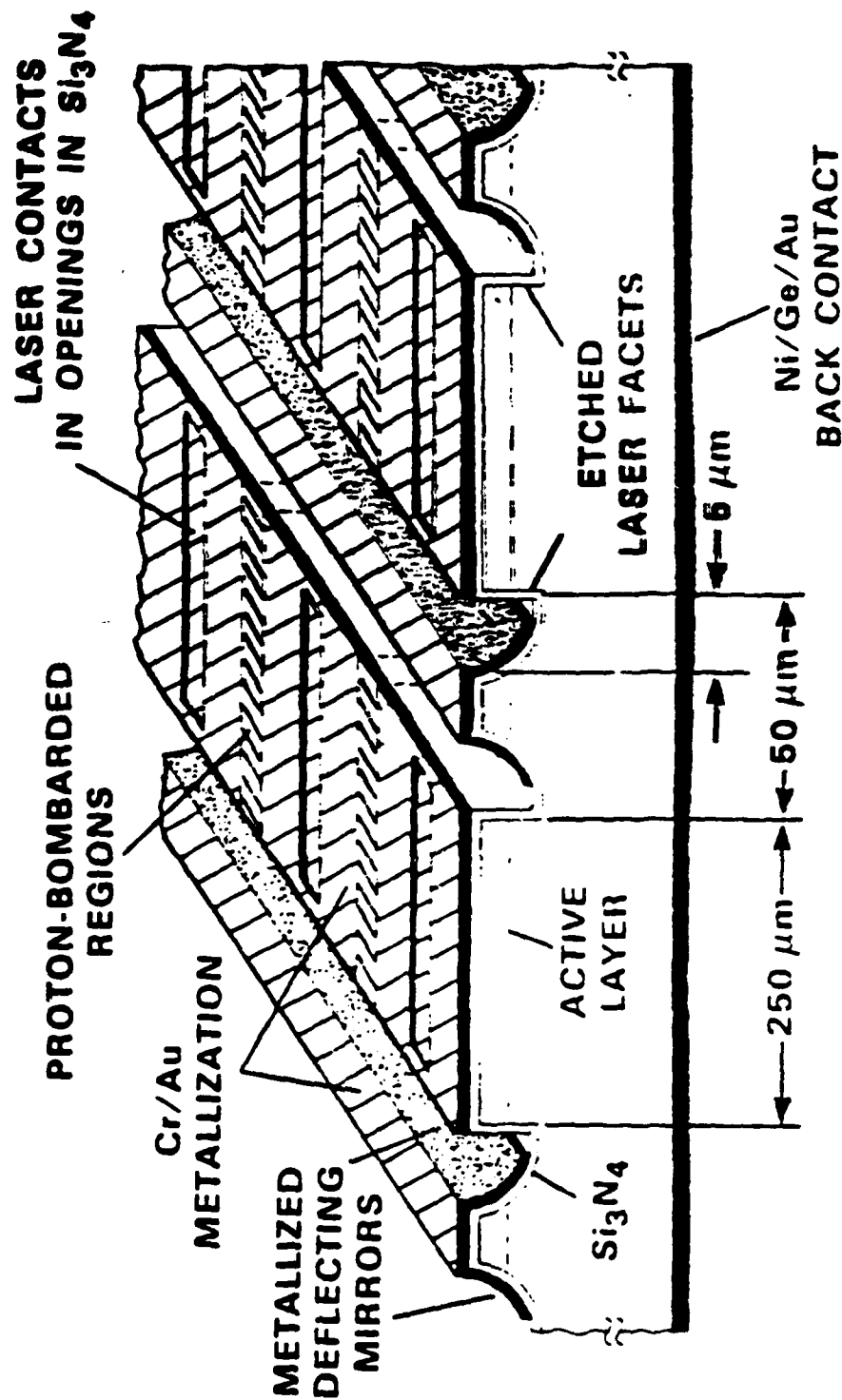


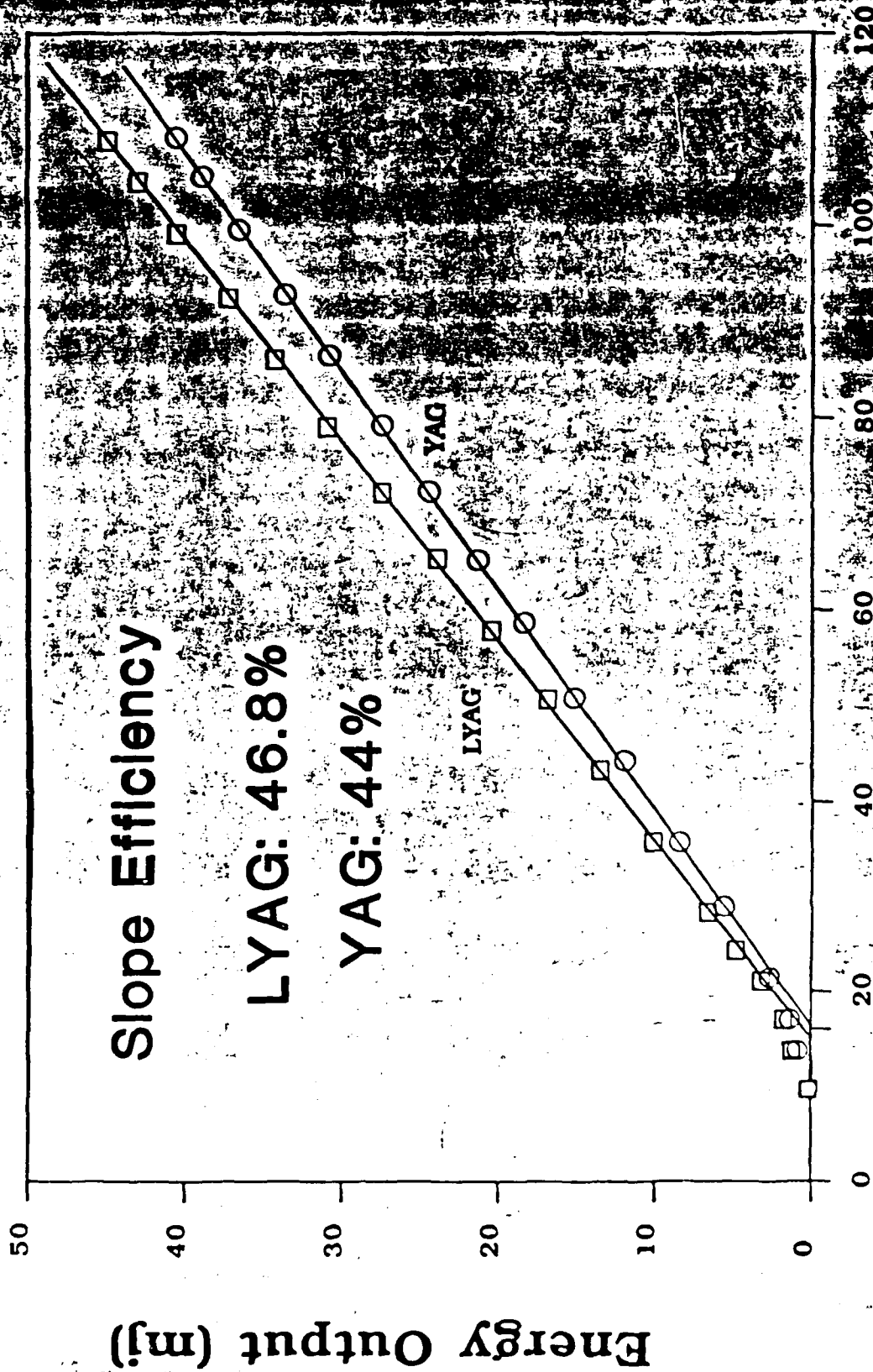
LASER WITH A GRATING FOR OUTPUT COUPLING

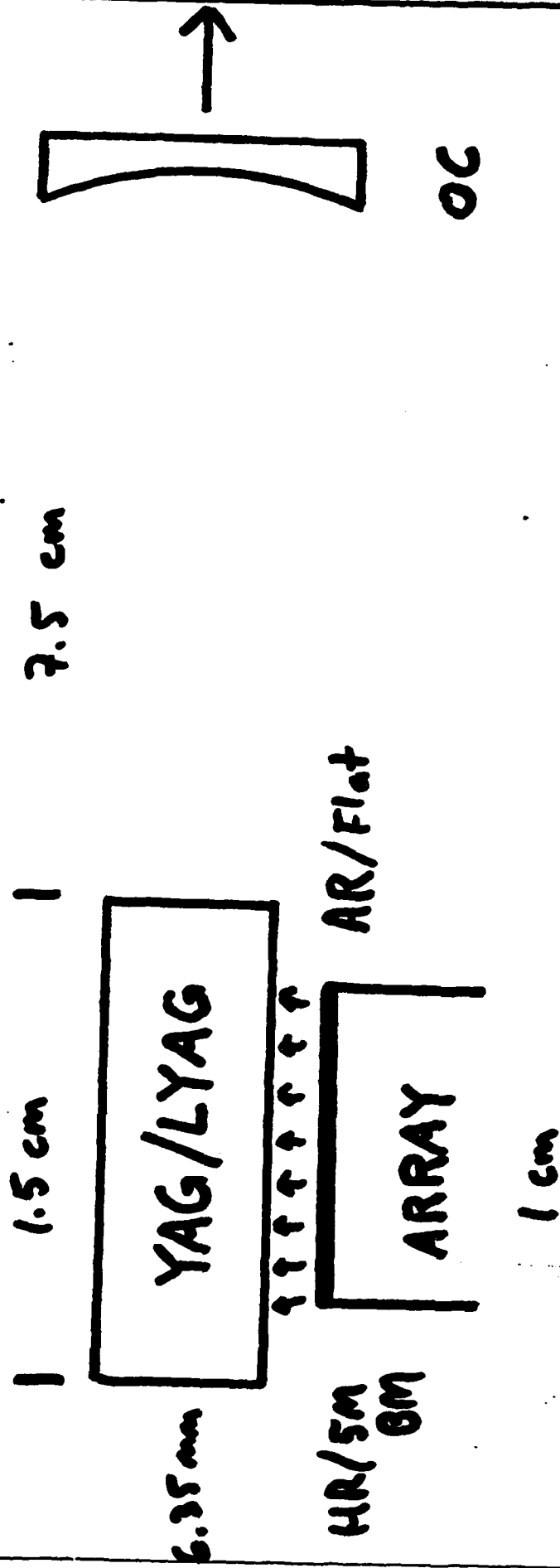
MDAC ARRAY CHARACTERISTICS

Dimensions	5 mm x 10 mm
Pulse Energy, 300 μ sec	100 mJ
Wavelength at 10 C	808 nm
Bandwidth at 10 C	< 2.7 nm FWHM
Array Efficiency	20.8%
Driver Efficiency	84%
Overall Efficiency	17.5%

MONOLITHIC TWO-DIMENSIONAL SURFACE-EMITTING AlGaAs/GaAs DIODE LASER ARRAY







Cavity Configuration

Temperature (°C)

25

20

15

10

Energy Output (mj)

42

40

38

36

34

32

30

LYAG

YAG

812

810

808

Input Wavelength (nm)

Energy output vs pump wavelength at 100 mJ/pulse

LIST OF ATTENDEES

4. LIST OF ATTENDEES

OPTOELECTRONIC WORKSHOP

SUPERLATTICE DISORDERING

December 7, 1988

NAME	ORGANIZATION	PHONE
Rudolf Buser	NVEOC	703-664-3067
Paul Amirtharaj	NVEOC	703-664-5043
Frederick Carlson	NVEOC	703-664-5036
Ronald Graft	NVEOC	703-664-5780
John Dinan	NVEOC	703-664-5825
Jan Davis	NVEOC	703-664-
Unchul Lee	NVEOC	703-664-5780
Michael Martinka	NVEOC	703-664-5043
John Pollard	NVEOC	703-664-5780
Gary Wood	NVEOC	703-664-5767
Ronald Antos	UR, Optics	716-275-4179
Susan Houde-Walter	UR, Optics	716-275-7629
Brian Olmsted	UR, Optics	716-275-5101